An investigation into the nature of sources associated with the gamma ray burst phenomenon

A THESIS

SUBMITTED FOR THE DEGREE OF
DOCTOR OF PHILOSOPHY

in
Department of Physics
Mangalore University

S. G. Bhargavi

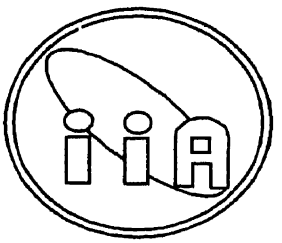

Indian Institute of Astrophysics
Bangalore 560 034, India
July 2001

Declaration

I hereby declare that this thesis, entitled '*An investigation into the the nature of the sources associated with the Gamma Ray Burst phenomenon*' submitted to the Mangalore University, Mangala Gangotri, for the award of a Ph.D. degree, is the result of the investigations carried out by me at Indian Institute of Astrophysics, Bangalore, under the general supervision of Professor Ramanath Cowsik. The results presented herein have not been subject to scrutiny, by any university or institute, for the award of a degree, diploma, associateship or fellowship whatsoever.

R. Cowsik

Professor Ramanath Cowsik
(Thesis Supervisor)

S. G. Bhargavi
(Ph.D. Candidate)

Indian Institute of Astrophysics
Bangalore 560 034, India

12 July 2001

Certificate

This is to certify that the thesis entitled '*An Investigation into the nature of sources associated with the Gamma Ray Burst (GRB) phenomenon*' submitted to the Mangalore University by S. G. Bhargavi for the award of the degree of Doctor of Philosophy in the department of Physics, is based on the results of the investigations carried out by her under my general supervision and guidance, at the Indian Institute of Astrophysics. This thesis has not been submitted for the award of any degree, diploma, associateship, fellowship, etc., of any university or institute.

Dr Ramanath Cowsik
(Thesis Supervisor)

Bangalore 560034
12 July 2001

Acknowledgements.

The expedition to 'search for the unknown sources of GRBs'
-one of the front-line topics of research in current astronomy,
was indeed a wonderful and rich experience
– a strange mixture of pleasant and bitter feelings!.
When I began with it, Ph D was a necessity; it became a duty at some stage (to fulfill the promises made); much later, along the long twisting path of risk and uncertainties, it appeared as a dream! It is the warmth and care of my family members and some wonderful friends and collegues besides self determination that helped me to overcome the "thesis blues".

It is with pleasure that I extend my sincere gratitude to Professor Ramanath Cowsik for accepting to be my thesis advisor when I was going through a phase of detestation and hostility. A major portion of the thesis contains the work carried out from mid-1999 onwards as the recent developments in the GRB field made my previous efforts un-publishable and out-dated. I have been privileged to be guided and motivated by Prof Cowsik to complete the thesis in 2 years with most recent results. The academic freedom and moral support he gave all along the PhD program are precious and gave me an opportunity to interact freely with the GRB community. I am grateful for his useful comments on this manuscript. His patience and enthusiasm for scientific discussions - several times after the long and exhausting hours of administrative duties of Director - were very inspiring.

I am indebted to two persons who gave constant encouragement and unlimited support in completing this thesis. First: Dr Jochen Greiner who tendered valuable scientific advice all along and has been a kind hearted friend. I gratefully acknowledge his comments on the manuscripts and the hospitality and facilities provided during my stay at AIP, Potsdam. Second: Dr Shiv Sethi who collaborated in two research projects. I thank Shiv for the help in numerical computations and several fruitful discussions.

All the university formalities (starting from recognition of IIA as a PhD center, onwards to thesis submission) were very smooth with the kind co-operation of Prof P Mohan Rao, Prof Prakash Karat, Prof J Ucchil and the Registrar of Mangalore University. I am grateful for their help and pleasant interaction.

Some of the data used in this thesis were observed by collegues and grad. students during the time allotted for other research (see the footnotes in relevant chapters). I acknowledge their kind co-operation. I thank all the assistants and telescope operators at VBO for their co-operation and help in obtaining the data.

Drs. Fred Vrba and Arne Henden (US Naval Observatory) are gratefully acknowledged for supplimenting the calibration data for IPN GRB studies presented in chapter 5 of this thesis.

I thank several other collegues who indirectly helped in obtaining the data from VBO: former and present chair-persons of GC-2 & time allocation committee; the former and present scientists-in-charge of VBO. I acknowledge the kind co-opertaion by the Heads and staff members of Engineering (electronic, mechanical and optical) division for, without the smooth operation of the telescope I would not have got any data and completed this thesis.

I am grateful to computer systems administrators, Mr AV Ananth and Mr JS Nathan for generously providing disk space and tolerating my extended use of the Sun system at fifth floor. I enjoyed the beautiful view besides solitude. I also thank Dr S Perumal and Mr KN Kutty for their help at VBO computer center.

I thank the Dean and the chair-person of BGS for their encouragement & help in matters related to Ph D program and approving several of my academic tours.

I wish to thank all the staff members of Director's office: Mr KT Rajan (also for putting up with my harsh words), Ms Pramila, Mr Ramesh and Mr Khan (also for his humour on my working hours!) for the timely help and fixing the appointments.

The Librarians, Ms Vagishwari, Ms Christina Louis and staff members are thanked for every help they provided. Thanks also to the staff members of Admin, stores and other non-academic divisions for providing all the facilities over the years during my stay at IIA. I thank Mr Elongovan & Mr Prabhakar for xeroxing and Mr Kanakaraj & Mr Thiyagarajan for binding this thesis in a shortest time.

It is my pleasure to thank GRB collegues:
Prof J Ryan who introduced me to GRBs during ICNAPP in early 1994 at IIA. Drs. K Hurley & R Hudec for communicating IPN positions; Profs. D Hartmann, A Loeb, P Kumar, P Mészáros & Shri Kulkarni and Drs. M Kippen, F Vrba, J Rhoads for promptly replying to my e-messages and useful discussions; Profs. Tsvi Piran and Ramesh Narayan for inviting me to the Jerusalem Winter School and

supporting the trip; all the lecturers of the school for inspiring lectures and useful discussions; younger collegues: (Drs.) Rosalba, Andrew, Johana, Re'em, Rennan, Nicola and several others for joyful company/e-mail updates and useful discussions.

I also thank collegues from sister-organizations: the Grad. course instructors, Dr D Bhattacharya (GRB lecture course), Dr PN Bhatt (initial discussions and hospitality at TIFR), Dr. S Sinha (from ISRO), the Director of MRI (computing facilities during my personal visits), the Director of UPSO (telescope time and hospitality), Prof. A Kembhavi (IUCAA databases and computing facilities), Organizers of various schools and workshops at IUCAA for support and hospitality.

I acknowledge several collegues who contributed to my knowledge: earliest lessons in astronomy by Prof R Rajamohan and those by Dr AK Pati on CCDs and telescopes; Grad. courses by Profs. M Parthasarathy & Ram Sagar; useful discussions with Drs. KN Nagendra and Baba Verghese; Prof C. Sivaram and Dr AV Raveendran (for feedback on the manuscript); Profs. BP Das & J Murthy and Dr Rajat Roy-Chowdhuri; Profs. Vinod Krishan & R Srinivasan (the first people I met in IIA). Drs. Vasundhara, Sushma Mallik & Mrs Usha Shekhar (pleasant company).

I thank all the Grad. students: to mention a few, Dr R Srikanth for several useful discussions, help with thesis presentation along with Mr Pavan Chakraborthy and Dr Rajguru. Mr Sridharan & Mr S Subrahmaniam (discussions on IDL),Dr Angom Dilip, Ms Mangala Sharma, Ms Preeti Kharb, Drs. Aruna Goswami& Anju Sharma (lunch dates); Ms Latha, Ms Shalima and Ms Rajalakshmi (smiling neighbours), Mr Sonjoy Majumder & Mr Kathiravan (company at 5th floor); Mr N Naidu, Mr Ambazhagam and Mr PK Mahesh for helpful discussions.

Over the years life in IIA campus was fun, exposing me to a variety of people: A situation where no justice was made to reward my 3 years of services to the institute forced me to write the PhD entrance test and enroll myself in the PhD program of IIA. I acknowledge several collegues who supported me through panic and difficult time. I would also thank those who discouraged me - for, they made me more stubborn and firm to complete this thesis. I also thank people who tolerated my diverse states of mind.

Nature became the best refuge to forgive and forget many instances of repeated bitterness in academics: Mountains, as always, brought immense joy and so did the company of all mountaineer friends (Navita, Radhi, Faisal, Vatsa, Lacchi, Sampath, Raju, Asha & Sudhakar, Usha Ramiah, Mahesh, Badri & Amar) whom I thank profusely for their delicate humour, and warmth of friendship during, week-end rock climbing or mountain expeditions. I also thank all my instructors from the national mountaineering institutes for, the tough mountain training and their reassuring words made me strong and determined to complete this challenging project. I thank all my friends who always cheered me up - particularly, Madhu & David, Vishala, Aparna, Rajeev & Namrata.

Several distractions helped to catch up peaceful sleep after hours of scrolling on the computer terminal: Indian music & heaps of books - particularly the writtings by Chris Bonnington and J Grisham and the famous 'Harry Potters'! Thanks to Kanhaiya (Aerobics), Prasad and Kartik (Merlin Nature club) and Dr Amber Habib for training on bird identification- it gave me a wonderful opportunity to sneak into the forests and valleys around Kavalur observatory -alone and fearless - esp. after cloudy observing runs.

Special thanks to my cute little nephews: Shree, Atreya, Aditya and Hemanth who always kept me cheerful through their entertaining company & sweet conversations; several close relatives including Vaman, Sudhir, Sunda and Arun for their support and affection esp. during the period of grief.

This thesis is dedicated to special people in my life:

to the fond memory of my father

who motivated me into science and encouraged my studies through most difficult days

and who taught me to admire Nature's hostile phenomena;

to my loving mother

who built courage & strength in me and taught me to face hardship with dignity;

to my sisters

who shared all ups and downs all along the Ph D days

with their deep love and care;

and

to my S.O

who came into my life when I lost my father in the midst of Ph D and thereafter remained a source of inspiration along the long years of the PhD program with his patience and unwavering love!

Preface

"Tamsoma Jyothirgamaya"

Lead us from Darkness to Light – The vedas

Today, Gamma Ray Bursts (GRBs) are the most intriguing of observed phenomena in modern astronomy. This thesis entitled "An investigation into the nature of sources associated with gamma ray burst phenomenon" is a study carried out during a "turn over", period i.e, from "*darkness*", when very little was known about these spectacular, momentary, flashes of gamma-rays that outshine all the cosmic sources put together, to "*light*", when the afterglows began unraveling the mystery.

This thesis is devoted to the study of the optical counterparts of gamma ray bursts, based mainly on the observations we have carried out at the Vainu Bappu Observatory. Statistical studies to address some of the current problems in GRB astronomy viz., the clustering properties and luminosity functions of GRBs have also been carried out using the BATSE catalog. No theoretical modelling has been done, although the existing theories in observational cosmology have been used for the statistical analysis.

Broadly, 3 pieces of work have been put together here: First, optical observations of GRB afterglows, second, statistical analysis of the BATSE catalog to determine the luminosity functions of GRBs and application of the results to an observational study of IPN[3] GRBs. Third, a statistical analysis of GRB catalogs to study their clustering properties. However, principal goal of all studies is to investigate the cosmological nature of GRBs. A brief description of the research work carried out in each chapter is presented below.

We begin with an overview of Gamma Ray Bursts in Chapter 1. This is followed by a section describing the observing techniques, localization of GRBs and various dedicated instruments flown in the successive generations of satellites to observe the GRBs. We then summarize the global properties of GRBs viz., temporal, spectral and their spatial distribution. A brief review on the status of the current research both in observations and theory is presented in §1.4 of Chapter 1 also refering the reader to some of the excellent review articles.

Chapter 2 gives the details of optical observing techniques: the telescope & detector systems, data acquisition and analysis tools. The methods of image pre-processing, photometric data reductions and analysis for general purposes as well as specific to observations of GRB afterglows are presented. Our goal and the procedures we followed to observe the GRB afterglows are stated. About a dozen GRB follow-up observations -including the observations of X-ray counterparts of GRB 920622 - were attempted since 1997 though, with no success due to bad weather conditions at our observing site or due to the afterglow being fainter than our detection limits. Some times our efforts were rewarded with the detection of asteroids in these fields, 2 of which were new. These attempts are summarized in Chapter 2. Short sections are added in Chapter 2 on observations and analysis of GRB 010214 and GRB 010222, made during the writting of this thesis.

In Chapter 3 we discuss in detail the afterglow of GRB 000301c which was detected in our observations in March 2000. The details of observations, data reductions and analysis are presented, along with a fit to its light curve and an analysis to all the available data in the literature. We propose a two-burst model from the empirical fit to the light curve and perform some statistical tests to compare our results to that of a single-break fit by other authors. We discuss some of the theoretical models that could give rise to a bi-modal burst and color evolution which might test the validity of such a suggestion. Statistical tests have been performed to check for the chromatic behaviour in the light curve on the basis of B–R data. We conclude saying that better coverage on the light curve data is required to confirm and characterize the possible existence of a secondary burst.

Chapter 4 is devoted to a study of luminosity functions of GRBs. To fit the $\log \mathcal{N}$ - $\log \mathcal{F}$ curve theoretically, we assume a cosmological model with $\Omega_m = 0.3$, $\Omega_\lambda = 0.7$, $H_0 = 65\,\mathrm{Km/s/Mpc}$ that is most favoured by recent observations and various luminosity functions of galaxies (viz. Schecter, scale-free and log-normal) each with 'no-evolution' or with some of the evolutionary models consistent with star-formation histories. We check if the luminosity function obtained from the $\log \mathcal{N}$ - $\log \mathcal{F}$ relation for BATSE GRBs is consistent with the one determined for a sample of GRBs where redshift measurements are available from afterglow observations. In concluding, we find that if the evolution of GRBs follow the star-formation history of universe, then the only model which is marginally consistent with both approaches is Log-normal luminosity function.

Chapter 5 is a study of optical fields of GRBs localized by the third Inter-Planetary Network (IPN^3) before the afterglow era. After a brief review of the searches for the optical counterparts we present the details of the reductions and analysis of the data obtained from Vainu Bappu Observatory. Based on the results of our study of the luminosity function of GRBs in Chapter 4 we determine the most probable range of redshifts from which the IPN - GRB of a given flux could have come from. We also estimate the average redshifts of host galaxies for our magnitude-limited sample. We then discuss the various uncertainties in these measurements and whether the observed fields contain any potential candidates for the GRB hosts.

Chapter 6 is concerned with a study of the large scale structure of the universe implied by the clustering of GRB population. Having said that the cosmological origin of GRBs has been established from the recent afterglow studies, we address the question, whether GRBs show the clustering properties as expected of cosmological objects. The large scale structures observed today represent the conditions that existed in the early universe. If GRBs are associated with the underlying large scale structures in the universe, then they would serve to be the best objects to probe the early universe.

One of the widely used technique to measure the degree of clustering of objects in cosmology is 'Two-Point Correlation Function'. After giving a brief review on statistical studies in GRB physics we summarize various estimators for two-point correlation function available in the literature. For our analysis we use the estimator by Landy & Szalay (1993) which has the smallest variance in comparison to other estimators. Assuming the BATSE catalog to be a volume-limited sample upto $z \sim 1$ we determine the angular two-point correlation function of the GRBs in the 4th (current) BATSE catalog. We show that the two-point correlation function of the BATSE catalog is consistent with zero at nearly all angular scales of interest. Our analysis suggests that nearly 10^5 GRBs are needed to make a positive detection of the two-point angular correlation function at a typical angular scale of $\theta \approx 5°$.

In Chapter 7 the conlusions drawn from the study presented in this thesis are summarized and prospects for future work are discussed.

References are presented at the end of each chapter.

It **may be noted** that the results presented in Chapter 3 of this thesis have been published in Astrophysical Journal Letters (Bhargavi & Cowsik 2000a); the work in Chapter 4 and §5.5 carried out independently in collaboration with Dr S Sethi, has been accepted for publication is A & A (2001) and is included here in support of the thesis; the results of Chapter 6 were presented as a poster paper at 5th Huntsville GRB meeting held in October 1999 (Sethi, Bhargavi & Greiner 1999); The results of observations of GRB 010222 have been included in the paper Cowsik *et al.* submitted for publication in BASI (2001).

I acknowledge the extensive use of Digitized Sky Survey (DSS) images both at ESO and STSci home pages, astronomical catalogs at NASA's Astrophysics Data System (ADS), finding charts at USNO/Flagstaff home page, GRB catalogs at CGRO/BATSE science center, the GCN circular services by Dr Scott Barthelmy and the contributing authors, astro-ph preprint services of LANL, Jochen Greiner's home page on GRB afterglows, software packages: IRAF, STSDAS, IDL graphic package, Numerical recipes and several other internet based facilities in completing this thesis.

List of publications

- *Deep CCD imaging of GRB fields*, S. G. Bhargavi, R. Cowsik, A. K. Pati and Ram Sagar, 1998, BASI, 26, 597 1998.
- *On the clustering of GRBs on the sky*, Shiv Sethi, S. G. Bhargavi, and Jochen Greiner, 1999, in *Gamma Ray Bursts: 5th Huntsville Symposium, Huntsville, Alabama, Oct 1999*, (ed). Kippen, M. R. et al., AIP-526, page-107; astroph/0001006
- *Early observations of afterglow of GRB000301c*, S. G. Bhargavi & R. Cowsik, 2000, ApJL, 545, L77; astroph/0010308
- *Luminosity function of GRBs*, Shiv Sethi & S. G. Bhargavi, 2001, A & A (accepted for publication).
- *Optical Photometry of the GRB 010222 Afterglow*, R Cowsik *et al.*, 2001, astro-ph/0104363 (submitted to BASI).

GCN Circulars

http://gcn.gsfc.nasa.gov/gcn/gcn3: # 537, 554, 591, 630, 978, 1051

Contents

List of Tables

List of Figures

Chapter 1

Introduction

1.1 Overview

Gamma Ray Bursts (GRBs) are energetic, brief flashes of γ-radiation from the cosmos, observed by space borne radiation detectors. They were first discovered serendipitously in 1967 by American *VELA* satellites (Klebesadel *et al.* 1973) and there after were reported by various dedicated space-borne instruments designed to detect them. GRBs are detected, on an average once a day, randomly in time, at random directions on the sky and during the short burst interval appear to release energies much larger than that is seen in SuperNovae (SNe). The event is not known to repeat from the same location and one can not predict the time or position of occurence of the next burst in the sky. The nature of sources and physical mechanism producing this mysterious phenomenon were not understood until recently.

While a quest for their origin had been – and still remains – the principal goal of all studies in GRB astronomy, the large positional uncertainties due to the poor directional senisitivity of γ-ray detectors hindered the identification of their counterparts in other wavelengths and hence their association with any known class of astronomical objects. Most of the theoretical models before 90s supported Galactic origin of GRBs suggesting a compact object (NS/WD) as a source – a view accepted on the basis of the short time structures in the γ-ray light curves of GRBs that set an upper limit to the source size. Nevertheless, models supporting cosmological origin of GRBs were also proposed (Usov & Chibisov 1975; Van den Berg 1983; Goodman 1986; Paczyński 1986). The proceedings of GRB conferences (Paciesas & Fishman 1992, Fishman, Brainerd & Hurley 1994; henceforth 1hGRB and 2hGRB

respectively) give a clear idea of the status in early 90's.

The first major progress in the understanding of GRB physics came about after the launch of *Compton Gamma Ray Observatory (CGRO)* (see §1.2.2) in Apr 1991 and a subsequent increase in the database of GRBs. The Burst And Transient Source Experiment (BATSE) onboard CGRO has detected nearly 3000 bursts and these show an isotropic and inhomogeneous (paucity of fainter sources) distribution (Fishman & Meegan 1995) favouring a cosmological origin of GRBs. With these results although the Galactic disk models were abondoned, there remained 'extended halo models'. In extended halo models NS ejected from the Galaxy with high kick-velocities form an isotropic population of sources in the halo of our galaxy. Thus, a fresh debete on galactic halo v/s cosmological origin of GRBs (75th Anniversary Astronomical Debate 1995 : Paczyński(1995), Lamb(1995)) was opened up. A large number of models emerged in mid - 90's (For a list of over 100 models, see Nemiroff 1994 and references therein). It was then realized and discussed that only way to sort out the distance scale issue is by identifying the counterparts of GRBs in other wavelength bands. Procedures were developed to quickly localize the GRBs and to distribute these positions to an eager set of astronomers networked around the globe to make rapid follow-up observations in other wavelength bands. Gamma-ray burst Co-ordinate distribution Network (GCN) is an unique service that alerts the GRB astronomers over electronic-mail, web or beepers within a few minutes after the burst.

For about 30 years GRBs remained a puzzling phenomenon, despite the extensive studies in theory and observations. It is in early 1997 that the Italian-Dutch satellite *BeppoSAX* (see §1.2.2) made a break-through in GRB field with its capabilities to rapidly determine the GRB positions accurate to a few arcminutes and to immediately slew its X-ray detectors to follow-up the burst and then to refine the localizations to an accuracy of $2' - 3'$. This in turn led to the discovery of the first X-ray counterpart to GRB 970228 (Costa *et al.* 1997). In the meanwhile the rapid distribution of the accurate position of GRB 970228 enabled follow-up observations in optical wavelength bands and the first ever Optical Transient (OT) was discovered (Van Paradijis *et al.* 1997). Follow-up observations were made at 4.2 m William Herschel Telescope (WHT) 21 hours as well as 8 days after the burst. When the images of two epochs were compared a source was found to fade by 1.5 magnitude. The source position was consistent with the X-ray counterpart and its fading be-

haviour confirmed it to be the optical counterpart of GRB 970228. After the OT became faint for ground-based observations it was observed with *Hubble Space Telescope (HST)* which showed that the OT was hosted by a faint galaxy (Sahu *et al.* 1997) at $z \sim 1$ thus establishing the cosmological origin of GRB 970228. The fading counterparts of GRBs in other wavelength bands are now popularly called **GRB afterglows**. Fig 2.6 demonstrates the fading behaviour of a GRB afterglow in case of GRB 010222 observed from Vainu Bappu Telescope (VBT) of Indian Institute of Astrophysics located at Kavalur, India. In the case of GRB 970508, the second OT, the redshift was measured to be (Metzger *et al.* 1997) $z \geq 0.835$. This confirmed its cosmological origin. To date about 25 optical and 15 radio counterparts have been detected. The typical magnitudes of host galaxies are R $\sim$ 26. In about 15 cases redshifts have been measured by optical spectroscopy; the redshifts cover a range from $z = 0.4 - 3.42$. In §1.4 we summarize the properties of several interesting afterglows. For a comprehensive list of references on afterglow observations see Greiner's home-page (Greiner 2001).

The afterglow observations and analysis have contributed to a great deal in understanding the physical processes associated with the GRB phenomenon and confirming the generic **fireball** models (see §1.4.2 for more details) initially proposed by Paczyński and Rhoads (1993), Katz (1994a, 1994b), Shemi & Piran (1990) and Mészáros & Rees (1997). The observed diversity in the light curves of afterglows have been explained by several authors (Mészáros, Rees & Weijers 1998; Sari, Piran & Narayan 1998; henceforth SPN 98) through more complicated fireball models which include non-isotropic expansion, non-uniform distribution of external medium and so on. The observed γ-ray fluences and measured redshifts imply that GRBs radiate prodigious amounts of energy ranging from 10^{52-54} erg in gamma rays within a short time, making them the most energetic events in the universe. Afterglow observations have shown that in some GRBs the energy is emitted into collimated jets and in such cases the total energies would be reduced by a factor $\approx \theta^2/2$ (typically few hundreds). The most popular models for sources of GRBs involve a BH and an accretion disk formed either through core collapse of a massive star in a star-forming region (Paczyński 1998; MacFadyen & Woosley 1999) or a merging NS–NS/NS–BH binary (Paczyński 1986; Eichler *et al.* 1989; Narayan 1992). Reviews by Kulkarni(2000) on afterglow observations, by Piran (1999) on theories and several papers in the Proceedings of Huntsville symposia (see end of this Chapter) give a clear

picture of current status of GRB research.

While the afterglow theories and observations are progressing on one hand, efforts have also been made towards the understanding of several other issues in cosmology, of these the most important are: clustering properties & Luminosity Function (LF) of GRBs. These aspects are reviewed in Chapters 4 and 6.

In the next section §1.2 we summarize the observing techniques in γ-ray astronomy, localizations of GRBs, followed by short notes on various GRB missions used in detecting GRBs. In §1.3 we describe the temporal, spectral and spatial properties of GRBs. Section §1.4 is a review on observations and models of GRB afterglows. Section §1.5 gives an outline of the thesis.

1.2 GRB Observations in γ-Ray Domain

1.2.1 Gamma Ray Detectors

In the following, some basic aspects of γ-ray detectors is presented. More details may be found in Ramana Moorthy & Wolfendale (1993) and Hillier (1984).

Gamma radiation is attenuated during propagation through the earth's atmosphere due to phtoelectric effect at < 60 keV, Compton scattering at energies between keV to few MeV and pair production ($\gamma \longrightarrow e^+e^-$) above few MeV. Therefore γ-ray detectors have to be flown in the space-crafts. Energy loss mechanisms are different at different energies. Depending upon the scientific goal the detectors are suitably chosen and the design of the detectors depends on the interaction process that is dominant in a given energy range. The γ-ray detectors have to be accompanied by some shielding material to attenuate the background radiation. One of the contribution to background radiation is the γ-flux produced as a result of interaction of cosmic ray particles in interstellar space. Shielding is generally achieved by using a second detector in anticoincidence with the central main detector.

The γ-ray telescopes operating in the low energy regime, use scintillaton counters or solid state detectors. A scintillator converts the fraction of energy lost by the charged particle into light and the photo-multiplier tube coupled to the detector converts the light signal to electric signal. For example, inorganic materials NaI and CsI have high cross section for photoelectric effect, but they are costly. The plastics loaded with organic compounds are less expensive. Generally a collimator is used

in front of the main detector to sense the direction of photons.

The angle between the secondary photon & electron in a compton scattering becomes narrower as the energy of primary photon increases. At MeV energy range, the direction of secondary particle can be used to define the direction of primary photon. The telescope based on this principle is called **Compton telescope**. The COMPTEL instrument (see next section) onboard *CGRO* was based on this principle.

At E > few MeV, pair production ($\gamma \longrightarrow e^+ + e^-$) becomes the most important interaction mechanism. The direction of motion of secondary particle is more closely aligned to that of primary photon and enables determination of arrival direction of γ-rays. Spark chambers are generally used in this energy region. The EGRET (see next section) instrument onboard *CGRO* detected γ-rays through pair-production.

1.2.2 Inter-Planetary Network (IPN) & GRB Localization

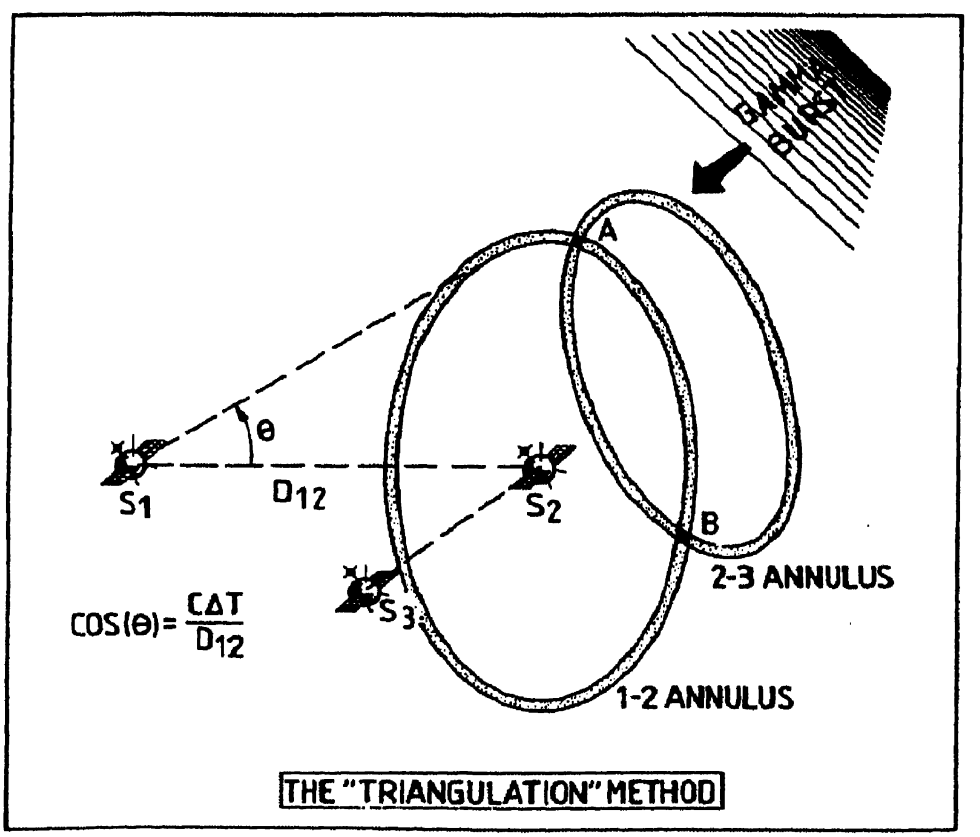

Figure 1.1: Triangulation Method. Courtesy: K Hurley

IPN is a group of satellites carrying GRB detectors that use **Triangulation** technique to localize the GRBs. Fig 1.1 illustrates the principle of triangulation method. Let S_1, S_2, S_3 be space-crafts seperated by distances D_{12}, D_{23} and D_{13}. Each pair of satellites gives an annulus of possible arrival direction whose center is defined by the vector joining the 2 space-crafts and whose radius θ depends upon the difference in arrival time divided by the distance between the 2 space-crafts. If D_{12} is the distance between the two detectors and ΔT is the time delay with which the signal arrives at the detectors then, the arrival direction θ is given by

$$cos\theta = \frac{c \times \Delta T}{D_{12}} \tag{1.1}$$

The location accuracy is better when the detectors are farther apart. If another detector has recorded the same burst, then another annulus intersecting the first one is obtained. Then the source is assumed to be within the regions of intersection of two annuli.

Successive generation of satellites used for triangulation are referred to as IPN^1, IPN^2 and so on. Third inter-planetary network began operating in 1990 with the launch of *Ulysses* space-craft. It carried both hard X-ray detectors (15–150 keV) and soft X-ray detectors (5–20 keV) to study the Solar flares and to observe GRBs(Hurley 1992). The *(CGRO)*, *Pioneer Venus Orbiter (PVO)*, *Mars Observer*, and *NEAR* were part of IPN^3 while they were operating. At present the 4th IPN uses *Ulysses* along with *RXTE*, *WIND*, *SAX*,*HETE-2* and Indian sl Stretched Rohini Satellite Series (SROSS)-C2 for triangulation. The timescale for distribution of IPN localizations varies from few hours to 2 days. See *http://ssl.berkeley.edu/ipn3/index.html* for further details.

1.2.3 Recent Space-borne Telescopes

The *(CGRO)* was designed to perform an all-sky survey of γ-ray sources in broad energy range of 15 keV–30 GeV with better sensitivity than the previous missions. It was launched in April 1991 and was de-orbited in June 2000. *CGRO* carried 4 scientific instruments: Burst and Transient Source Experiment (BATSE), Compton Telescope (COMPTEL), Energetic Gamma Ray Experiment Telescope (EGRET) and Oriented Scintillation Spectroscopy Experiment (OSSE). For further details see *http://cossc.gsfc.nasa.gov/*.

The BATSE consisted of 8 identical modules placed at 8 corners of the space-craft. Each module had a Large Area Detector (LAD), a scintillator of NaI crystal sensitive to the energy range 30 keV–1.9 MeV, a Spectroscopy Detector (SD) to operate in the range 15 keV–110 MeV. When BATSE detected GRBs it sent signals to other instruments to switch them to burst data collection mode. It also observed γ-rays from pulsars, black-holes and other objects. BATSE provided single space-craft detemination of burst localizations. Each burst was viewed by atleast 4 LADs. Direction of GRBs was determined by comparing the count rate in each of the 4 detectors. The count rate is a function of cosine of the angle θ between the detector normal and burst source. Typically uncertainties in localizations were $\sim 4^{\circ}$ in radius (statistical error). The current catalog contains 2702 burst events.

COMPTEL consisted of two detector arrays: upper liquid scintillator and a lower NaI crystal. Gamma rays are detected by 2 successive interactions: the incident γ-ray first gets compton scattered in the upper detector and then gets totally absorbed in the lower. The locations of the interactions and energy losses in both detectors are measured. Energy loss measurements combined with trajectory of photon are used to construct the liklihood map of probable source direction. In its burst mode COMPTEL detected γ-ray bursts in the range 100 keV–10 MeV. About 30 bursts are available in comptel catalog.

EGRET covered the energy range from 20 MeV–30 GeV and had very low background. It detected γ-rays through pair-production mechanism. In its burst mode it detected GRBs in the NaI crystal detector, where energy spectra could be measured in 0.6–140 MeV range.

OSSE was designed to observe the astrophysical sources (mostly pulsars) in the 0.1–10 MeV range.

The **Rossi X-ray Timing Explorer (RXTE)** is an X-ray satellite that observes variabilities in X-ray intensities on microsecond time scale since Dec 1995. It carries three instruments: The Proportional Counter Array (PCA) at low energy, the High Energy X-ray Timing Explorer (HEXTE) and the All-Sky Monitor (ASM). ASM scans about 80% of the sky per each orbit. The Experiment Data System (EDS) processes the data onboard from PCA and ASM. The HEXTE consists of two clusters of of 4 NaI/CsI phoswich scintillation detectors, which are sensitive to X-rays from 15 to 250 keV. PCA is an array of five proportional counters with a total collecting area of 6500 cm^2 operating between 2–60 keV, with a time resolution of 1

microsecond. The ASM operates between 2–12 keV range. Besides monitoring the X-ray sky, it also senses any transient phenomenon. It consists of three Scanning Shadow Cameras (SSCs) mounted on a rotating assembly. Each Camera has a field of view (FWHM) of $6° \times 90°$ and a position sensitive proportional counter. (for more details see *http://heasarc.gsfc.nasa.gov/xte/*)

BeppoSAX : SAX (Satellite italiano per Astronomia X) also known as *BeppoSAX* in honour of Giuseppe (Beppo) Occhialini is a joint Italian-Dutch satellite and was launched in April 1996 (Boell et al. 1996). It covers an energy range of 0.1–300 keV and is suitable for the study of spectral and temporal behaviour of weak and variable sources. The payload has Narrow Field Instrument (NFI) and Wide Field Camera (WFC).

NFI has 3 units of Medium Energy Concentrator Spectrometer (MECS) operating in 1–10 keV energy range (Conti *et al.* 1994) and a single unit of Low Energy Concentrator Spectrometer (LECS) operating in 0.1–10 keV range (Parmar *et al.* 1996). These are grazing incidence telescopes with position sensitive gas scintillation proportional counters in their focal planes. It also contains a collimated High Pressure Gas Scintillation Proportional counter (HPGSPC) operating in 4–120 keV (Manzo *et al.* 1996) and a collimated Phoswich Detector System (PDS) operating in 15–300 keV range (Frontera *et al.* 1996); Gamma Ray Burst Monitor (GRBM) is a part of PDS and operates between 40–700 keV.

Perpendicular to the NFIs there are two WFCs (coded mask proportional counters) operating in the range 2–30 keV (Jager *et al.* 1996), each with a FOV of $20° \times 20°$ with a resolution of $5'$. The method followed to localize the GRBs by BeppoSAX is based on the comparison between the relative intensities registered by the 4 GRBM detectors and expected values determined from the detector response functions (Preger *et al.* 1996). The error boxes are accurate to $< 3'$.

HETE-2

The *High Energy Transient Explorer (HETE)*, the most recent multi-wavelength mission is designed to observe GRBs and to distribute the GRB co-ordinates to the astronomical community in real-time for immediate follow-up observations. *HETE-2* was launched on 9 Oct 2000. It consists of one gamma-ray detector (6–400 keV), a wide-field, medium-energy X-ray imaging system (2–25 keV), a wide-field, low-energy X-ray imaging system (0.5–10 keV) and a set of optical imaging cameras. The

X-ray detectors are coded-aperture imagers, and can localize GRBs to an accuracy of $10' - 10''$. Sophisticated on-board processing software allows the location to be calculated on board in real time, and ground based post-burst analyses will provide refined localizations. *HETE* will always point atleast 120° from Sun and therefore convenient for rapid optical follow-up. About 50 GRBs/yr may be localized by *HETE-2*. For more details see http://space.mit.edu.

Swift

Swift is a multi-wavelength mission to catch the GRBs on the fly and is named after the birds called swift that feeds on flying. *Swift* is expected to be launched in year 2003 and would carry three instruments: Burst Alert Telescope (BAT), X-Ray telescope (XRT), and Ultra-Voilet/Optical telescope (UVOT). BAT is a coded aperture instrument with a wide FOV (2 str) designed to operate in 10–150 keV energy range. It will observe and locate one GRB/day with an accuracy of 1–4 arcmin and would relay the positions to ground within 15 sec of a burst. *Swift* will then point XRT and UVOT at the initial burst position to study the afterglow. XRT and UVOT will produce arcsecond positions and multi-wavelength light curves as well as redshifts to GRB afterglows. These data would be useful in classifying the GRBs, locating the afterglow w.r.t. host galaxy, in probing the GRB environments and studying the early universe.

Further details may be obtained at sl http://swift.sonoma.edu.

1.3 Temporal, Spectral and Spatial Properties of GRBs

Temporal Properties

Light curve or time history of a burst is characterized by a rapid rise followed by decay. The light curves show remarkable diversity varying from smooth, single peaked, sharp and spiky to complex, multi-peaked structures (see *http://www.batse.msfc.nasa.gov* for some examples). Rapid fluctuations seen in the light curves provide limits to the size of the emitting region; typical variations of ~ 5 millisecond imply a source size of < 1500 km. Periodicities have not been seen in BATSE GRB light curves. Periodicities if found, may be attributed to the rotation of the source and to put an upper limit to the density of the source object. For instance, the 5ms periodicity

seen in GRB790325 -which is now classified as SGR - implies a density corresponding to a NS.

Duration of a burst event is the total time from the onset of burst until the time when the detector records counts just above the noise level. For instance, in BATSE the burst duration is defined by parameters T_{90} & T_{50}. T_{90} is the time interval during which 90% of the total observed counts have been detected, i.e, the time during which integrated counts increase from 5% to 95% of total counts. The durations of BATSE bursts shows a bimodal distribution with short (< 2 s) events peaking at ~ 0.1 s and long bursts (> 2 s) peaking at around 40 s (see Fishman & Meegan 1995).

Hardness Ratio is the the ratio of the fluence in the channel with higher energy band (100-300 keV) to the fluence in the channel with lower energy band (50-100 keV). Distribution of duration v/s hardness ratio for BATSE bursts shows two distinct groups: short/hard and long/soft events (see Kulkarni *et al.* 2000).

Fluence is the total energy integrated over the burst duration and is expressed in ergs/s/cm^2.

Spectral Properties

The observed spectra of GRBs are invariably non-thermal in the 50–300 keV range with a flattening at lower energies so that only very few bursts are seen at ~ 10 keV in prompt emission. The low energy part of the spectrum between 50 to 300 keV can be fit with a power-law of the form

$$F(E)dE = E^{\alpha}dE \tag{1.2}$$

with observed values of α lying in the range -3.5 to +0.5 with a broad peak around -1.8 to -2. The flat spectra with slopes $-1/2 < \alpha < 1/3$ at the lowest energies suggests that the radiation could be due to the synchrotron process by relativistic electrons accelerated in a shock. Such a power-law steepens at high energies to a form fit by Band *et al.* (1993) by the function

$$\begin{aligned} F(E) &= N_0 E^{\alpha} e^{-E/E_0} \qquad \text{for } E \leq H \text{ and} \\ F(E) &= N_0 \{(\alpha-\beta)E_0\}^{(\alpha-\beta)}\, e^{(\beta-\alpha)} E^{\beta} \qquad \text{for } E \geq H, \\ \text{with} \quad H &= (\alpha-\beta)E_0 \end{aligned} \tag{1.3}$$

In this form the luminosity peaks at $E_p = \frac{(\alpha+2)}{(\alpha-\beta)}H$ and the distributions in H is shown in Fig. 3 (Band *et al.* 1993, Cohen *et al.* 1998).

Distribution on the sky

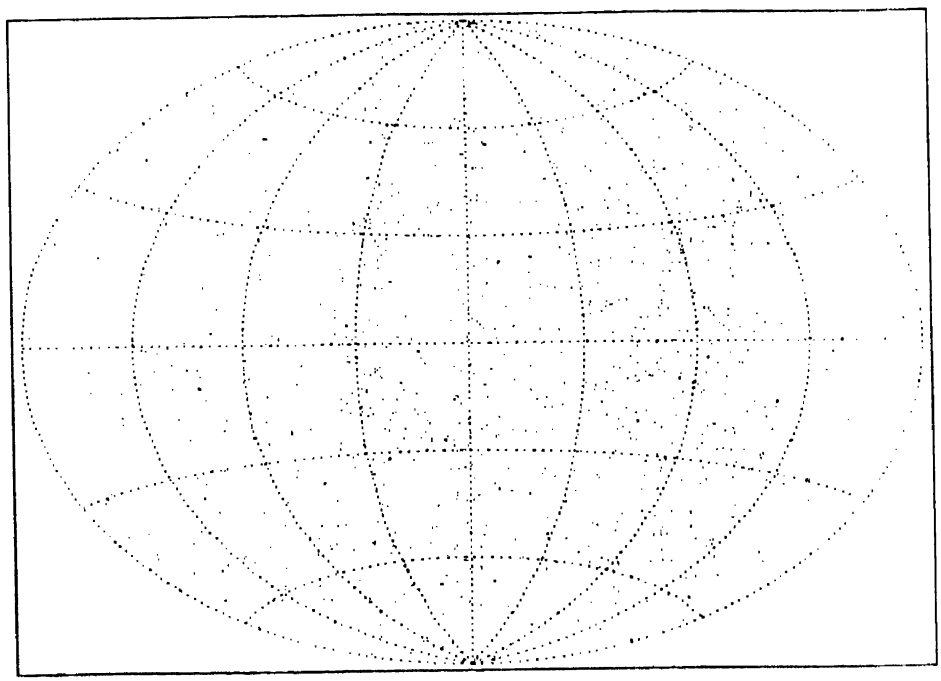

Figure 1.2: Distribution of 2704 BATSE GRBs on the sky.

Fig 1.2 shows the distribution of 2704 BATSE GRBs on the sky. The distribution is isotropic with no concentration of bursts either at the Galactic center or in the plane. Two parameters are used to quantify the degree of isotropy: **Galactic dipole moment** is given by,

$$\frac{1}{N}(\sum_{n=1}^{n=N} \cos\theta) \tag{1.4}$$

Here, θ is the angle between GRB source and galactic center; N is the total number of bursts. Then $\langle \cos\theta \rangle = 0$ for isotropic distribution. The **quadrupole moment** of the distribution is given by,

$$QM = \frac{1}{N} \times \sin^2 |b| - 1/3 \tag{1.5}$$

where b = galactic latitude. These quantities for BATSE bursts have been reported (Fishman & Meegan 1995) to be:

$$\begin{aligned} \langle \cos\phi \rangle &= 0.017 \pm 0.018 \\ \langle \sin^2 b - 1/3 \rangle &= -0.003 \pm 0.009 \end{aligned} \tag{1.6}$$

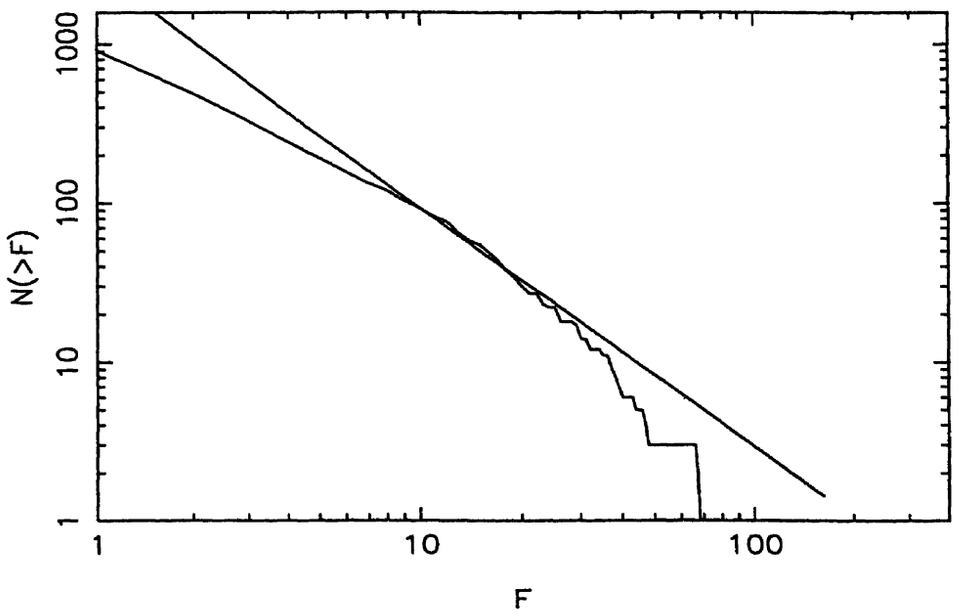

Figure 1.3: $\mathcal{N}$–F relation for BATSE GRBs.

Distribution in Space (radial)

In Fig. 1.3 we show the flux distribution of current (4B) BATSE catalog containing 2093 GRBs recorded between 19 Apr 1991 to 10 July 2000. On the x-axis are plotted log of peak fluxes (for energy range 50–300 keV) on 1024 millisecond time scale in units of photons/cm^2/s. The number of bursts above a certain flux level ($N > F$) is plotted on the y-axis. If GRBs are assumed to be standard candles then, in a flat euclidean space, the flux from a burst of luminosity L, located at distance r is given by:

$$f = \frac{L}{4\pi r^2}\,; \qquad r = (\frac{L}{4\pi f})^{0.5} \tag{1.7}$$

If GRBs are uniformly distributed in space with mean density n then number of GRBs $N(> F)$ brighter than some flux limit F is given by:

$$N(> F) = nV \tag{1.8}$$

where, V is the volume of a space out to a distnace r and $V \propto r^3$.

$$N(> F) \propto nr^3 \qquad \text{hence } N(> F) \propto f^{-3/2} \tag{1.9}$$

Fig 1.3 shows that N v/s F follows -3/2 power-law at the brighter end as expected for a homogeneous sample of sources but flattens out at the fainter end indicating that there is a deficiency of weaker bursts. We discuss $\mathcal{N}$–F distribution in greater detail in Chapter 4.

V/V_{max} test

Alernatively, a statistical test called V/V_{max} is also used to determine the brightness distribution of a population of sources. Assuming, all GRBs to have same intrinsic luminosity, the brighter sources would be nearer and the fainter ones would be far away. Let the distance of a faintest burst - detected just above the background level be R_{max} and the corresponding count rate be $C_{min} = C_{threshold}$. The spherical volume defined by this distance R_{max} is V_{max} . Similarly, for a nearest burst distance can be as close as R, and the volume of the corresponding sphere with radius R is V and the count rate is maximum (C_{max}). The quantity $V/V_{max} \propto R^3/R^3_{max}$ and varies from 0 to 1. (i.e, for a bright burst R can be as close as zero and then $V/V_{max} = 0$; for a faint burst $R \sim R_{max}$; $V/V_{max} = R_{max}/R_{max} = 1$). In BATSE, V/V_{max} is given by $(C_{max}/C_{threshold})^{3/2}$ and is found to be 0.32 which implies that GRBs are not homogeneously distributed in space.

1.4 Current Status of GRB Research

1.4.1 Afterglow Observations and Models

Afterglow is the slow fading radiation associated with a GRB that can be seen for a longer period at longer wavelength bands. Afterglow observations of GRBs have established the cosmological origin of GRBs (particularly that of the long duration bursts).

- GRBs are hosted by distant, faint galaxies (typically $R \sim 26$).
- The total amount of energies estimated in γ-rays from the measured redshifts and observed fluences, assuming isotropic emission are in the range $10^{51} - 10^{54}$ erg.
- GRBs are not standard candles.
- The afterglow light curves decay as a power-law; $F_\nu(t) \propto t^{-\alpha}$, where the slope $\alpha \sim 1.0 - 2.0$; In some cases afterglows displayed a single power-law, while in about 7 cases the slope of the light curve changed from flatter to a steeper one, the break occuring at few days after the burst. In some cases the late-time curve flattened perhaps indicating the presence of an underlying host galaxy.
- The afterglow spectrum is a power-law $F_\nu \propto \nu^\beta$, typical value of $\beta \sim -0.7$ for a broad range of frequencies.
- The power-law spectrum indicates that the emission mechanism is synchrotron arising from relativistic electrons.

Fireball Model

Fireball model is the most popularly accepted model of GRB afterglows. The generic model of the nature of afterglows at longer wavelengths was predicted (Mészáros & Rees 1997) much in advance of the actual observations. The subsequent observations were largely in agreement with the theory. In this model the explosion triggered by an 'unknown' central source results in a relativistic blast-wave that expands into the ISM. As the ejecta encounters with the ambient gas, it produces two shocks: a short-lived reverse shock (which can give a prompt flash in real time) and a long-lived forward shock. Both the gamma-ray (what we call a GRB) and the afterglow

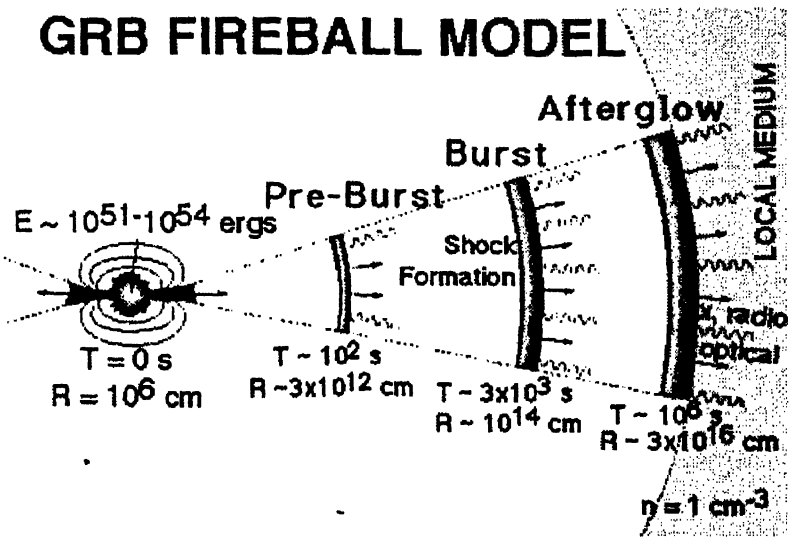

Figure 1.4: Fireball Model. Courtsey: B. J. Teegarden.

arise from the forward shock. The gamma ray emission comes from shocks occuring within the wind (internal shocks), while the afterglow is produced by the interaction of blast wave with ISM (external shocks). A schematic diagram of the fireball model is shown in Fig 1.4.

The relativistic expansion is required to overcome the **"compactness problem"** which is described below:

As mentioned in §1.1, the γ-ray fluences imply total energies of $\sim 10^{52-54}$ erg at cosmological distances when isotropic emission is assumed. such energies are $> 10^{19} L_{\odot}$ and are in excess of Eddington luminonity[1] limit for any object at equillibrium (Paczyński & Rhoads 1993). Therefore radiation pressure must drive an ultra-relativistic wind. This conclusion is valid even if the radiation is beamed into a solid angle.

The temporal properties of GRBs imply a compact emitting region (see §1.3). When a large amount of energy is suddenly deposited into a compact region it is referred to as **fireball**. Here, the energy densities are of of the order of 10^{12} erg cm^{-3} and optical

[1] Eddington luminosity is the maximum luminosity which a spherically symetric source of mass 'M' can emit in a steady state. It is determined by balancing inward force of gravity v/s outward radiation pressure and is given by $L_E = 1.3 \times M/M_{\odot}\,\mathrm{erg\,s^{-1}}$.

depths [2] for the process $\gamma\gamma \longrightarrow e^+e^-$ are of the order of $\sim 10^{10}$. With high optical depth the conditions can be treated close to thermodynamic equillibrium (LTE) which means that γ-ray spectrum should be close to that of a black-body [3] with $F_\nu \propto \nu^2$. However, the observed spectrum is non-thermal and broad (sometimes extends even to GeV range) with large fraction of high energy photons. There is no evidence for pair-creation cut-off seen at 512 keV. This clearly indicates that the sources must be optically thin. Therefore to reconcile the observed γ-ray spectrum it has been suggested that the γ-rays detected in a GRB event do not come from the site of explosion, but are generated later on at a larger distance when the fireball becomes optically thin.

In a relativistically expanding fireball the Lorentz factor is of the order of few hundreds. The size of the expanding sphere characterized by a Lorentz factor γ, appears larger by a factor γ^2 (i.e, $R = \gamma^2 \times c\Delta t$), thus reducing the photon densities (L/R^3) by a factor of γ^6. For a typical variability of t = 10ms, the shock radius $R = c\Delta t\gamma^2 \sim 10^{13}$ cm. Shocks convert the KE to internal energy of accelerated particles, which in turn emit the γ-rays. At this stage the system is optically thin and the γ-rays can easily escape.

[2] Optical depth :

$\tau \sim 1.7 \times 10^{-37} D^2 l/A$ where $A = l^2$; $l = c\delta t$ is the thickness of emitting region; and δt is the observed variability in the burst light curve. (Fenimore 1992).

[3] $F_\nu = (2h\nu^2/c^3) \times e^{-h\nu/kT}$

Afterglow mechanism: Synchrotron emission

The emission process for both the GRB and the afterglow is synchrotron. The emitting electrons have a power-law energy distribution given by, $N(E) \propto E^{-p}$.

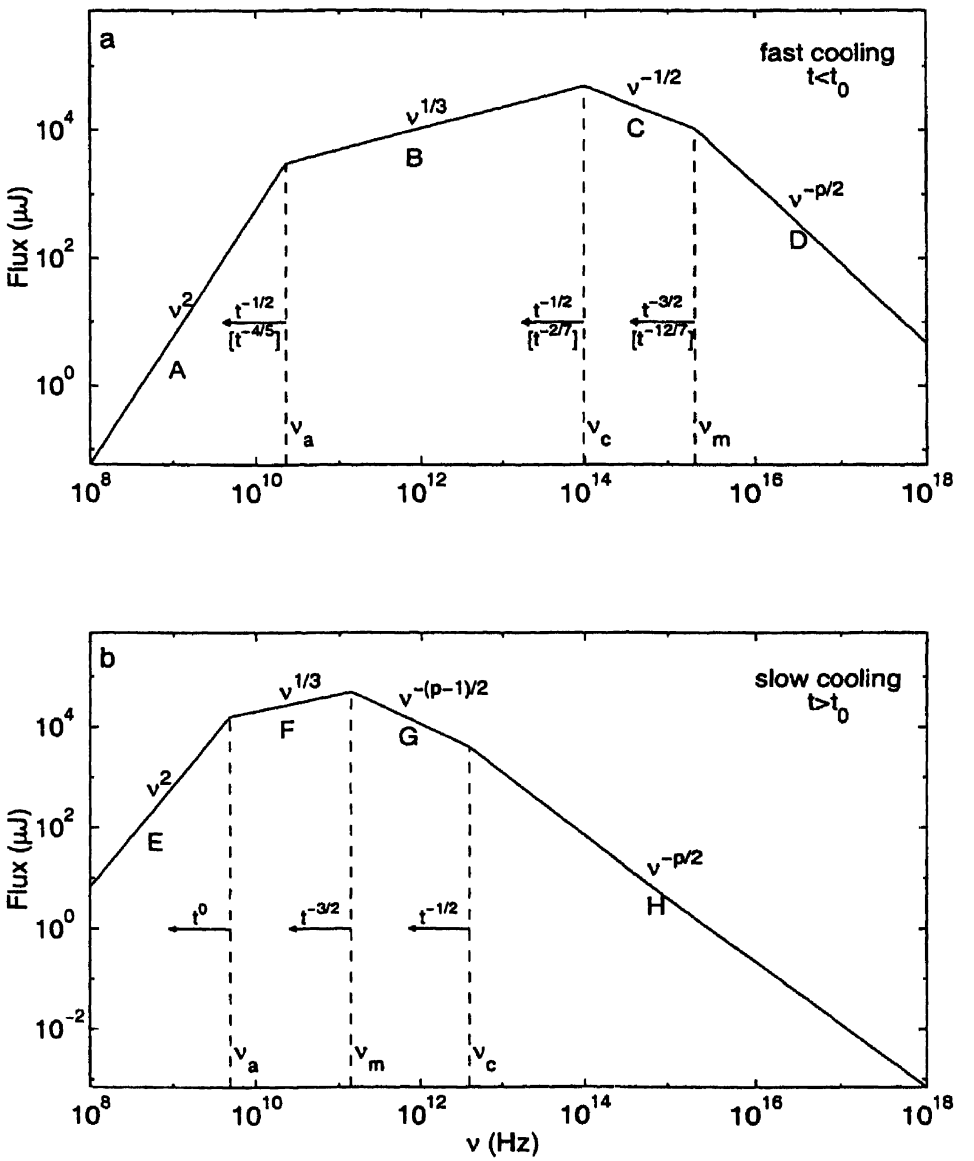

Figure 1.5: Synchrotron spectrum of a relativistic shock with a power-law distribution of electrons. (a) The case of fast cooling, which is expected at early times ($t < t_0$) in a γ-ray burst afterglow. The spectrum consists of four segments, identified as A, B, C, D. Self-absorption is important below ν_a. The frequencies, ν_m, ν_c, ν_a, decrease with time as indicated; the scalings above the arrows correspond to an adiabatic evolution, and the scalings below, in square brackets, to a fully radiative evolution. (b) The case of slow cooling, which is expected at late times ($t > t_0$). The evolution is always adiabatic. The four segments are identified as E, F, G, H (Reproduced with kind permission from authors: Sari, Piran & Narayan 1998).

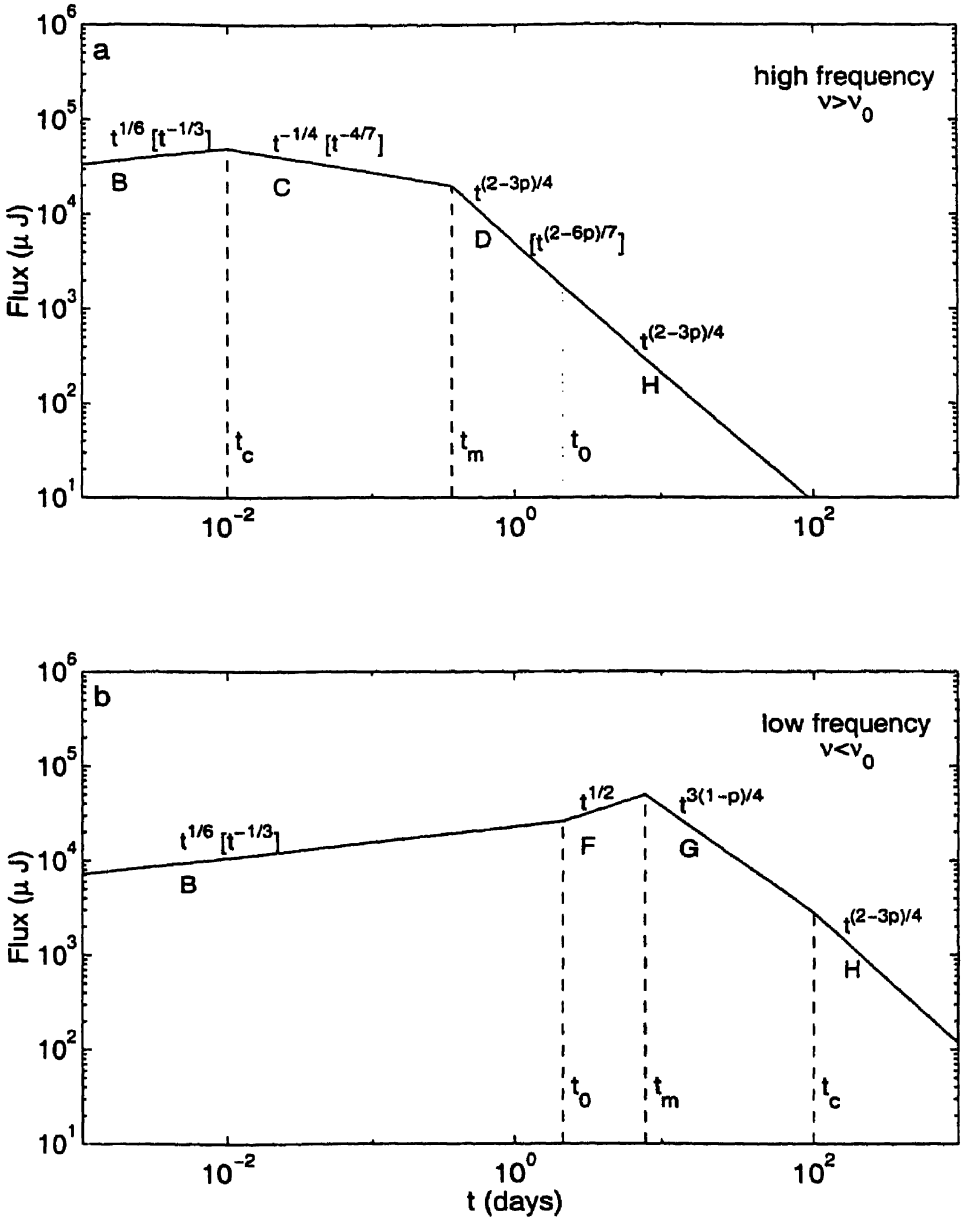

Figure 1.6: Light curve due to synchrotron radiation from a spherical relativistic shock, ignoring the effect of self-absorption. (a) The high frequency case ($\nu > \nu_0$). The light curve has four segments, separated by the critical times, t_c, t_m, t_0. The labels, B, C, D, H, indicate the correspondence with spectral segments in Fig. 1.5. The observed flux varies with time as indicated; the scalings within square brackets are for radiative evolution (which is restricted to $t < t_0$) and the other scalings are for adiabatic evolution. (b) The low frequency case ($\nu < \nu_0$) (Reproduced with kind permission from authors: Sari, Piran & Narayan 1998).

This distribution has a cut-off at low energies which is determined from n_e - the electron density and e_e - the elctron energy. $E_{min} = e_e/(p-2)n_e$. Since largest

number of electrons are available at E_{min}, it is also called the characterisitic electron energy. Electrons with this energy have synchrotron frequency ν_m. The power-law indices, ($F_\nu \propto t^{-\alpha}\nu^{-\beta}$) α and β are both functions of 'p' - the power-law index of electron energy distribution.

Fig 1.5 shows theoretical afterglow spectrum (SPN 98) which is a broken power-law with 4 segments:
Between each 'break' point the radiation spectrum is a power-law; and exponent of power-law changes at each break point. The break frequencies are:

1 . ν_m : The characteristic frequency of emission of lowest energy electrons.

2 . ν_{sa} : The frequency at which the emitting plasma becomes optically thick to synchrotron radiation.

3 . ν_c : The cooling frequency which is the characteristic frequency of emission for an electron whose cooling time = age of the GRB remnant.

GRB afterglow models predict the evolution of these break frequencies as a function of time. The light curve can be predicted from the evolution of break points combined with the spectrum. Fig 1.6 shows the light curves due to synchrotron emission for spherical case (SPN 98). Wijers & Galama (1999) have treated GRB 970508 and GRB 971214 for spherical case and the jet-like case is presented by Rhoads (1999).

1.4.2 Survey of Afterglow Observations

In Table 1.1 we have listed all those GRBs with optical afterglows along with their redshifts and host magnitudes (where ever available). The table does not include those GRBs with X-ray and/or radio afterglow alone. As of June 2001, we have :

- 24 Optical transients: (XOR(10)+XO(4)+OR(4)+O(6)=24);
  10 of them had no XA; 10 of them had no RA.
- 17 Radio afterglows (XOR(10)+OR(4)+XR(3)=17);
  3 of them had no OT. (990506, 981226, 970828)
- 17 redshift measurements -including GRB 980425 SN-GRB.

Here, X, O and R refer to the X-ray, optical and radio afterglows respectively, following the notations by Greiner (2001) & Frail (1999a).

In the following, we summarize the properties of some of the interesting cases. We also warn the reader that at this stage strict classification of afterglows is difficult, although we have tried to group them.

1. Afterglows with no OT

From Table 1.1 we see that three of the GRBs do not have optical counterparts, although their X-ray and radio afterglows were detected. The non-detection of radio counterparts in some cases is due to lack of sensitivity Frail (1999a). Various factors viz., late notification, large error boxes, proximity to Sun/Moon, deep south or low galactic latitude contribute to the non-detections. However, in case of GRB 970828, GRB 981226 and GRB 990506 none of these were the reasons and extensive efforts were made to search for the optical counterparts. Extinction by dust in the host galaxy or absorption in the intargalactic medium along the line of sight seems to be the more likely explanation (Kulkarni *et al.* 2000). This would support the failed SN (Woosley 1993) and the 'hypernova' model (Paczyński 1998) in which GRBs come from high density, dusty, regions of active star-formation.

GRB 970828 revealed no OT down to a limiting magnitude of $R = 23.8$ despite the observations carried out starting from 4 hr–8 days after the burst Groot *et al.*

(1998a). Since X-ray and radio afterglow were detected in this case, the absence of OT has been thought to be due to optical extinction.

GRB 981226, an X-ray rich burst displayed no OT down to the limit $R = 23$. Several groups (Galama *et al.* 1998b, Castro-Tirado *et al.* 1998, Wozniak 1998, Lindgren *et al.* 1999) proposed candidates for optical counterparts but none got confirmed. A variable radio counterpart was detected (Frail *et al.* 1999b) inside the NFI error circle in 8.46 GHz (VLA). The interesting feature of this GRB is that it had a short-lived radio afterglow, unlike the previous radio afterglows which rised to peak flux a week after the burst. The observations were fitted by a simple spherical blast wave model, with a electron power-law index $p = 3.7$ which was found to be larger than the typical value of 2.4. The jet model fitted well, with the parameters similar to GRB 990510 (Harrison *et al.* 1999). The radio observations were explained using spherical, jet or circumstellar models (Frail *et al.* 1999b) without requiring extinction (within the host galaxy) to explain the absence of optical afterglow. The position of radio afterglow was imaged in June 1999 with LRIS/Keck II telescope to search for the host galaxy and was identified. The magnitude of the host galaxy was $R = 24.85 \pm .06$

No optical counterpart was detected in case of **GRB 990506** despite the extensive search down to the limit $R = 23.5$. The radio afterglow was detected within 1.5 day which rapidly faded after 5 days. The host galaxy was detected $\sim$ 36 days after the burst in the images acquired by Keck-II telescope which appeared to be a pair of merging galaxies with $R = 24.4 \pm 0.3$, $R = 24.0 \pm 0.3$ (Taylor *et al.* 2000).

2. *Dim optical afterglows*

GRB 980329 provided the first evidence for heavy obscuration. It was one of the brightest burst in γ and X-rays. The optical afterglow was detected after the identification of radio afterglow. The R magnitude was $23.6 \pm .2$ on Mar 29.9 UT and the OT was not detected on Apr 1.95 UT down to the limit R = 25.5 (Palazzi 1998). The afterglow observations were fitted with the simple relativistic blast-wave model having a temporal decay index of $\alpha = -1.35 \pm .03$ and spectral index of $\beta = 1.4 \pm .4$ (In't Zand *et al.* 1998). Further, R, I, J and K observations were reported by Reichart *et al.* (1999a). If the flux density of $325 \mu Jy$ at 8.3 GHz is

extra-polated to R-band using the power-law and predictions of fireball model, it would imply $R \sim 17$. But the observed magnitude was fainter than $R = 20$ and brighter in K-band and therefore the large $R - K$ color indicated that OT was very red. Thus large IR/optical flux ratio for this GRB clearly showed that strong obscuration along the line of sight has made the optical afterglow dim. The host galaxy was $26.8 < R < 29$ (Gorosabel *et al.* 1999).

An alternative explanation for the very red color of optical afterglow of GRB 980329 was given by Fruchter (1999) that GRB might have occured at $z \sim 5$. The decrement of about 2 magnitudes in $R-I$ color, while $K-I$ or $J-I$ were unaffected has been explained by the absorption of light by Ly_α clouds at high redshift. For a $z \sim 5$ object Ly_α break occurs $\sim 7300A$ in the observer's frame, thus decreasing the R flux. However, Djorgovski reported $z < 3.9$ based upon the non-detection of Ly_α forest in the Keck II spectrum.

In case of **GRB 990705** and **GRB 000418** the afterglow was first identified in near-IR. The afterglow of GRB 990705 was extremely red and dust obscuration was suggested to be the likely reason (Masetti *et al.* 2000a). The afterglow of GRB 000418 showed a single power-law with a slope of -1.22 which flattened out at a later time indicating the host galaxy. The OT was very red with $R - K \approx 4$ mag. The observations were consistent with a spherical fireball with a heavy reddening due to dust extinction in the host galaxy (Klose *et al.* 2000).

3. *Rapidly decaying afterglows*

In case of **GRB 980326** no X-ray afterglow was detected. The optical couterpart exhibited rapid decay with a slope of $\alpha = -2.1 \pm 0.13$ (Groot *et al.* 1998b). The slope was much steeper than that of previous OTs. Since extinction due to dust is negligible above 5 keV, it can not explain the absence of X-ray afterglow (Taylor *et al.* 1998). Therefore rapid decay seems to be a viable explanation. Various cases of blast wave model have been assumed to derive the spectral slope β and electron slope p. Only in jet-like blast wave model the the derived value of $\beta = 0.55$ was consistent with the observed optical color.

The afterglow of **GRB 980519** showed a steep temporal decay with $\alpha = -2.05$ and flat broad-band spectrum of the form $\nu^{-1.2}$ (Halpern 1999). Such a combination of

α and β was inconsistent with the simple spherical fireball model but was consistent with the predictions of an expanding jet. The transition from spherical to jet phase occured $\sim$ 8.5 hr after the burst (Sari, Piran & Halpern 1999).

GRB 991208 was the first IPN localolized GRB for which afterglow was detected. The optical afterglow displayed rapid decay with index $\alpha = 2.2 \pm 0.1$ (Sagar *et al.* 2000a, Hurley *et al.* 2000).

4. *Afterglows of dark hosts*

The optical afterglow of **GRB 990308** was identified by comparing the images of the field taken at the 1m schmidt telecsope of Observatorio Nacional de Llano del Hato, Venezuela, 3 hrs after the burst with those taken with Yale 1m telescope on 29 May 1999 (Schaefer *et al.* 1999). The OT was R = 22.1 three hrs after the burst. No host was seen down to R = 25.7 in images taken with Keck-II on June 19, 1999. No radio counterpart was detected with VLA (8.56 GHz) down to 256 micro-Jy level.

The spectral slope was $0.38 \pm .25$ consistent with fireball model in $\nu^{1/3}$ regime (SPN 98). But the measured temporal slope -2.1 ± 0.1 was higher than the slope of previous afterglows. The possibility that the progenitor could be ejected out of its host galaxy is ruled out statistical grounds, since all the host-galaxies seen so far were within sub-arcsec of their counterparts. The absence of the host could be due to high redshift $z > 1.2$.

The afterglow of **GRB 000630** showed a single power-law decay with a slope of $\alpha = -1.03 \pm 0.097$. The OT was $R = 23.04 \pm 0.08$ about 21 hr after the burst. The images taken 25 days after the burst didnot show any host galaxy down to the limit $R \sim 24.6$ mag (Fynbo *et al.* 2001). Whether a separate class of GRBs with dark hosts exist needs to be investigated.

5. *Very High-z GRBs*

The optical afterglow of **GRB 971214** was reported by Ramprakash *et al.* (1998) from the IR observations. A break in the VRIJK spectrum was identified at a

wavelength of $\sim 1\mu$ about 0.58 days after the burst and was interpreted as peak frequency ν_m. Wijers & Galama (1999) gave a detailed analysis of synchrotron spectra arising from the blast wave and argue that the break is more likely to be cooling frequency ν_c. After the OT faded the host galaxy became visible and its redshift was measured to be 3.42 (Kulkarni *et al.* 1998). The afterglow showed evidence for strong reddening (Halpern *et al.* 1998, Ramprakash *et al.* 1998). Reddening suggests that the progenitor is located in a region of dense gas.

6. *Jetted GRBs*

Several astrophysical sources have non-spherical emitting surfaces: quasars, pulsars, stellar BHs and so on. Such a geometry was suggested for GRB sources to relax the energies. If the jet opening angle is θ_o, then the total energy is reduced by a factor $\approx \theta_o^2/2$. As the relativistically expanding ejecta slows down, a transition from spherical-like phase to expanding jet-like phase can occur. This happens when the bulk Lorentz factor Γ falls below θ_o^{-1}. At this stage, lateral spreading of jet will begin and observed light curve will show a break (Rhoads 1999).

The best studied afterglows of **GRB 970228** and **GRB 970508** demonstrated single power-law fit consistent with the simplest fireball model with spherical emission. The afterglows of **GRB 990123**, **GRB 990510**, **GRB 991216**, **GRB 000301c** (see Chapter 3), **GRB 000926** and recently **GRB 010222** (see Chapter 2) showed a break in the light curve. In Table 4.1 we have tabulated the beaming factors for GRBs that showed evidence for beaming through break in the observed light curve.

GRB 990123 was one of the well studied burst. It is the only burst that showed evidence for a reverse shock. A prompt optical flash at $\sim 9^{th}$ magnitude was observed in real time which disappeared quickly. The optical afterglow showed a power-law decay with $\alpha_1 = -1.12 \pm 0.08$ and $\alpha_2 = 1.69 \pm 0.06$, with an early break at $t_b = 1.68 \pm 0.19$ day (Holland *et al.* 2000).

In case of **GRB 990510** the power-law index changed from $\alpha_1 = -0.76 \pm 0.01$ to $\alpha_2 = -2.4 \pm 0.02$ at 1.6 day after the burst (Stanek *et al.* 1999). The afterglow of GRB 990510 provided the first evidence for linear polarization of 1.6% at 0.86 day after the burst. The polarization is due to synchrotron nature of the emission (Wijers *et al.* 1999).

In case of **GRB 991216** the light curve steepened from $\alpha_1 = -1.22 \pm 0.04$ at early times to $\alpha_2 = -1.53 \pm 0.05$ at $\sim$ 2 day (Halpern *et al.* 2000). The light curve of the afterglow of **GRB 000926** decayed with a power-law. The initial slope of $\alpha_1 = 1.4 \pm 0.1$ steepened to $\alpha_2 = 2.6 \pm 0.06$ after about 1.6 days (Sagar *et al.* 2001). The jet angle was estimated to be .09 radians.

7. *SN-GRBs*

GRB 980425 is a unique burst having its optical transient associated with a luminous type Ic supernova, SN 1998bw (Galama *et al.* 1998a). It was located in a spiral arm of the face-on barred spiral galaxy ESO 184-G82 at a redshift of $z = 0.0085$. The SN was unusally bright in radio-band and the data indicated relativistic expansion unlike the typical supernova (Kulkarni *et al.* 1998). The light curve, when extrapolated in time indicated that the SN exploded within a day of the GRB event. Total energy of the ejecta was $(2 - 5) \times 10^{52}$ erg, and hence the name 'hypernova' was given. Iwamoto *et al.* 1998 modelled the observed light curve and spectra and showed that the explosion by a massive CO progenitor star. The peculier properties of GRB 940425 identifies it as a separate sub-class of GRBs. Following the suggestion that a sub-class of 's-GRBs' might exist, there had been attempts to fit the SN light curves on existing data. The light curve of **GRB 980326** showed steep decline upto 5 days after the burst. Between 3-4 weeks the OT re-brightened to $\sim$ 60 times than the expected flux obtained by extrapolating the light curve and again it faded to a undetectable level. Bloom *et al.* (1999) fitted the SN light curve to GRB 980326 data. The light curve of **GRB 970228** showed a bump that is consistent with a contribution from an underlying SN (Reichart 1999b). A recent revised analysis light curve of **GRB 990712** also showed a contribution from underlying SN (Björnson *et al.* 2001).

Table 1.1: Summary of GRB Afterglows

GRB	Afterglow	z	Magnitude of host-galaxy
GRB 970228	XO	.695	24.7
GRB 970508	XOR	.835	25.0
GRB 970828	XR	.958	–
GRB 971214	XOR	3.42	26.2
GRB 980326	O	∼1	> 27.3
GRB 980329	XOR	< 3.9	> 25.5
GRB 980425	XOR	.0085	14.1
GRB 980519	XOR	–	26.2
GRB 980613	XO	1.096	24.5
GRB 980703	XOR	.966	22.6
GRB 981226	XR	–	> 22
GRB 990123	XOR	1.60	24.4
GRB 990308	O	–	> 25.7
GRB 990506	XR	1.31	–
GRB 990510	XO	1.619	> 28.0
GRB 990705	XO	∼.25	–
GRB 990712	O	.434	21.78
GRB 991208	OR	.706	> 25
GRB 991216	XOR	1.02	24.5
GRB 000131	O	–	–
GRB 000301c	OR	2.03	28.0
GRB 000418	OR	1.118	–
GRB 000630	O	–	–
GRB 000911	OR	–	–
GRB 000926	XOR	2.066	-
GRB 001011	O	-	-
GRB 010222	XOR	1.477	–

Bibliography

[1] Band, D. L. *et al.* 1993, ApJ, 413, 281

[2] Bhargavi, S. G. & Cowsik, R. 2000a, ApJ. Lett., 545, L77; astro-ph/0010308

[3] Björnson, G. *et al.* 2001, ApJL, 552, L121

[4] Bloom, J. S. *et al.* 1999, Nature, 401, 453

[5] Boella, G. *et al.* 1996, AASS, 122, 299

[6] Castro-Tirado, A. J. *et al.* 1998, GCN Circular 173

[7] Cohen, E. *et al.* 1998, ApJ, 500, 888

[8] Conti, G. *et al.* 1994, SPIE Proc. 2279, 101

[9] Costa, E. *et al.* 1997, 387, 783

[10] Eichler, D. *et al.* 1989, Nature, 340, 126

[11] Fenimore, E. E. *et al.*, 1992, In 1hGRB, p. 158

[12] Fishman, G. J. & Meegan, C. A. 1995, Ann. Rev. Astron. Astrophy, 33, 415

[13] Frail, D. A. 1999a, astroph/9912171

[14] Frail, D. A. 1999b, ApJ, 525, L81

[15] Frontera, F. *et al.* 1996, AASS, 122, 357

[16] Frontera, F. 1998, IAU circ.7078

[17] Fruchter, A. S. 1999, ApJ, 512, L1

[18] Fynbo, J. U. *et al.* 2001, astro-ph/0101425

[19] Galama, T. J. 1998b, GCN Circular 172

[20] Galama, T. J. *et al.* 1998a, Nature, 395, 670

[21] Garnavich, P., Loeb, A. & Stanek, K. 2000, ApJ 544, L11

[22] Goodman, J. 1986, ApJ, 308, L47

[23] Gorosabel, J. 1999, A & A, 347, L31

[24] Greiner, J. 2001, *http://www.aip.de/People/JGreiner*

[25] Groot, P. J. *et al.* 1998a, ApJ, 493, L27; also in 4hGRB, p-557

[26] Groot, P. J. *et al.* 1998b, ApJ, 502, L123

[27] Halpern, J. P. *et al.* 1998, Nature, 393, 41

[28] Halpern, J. P. *et al.* 1999, ApJ, 517, L105

[29] Halpern, J. P. *et al.* 2000, astro-ph/0006206

[30] Harrison, F. A. *et al.* 1999, ApJ, 523, L121

[31] Hillier, R. 1984, *Gamma Ray Astronomy*, Clarendon Press: Oxford.

[32] Hurley, K. 1992, AASS, 92, 401

[33] Hurley, K. *et al.* 2000, ApJ, 534, L23

[34] Holland, S. *et al.* 2000, astro-ph/0010196

[35] In't Zand, J. J. M. *et al.* 1998, ApJ, 505, L119

[36] Iwamoto, K. *et al.* 1998, Nature, 395, 672

[37] Jager, R. 1996, A& AS, 122

[38] Kasturirangan, K. 1999, BASI, 27, 17

[39] Katz, J. I. 1994a, ApJ, 422, 248

[40] Katz, J. I. 1994b, ApJ, 432, L107

[41] Klebesadel, R. W., Strong, I. B. & Olson, R. A. 1973, ApJ. Lett., 182, L85

[42] Klose, S. *et al.* 2000, ApJ, 545, 271

[43] Kulkarni, S. R. 2000, Proc. SPIE, 4005, 9 (astroph/0002168)

[44] Kulkarni, S. R. *et al.* 1999, Nature, 398, 389

[45] Kulkarni, S. R. *et al.* 1998, Nature, 395, 663

[46] Kulkarni, S. R. *et al.* 1998, Nature, 393, 35

[47] Lamb, D. Q. 1995, PASP, 107, 1152

[48] Lindgren, B. *et al.* 1999, GCN circular 190

[49] Manzo, G. *et al.* 1996, AASS, 122, 341

[50] Masetti, N. *et al.* 2000a, A & A, 354, 473

[51] Masetti, N. *et al.* 2000b, A & A, 359, L23

[52] MacFayden, A. & Woosley, S. E. 1999, ApJ, 524, 262 (astroph/9810274)

[53] Mészáros, P. & Rees, M. J. 1997, ApJ, 476, 232

[54] Mészáros, P., Rees, M. J. & Wijers, R. A. M. J. 1998, ApJ, 499, 301

[55] Mészáros, P. & Rees, M. J. 1999, MNRAS, 306, L39

[56] Metzger, M. R. *et al.* 1997, Nature, 387, 878

[57] Narayan, R. 1992, ApJ, 399, 368

[58] Nemiroff, R. J. 1994, In 2hGRB, p-730

[59] Paczyński, B. 1986, ApJ, 308, L43

[60] Paczyński, B. 1995, PASP, 107, 1167

[61] Paczyński, B. 1998, ApJ, 494, L45

[62] Paczyński, B. & Rhoads, J. E. 1993, ApJ, 418, L5

[63] Palazzi, E. *et al.* 1998, A & A 336, L95

[64] Panaitescu, A. 2001, astro-ph/0102401

[65] Park, H. S. *et al.* 1997, ApJ, 490, L21

[66] Park, H. S. *et al.* 1998, In 4hGRB, p-842

[67] Parmar, A. *et al.* 1996, AASS, 136, 407

[68] Piran, T. 1999, Phy Reports, 314, 575 (astroph/9810256)

[69] Preger, B. 1996, AASS, 138, 559

[70] Ramana Murthy, P. V. & Wolfendale, A. W. 1993, *Gamma Ray Astronomy*, (2 ed.), Cambridge University Press.

[71] Ramprakash, A. N. 1998, Nature, 393, 43

[72] Reichart, D. E. 1999a, ApJ, 517, 692

[73] Reichart, D. E. 1999b, ApJ, 521, L111

[74] Rhoads, J., E. & Fruchter, A. 2001, ApJ, 546, 117

[75] Rhoads, J., E. 1999, ApJ, 525, 737

[76] Sagar, R. *et al.* 2001, BASI, 29,1

[77] Sagar, R. *et al.* 2000a, BASI, 28,15

[78] Sahu, K. *et al.* 1997, Nature, 387, 476

[79] Sari, R., Piran, T. & Haplern, J. P. 1999, ApJ, 519, L17

[80] Sari, R., Piran, T. & Narayan, R. 1998, ApJ, 497, L17 (SPN 98)

[81] Schaefer, B. E. 1999, ApJ, 524, L103

[82] Shemi, A. & Piran, T. 1990, ApJ, 365, L55

[83] Stanek, K. J. *et al.* 1999, ApJ, 522, L39

[84] Taylor, G. B. *et al.* 1998, ApJ, 502, L115

[85] Taylor, G. B. *et al.* 2000, ApJ, 537, L17

[86] Wozniak, P. R. 1998, GCN Circular 177

[87] Usov, V. & Chibisov, G. 1975, Sov. Astron. 19, 115

[88] Van den Berg, S. 1983, ApSS, 97, 385

[89] Van Paradijs, J. *et al.* 1997, Nature, 386, 686

[90] Wijers, R. A. M. J. & Galama, T. J. 1999, ApJ, 523, 177

[91] Wijers, R. A. M. J. *et al.* 1999, astro-ph/9906346

[92] Woosley, S. E. 1993, ApJ, 405, 273

Following abbreviations are used to cite the GRB conference proceedings that are frequently used in this thesis:

1hGRB = Paciesas, W. S. & Fishman, G. J. (eds). 1992, *Gamma Ray Bursts: First Huntsville Symposium, 1991, Huntsville, AL, AIP conf. proc. 265*, New York: Am. Inst. Phys.

2hGRB = Fishman, G. J., Brainerd, J. J. & Hurley, K. (eds). 1994, *Gamma Ray Bursts: Second Huntsville Symposium, 1993, Huntsville, AL, AIP conf. proc. 307*, New York: Am. Inst. Phys.

3hGRB = Kouveliotou, C., Briggs, M. F. & Fishman, G. J., (eds). 1996, *Gamma Ray Bursts: Third Huntsville Symposium, 1995, Huntsville, AL, AIP conf. proc. 384*, New York: Am. Inst. Phys.

4hGRB = Meegan, C. A., Preece, R. D. & Koshut, T. M. (eds). 1998, *Gamma Ray Bursts: Fourth Huntsville Symposium, 1997, Huntsville, AL, AIP conf. proc. 428*, New York: Am. Inst. Phys.

5hGRB = Kippen, M. R. *et al.* (ed). 2000, *Gamma Ray Bursts: Fifth Huntsville Symposium, 1999, Huntsville, AL, AIP conf. proc. 526*, New York: Am. Inst. Phys.

GCN Circulars may be found at *http://gcn.gsfc.nasa.gov/gcn/gcn3/*

Astro-ph is web based pre-print service available at *http://arXiv.org/abs/astro-ph*

Chapter 2

Optical Observations of GRB Counterparts

2.1 Introduction

Until the 1960's, astronomical observations were made mostly in the visible and the radio range of the electro-magnetic spectrum. With the advent of new technologies, observing facilities got extended to other wavelength bands viz., IR, UV, X-ray and γ-rays, thereby opening up new and exciting areas in astrophysics. Whenever observations were made in wavelengths other than optical and sources detected, it became the standard practice to identify those sources in the optical band. The optical identification of sources detected in other wavelength bands, is important because distances are generally determined through optical observations. Multi-wavelength observations have helped a great deal in the understanding of the related astrophysical phenomenon. Identification and follow-up observations of counterparts of Gamma Ray Bursts (GRBs) in longer wavelength bands have been a major activity in GRB astronomy in the last 4 years, ever since the first fading X-ray (Costa *et al.* 1997) and optical (Van Paradijs *et al.* 1997) counterparts of GRB 970228 were detected.

In this chapter we describe the optical observing techniques and the details of data analysis. The observing and analysis strategies specific to GRB counterpart studies are included in the discussions. In §3, the results of selected GRB afterglow observations are summarized.

2.2 Observational Techniques and Data Reductions

2.2.1 Telescopes and Detector systems

Most of the optical data used for this thesis has been obtained from Vainu Bappu Observatory (VBO), Kavalur, in Tamilnadu, India situated at longitude = 78°49′36″E, latitude = 12°34′36″N. The observatory houses several small and big telescopes 0.15 m to 2.34 m in diameter, of which, we used the 1.02 m Zeiss and 2.34 m Vainu Bappu Telescope (VBT) in imaging mode for our observations. Only in the case of GRB 010214 were observations made using the new 2.01 m telescope of 'Indian Astronomical Observatory' (IAO), Mt. Saraswati, Hanle, at longitude = 78°57′51″E, lattitude = 32°46′46″N.

In the imaging mode these telescopes use Charge Coupled Devices (CCDs) and broad-band filters. For the last two decades, CCDs have become the most popular detectors and the best choice for astronomical imaging because of their high quantum efficiency, wide spectral response, large dynamic range and low noise. Photographic plates are now out-dated (as astronomical detectors) in view of their low quantum efficiency (as compared to CCDs) as well as various strenuous and time-consuming processes involved in the data retrieval viz., dark room processing, digitization etc. The only disadvantage of CCDs is small Field of View (FOV) as compared to photographic plates. This is overcome by having large mosaics of CCDs[1] that are being developed in recent years. We briefly describe the basic properties and the principle of operation of CCDs. Further technical details may be found in comprehensive articles, viz. Mackay (1986), Jacoby (1990), Howell(1992), McLean(1997) and a text book by Howell(2000).

CCD Camera

A CCD is a miniaturized 2-d array of solid state detecors enclosed in a single silicon chip. The entire chip of a 1024 × 1024 CCD for instance, consists of 10^6 pixels and occupies only a few square centimeters! CCDs work on the principle of the photo-electric effect, wherein the incident optical photons upon hitting the silicon base generate free electron-hole pairs (within the device). Silicon can easily absorb photons of energy 1.1–4 eV and displace the electrons from their valence layer (

[1] a technique of forming images by joining together two or more chips.

where they are attached to atoms) to conduction layer (where they are free). The minimum energy required to liberate an electron in the case of Si is 1.14 eV (also called band-gap energy). [2]

If not held back, the photo-electrons created during the the exposure to optical radiation, can recombine into the valence layer in micro-sec time scale. Therefore suitable arrangements are available to apply voltages to each pixel for allowing it to accumulate the charges in a potential well and hold the electrons until the read-out, occurs. The size of a pixel is typically $\sim 10 - 20\mu$; For example, the TEK 1k CCD at VBO has a 24μ square pixel. A pixel can hold 50–500 kilo electrons depending upon it's well capacity. In a three-phase device, each pixel receives 3 sets of voltages in a time sequence through three different 'gate's, which can be repeated in a cyclical order, controlled by clock circuits to shift the charges accumulated (during integration) along a column to be read-out after the exposure is over. During the read-out, charges collected under each pixel are shifted along the columns from one pixel to another with a typical charge-transfer efficieny of 99.99%. Charges are then shifted into an output shift register from the entire final row, after which they are serially read out, one at a time into the output electronics and the process is continued until the entire array is read-out. The output from each pixel is read as voltage after amplifying it and finally converted into a digital number by Analog-to-Digital Converter (ADC).

The CCD camera used for astronomical imaging is generally housed in a cooled, vacuum chamber called 'CCD dewar'. Cooling is necessary to reduce the dark current (arising due to thermal electrons). The camera requires an electronic controller to interface between the CCD and host computer. The controller does the charge transfer, digitization and transferring of the digitized data to the host computer. The host computer runs the acquisition software- that acquires the digitized data and stores the images.

2.2.2 Some Practical Considerations

The choice of a CCD is dictated by the scientific goals one wants to achieve and in this regard, the size of the CCD pixel and typical '*seeing*' of the observing site are

[2]Note that this energy range 1.1–4 eV corresponds to the wavelength range 11000–3000 A° in visible band of electro-magnetic spectrum and for photons of energy outside this range the CCD under discussion is not useful.

important factors. The pixel size essentially defines the resolution of an image; a large pixel size would degrade the image resolution, and having too fine a pixel size is also not recommended, as the well depth is limited and reading noise increases. In optical astronomy, images are limited by atmospheric seeing (see below for brief explanation on seeing). A pixel size of about half the typical seeing is considered ideal because one needs, according to Nyquist theorem, at least two pixels to sample the smallest resolvable object (e.g., cosmic-ray event). Further, the total FOV depends upon the pixel size, total number of pixels and also f-ratio of the telescope.

The 2.34-m VBT at its prime f/3.25 and cassegrain f/13 foci have an image scale of 27″.12/mm and 6″.8/mm respectively. In imaging mode the FOV at the prime is 10′.4 × 10′.4. The 1.02-m Zeiss telescope at its f/13 cassegrain focus has a image scale of 15″.6/mm and the FOV is $\sim$ 6′ × 6′. The image scale (in ″/pix) and total FOV corresponding to various CCDs used are summarized in **Appendix** at the end of this chapter. The 2.01-m telescope at Hanle yields 0″.274/pix and with the TEK 1k CCD of 24μ^2 pixel the FOV is $\sim$ 4′.7 × 4′.7 (See section on GRB 010214 presented below).

Before describing the details of CCD reduction and analysis methods, it is worthwhile to stop here and discuss some of the problems one encounters during CCD imaging and certain factors that affect mesurements with CCDs.

Seeing: Atmospheric seeing smears out the stellar images. It is produced by the turbulence in the atmosphere (along the line of sight) that causes variations in the position and intensity, of an image by distorting the wavefront reaching the telescope. As a result, a point source is smeared into a seeing disc of a few arcseconds in diameter. The images however, look circular but the FWHM of the radial profile, which is a measure of seeing becomes large. Variation in humidity and temperature also affect the seeing. The typical seeing at VBT is 2″.5, whereas it is 1″.5 at 1.02-m telescope. The difference essentially has to do with the dome structure and surroundings, although the two telescopes are within half a kilometer distance of each other! Bad seeing conditions affect the detection of faint objects. Figure 2.1 shows 2 images of same field under good (*right-panel*) and bad (*left-panel*) seeing conditions. The faint objects in the right-panel image are better resolved as compared to those in the left-panel image.

Focus and guiding: Focussing and guiding are important processes in deep field imaging. An image can be elongated or doughnut-shaped if the detector is shifted

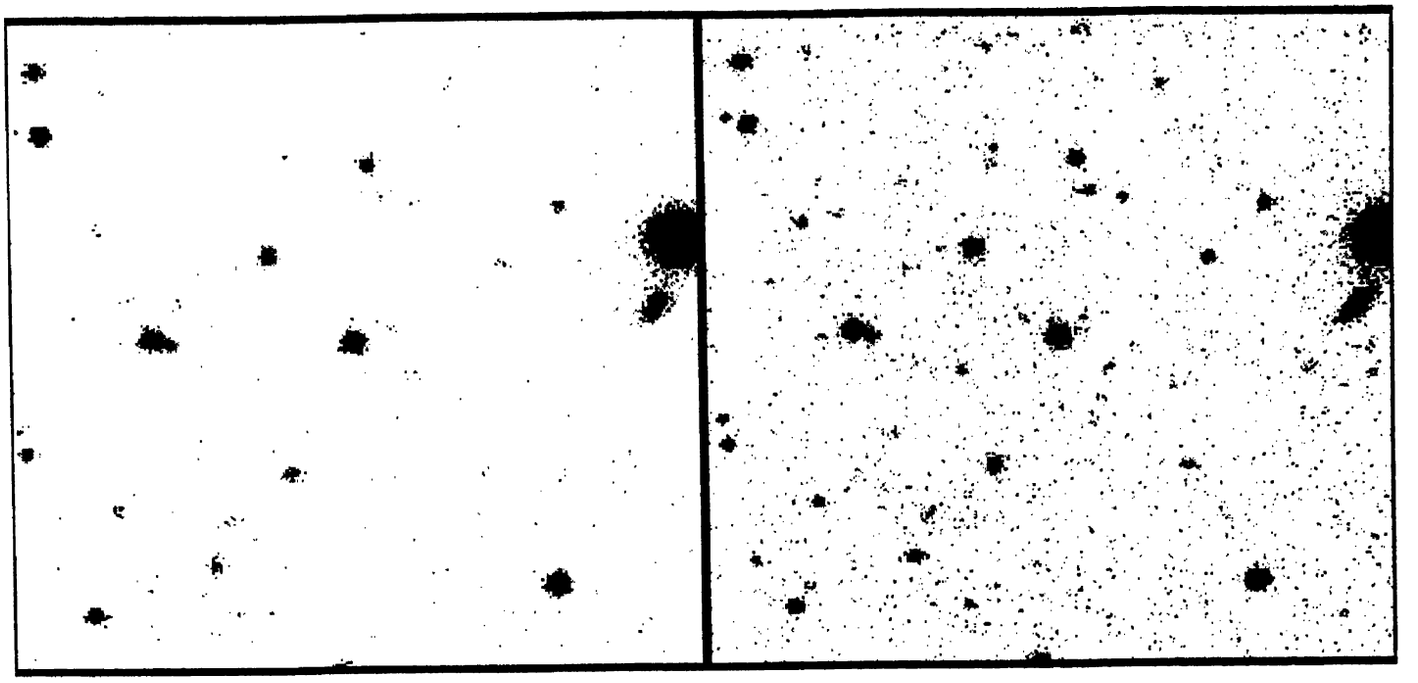

Figure 2.1: R-band (600 s)images of the same field taken under different seeing conditions. The FOV is $\sim 3' \times 3'$; the image on the *right-panel* detects many faint objects as compared to the *left-panel* image.

away from the true focal plane. This finite distance can be tuned and as the correct focus value approches, the images begin to look sharp and circular. Under bad seeing focussing becomes quite difficult and images might look fat. Focus also changes at different telescope positions and at high humidity. Therefore the observer has to spend adequate amount of time in checking the focus between the observing runs. Images might get elongated (in E-W direction) also due to bad guiding. Guiding is the process of applying small corrective motions to the telescope in addition to the sidereal tracking, to keep an object at the same position on the detector. The guider may fail to keep the guide star in position due to various reasons: clouds, bad seeing, problems with the tracking system (or a tired observer falling asleep - a rare possibility!).

Various practical aspects prompted us to follow certain guidelines while observing at VBO: in deep imaging studies it is customary to take several short exposure images and stack them together rather than have a single long exposure. This not only improves the Signal-to-Noise ratio (S/N) but also reduces the number of cosmic-rays events on each frame. This procedure suited the skies, when passing clouds were frequent. Often we took short exposure images and managed to store them before dark patches of clouds came to block the sky view, whereas a longer

integration would have trailed the images once the guide star disappered behind the clouds. Under poor sky conditions we also preferred taking repeated R-band images rather than in all bands in view of its broader spectral coverage and higher response of the CCD in the R-band. In all the runs, B-band observations were scheduled when the field/object was close to the meridian (smallest hour angle) so that the atmospheric extinction is smaller. Response of CCDs in B-band is $\sim$ 30%, while it is $\sim$ 80% in R-band.

2.2.3 Image Pre-processing

1. Data Conversion:

At the telescope we use PMIS 3.5 software system (on Windows 3.1) for data acquisition. The data read out from a CCD is in binary format (16-bit in the present system) and it is then converted into 'Flexible Image Transport System (FITS)' format- one of the widely used data formats in astronomy (Berry 1995).

2. Software Tools:

Several astronomical software packages are available for image re-construction, data reduction and analysis, viz. *Interactive data Reduction and Analysis Facility* (*IRAF*), *Munich Image and Data Analysis System (MIDAS)*, *DAOPHOT*(See Stetson 1987) and so on. These software packages work on various platforms: SUN/Solaris, PC/Linux and DEC-ALPHA/Unix, available at our Institute. All the CCD reductions used in this thesis are carried out in *IRAF* environment. For plotting analysed data, programs were written in *FORTRAN* or in *Interactive Data Language (IDL)* environment.

IRAF is a general purpose software which allows reductions of data from various instruments and contains several packages for photometric and spectroscopic data reductions. The reductions can be automated and every reduction operation gets recorded in the image header so that the subsequent tasks would take the information from these headers. It is possible to process a list of images simultaneously in a batch rather than one image. Each task has a number of parameters which can be controlled by a parameter file. For further details see user manuals available at *http://iraf.noao.edu.*

3. Image Pre-processing:

Image pre-processing consists of several standard operations such as the replacement of bad pixels by interpolation from neighbouring columns and rows, the removal of DC offset using the overscan region, the subtraction of bias level using zero second integration frame, the subtraction of dark current, the flatfield division and the trimming the frames of unwanted pixels (bad columns or rows and vignetted corners).

Bias Subtraction:

The small positive voltage used to hold the photo-electrons in their potential wells during the exposure will cause a nonzero current (DC) signal when the chip is read out. This offset level can be determined from the 'overscan' region which is a region of extra pixels masked off at the edge of each frame with no charge from the exposure. To remove this pedestal value one takes the average of all overscan pixels to form a single constant and subtracts that constant from the image. CCDs we use at VBO do not have the overscan region. The DC offset gets removed while subtracting the bias which is the image obtained with essentially a zero exposure (with shutter closed). The advantage of using the bias frame is that it gives a good statistical average, since the entire CCD chip is involved.

In addition to the individual DC level for each frame, a low spatial frequency variation in the amplifier readout may exist across the chip, especially when the temperature stability of the chip has not yet been achieved. Since this variation may occur both in rows and columns a 2-d subtraction is necessary. Therefore one prefers to subtract the entire frame than a single count. We average many bias frames (taken throughout the night before and after the object frames) to reduce the niose. The mean bias frame is subtracted from flat as well as object frames.

Dark Subtraction:

The dark frames are the long exposures taken with the CCD shutter closed. The dark current is very low in our data and we prefer not to subtract the dark frame because the procedure itself adds noise into the frame.

Flat Fielding:

Flat fielding is one of the most important of the CCD processing steps. Ideally, if a CCD is exposed to a uniform source, all pixels are expected to show a uniform, flat response. But generally a nonuniform response is seen with two components:

1. A small spatial scale (high frequency) component due to the variation in the response from pixel-to-pixel.

2. A large scale (low frequency) component due to the non-uniformity in the calibration lamp itself. (there is also a variation in the light received from center-to-edge, but this need not be corrected since is is present in all the frames.)

To remove the pixel-to-pixel variation from the object frame a calibration with uniform illumination is needed. The best observation for calibration is a region of blank sky. Blank fields are chosen from regions of the sky which have no observable objects. Finding a real blank sky is not easy and it also requires substantial amount of telescope time. Generally one uses a quartz lamp to illuminate a part of the dome (Dome flat). If such an illumination is truly uniform it is sufficient to remove the pixel-to-pixel variation.

If the lamp illumination is not uniform, it can introduce illumination patterns or gradients in the flattened object frames. To remove this effect either

a1. smoothen the flat field itself using the the task *mkillumflat*
(It basically fits a function to the flat and divides the flat by that function: we then get a flat which is free of large scale pattern, containing only pixel-to-pixel variation.) or

b1. correct the flat using a blank sky frame or highly smoothed object frame. (*mksktflat*).

Alternatively, one applies the uncorrected flat to the data and then applies illumination correction to the flattened data (using *mkillumcor*, *mkskycor*).

In deep field studies, one uses program frames themselves to generate a sky flat. This is acheived by the dithering technique. A large number of short exposures are taken in each bandpass. In between the exposures the telescope is moved by a few arcseconds in alternating cardinal directions. The sky flat is generated by taking a median of all such program frames in each band-pass. Any left-over stars have to be masked. Such smoothed sky flat is used as a illumination correction for the dome flats. The corrected dome flat is then applied to the program fields.

Since the flatfield response is wavelength dependent, the flat image in each bandpass is required. A master flat is generated in each band-pass by taking a median of all

the flats. It should be noted that the counts in twilight frames are scaled to pixel intensities and not exposure times. The master flat is then normalized to its mean value and used to flatten the program frames.

Dust rings:

Often ring like features appear in the CCD frames caused by the dust on the filters or CCD window. The larger rings are caused by dust on the filters and tend to move through the frame over the observing run since the telescope and filter wheel both are moved. It is difficult to get rid of them; these may be removed by median combining a large number of morning and evening flats. The smaller rings come from the CCD window. These are fairly stationary through the night (See Fig. 2.9).

Cosmic Rays:

These are high energy particles from outer space striking the CCD. They look like streaks or dots. The dots can be easily distinguished from a stellar image which has a gaussian profile. The radial profile of a cosmic-ray event is a delta function, quite sharp, and has all its light concentrated in 1-2 pixels. Cosmic rays events are removed by replacing the pixel values by an average value from neighbouring pixels. In *DAOPHOT* cosmic rays automatically get rejected by the star finding routines. Cosmic-ray removal can be done before or after combining the images. However we preferrred removing them before combining the images.

Image Summation:

After flattening the program frames, images of each field are summed in each band-pass. The final summed frame is an average of all input frames with average exposure time. Individual frames have to be registered and aligned before summing. Aligning is done by measuring the shifts and rotations in X and Y axis between the frames with respect to a few reference stars common to the frames. The *IRAF* tasks *Geomap* and *Geotran* are used for this purpose.

Good seeing conditions are essential for acquiring deep images. If an image with good seeing, say 1″.2, is combined with another frame observed with 2″.5 the image quality gets degraded in the combined image, compared to the better image. Therefore depending upon the scientific goal one wants to achieve one could choose between good S/N or good quality image.

2.2.4 Photometry and Calibrations

Photometry:

We have used aperture photometric techniques to measure the magnitudes of objects in the CCD frames presented in this thesis. The other technique of fitting Point Spread Function (PSF) is generally used to determine the photometry of objects in a crowded field. Most of the GRB fields studied here are located at high galactic latitudes and are not crowded. Further, these fields contain both stars and faint galaxies. Following Lilly (1991), we decided to use aperture photometry for faint galaxies in the field as opposed to isophotal photometry which is normally used in case of brighter galaxies.

The *IRAF* task *phot* was used extensively to measure the magnitudes. It computes accurate centers, a best estimate of sky value and magnitudes for given concentric aperture radii. The sky value per pixel is estimated from an annulus around an object and the total sky contribution within an aperture (i.e, sky/pixel × area) is subtracted from the total number of counts within that aperture area to obtain a value called flux of the object. The flux is then converted into magnitude using

$$\mathrm{mag} = \mathrm{zmag} - 2.5 \times \log_{10}(\mathrm{flux}) + 2.5 \times \log_{10}(\mathrm{itime}) \qquad (2.1)$$

Here, 'itime' is the exposure in seconds and 'zmag' is a normalizing constant.

Let us assume that in a given CCD frame there are objects ranging in brightness and we would like to determine their magnitudes. As discussed in previous section, we know that atmospheric seeing smears an image of a point source as described by Point Spread Function. The stellar profile (i.e, a row/column cut across an image) can be approximated by a gaussian function. A gaussian function is characterized by its FWHM (σ) and maximum intensity I_0. The FWHM of PSF is a measure of seeing. Since almost all the light is concentrated within 3×FWHM of a seeing disc, it had been a standard practice to measure the magnitudes within an aperture of radii 3–5 σ. The **growth curve**, a plot of magnitudes at concentric apertures as a function of aperture radii, (see Fig 5.12) is first plotted for a few well exposed, bright stars in the field, to decide the aperture radius r_a beyond which the magnitude does not change. If fainter objects in the field are measured at this radius r_a, large fraction of the aperture area would receive contribution from the sky background and hence will yield poor S/N. In such cases we go for **aperture corrections**. The fainter objects are measured using a smaller aperture radius, r_f where the

derived magnitudes just begin to get contaminated by sky background. For objects fainter than 20 mag one would use an aperture radius of 1–1.5σ by drawing circles and visually inspecting the image display window. Then a correction factor Δ_{ap} is added to obtain their magnitudes at r_a. The correction factor is the difference in magnitudes: m[r_f]− m[r_a] obtained from the well exposed reference stars.

Transformation to standard system: To transform the magnitudes of program objects thus obtained to Jhonson's standard system it is necessary to observe a few standard stars in photometric sky conditions on the same night. Generally a star cluster (where all stars have the same airmass) or Landolt standard field (Landolt 1992) with a good color range located close to the program object is chosen.

The transformation coefficients and photometric zero points are determined by fitting least square linear regression to BVRI indices of several standard stars as a function of observed (instrumental) magnitudes/colors of the same standards using the following equations.

$$\begin{aligned} B - V &= \mu_{bv} \times (b - v)_0 + \zeta_{bv} \\ V - v_0 &= \epsilon_v \times (B - V) + \zeta_v \end{aligned} \tag{2.2}$$

Here, $B - V$ and V refer to the standard color and magnitude; $(b - v)_0$, v_0 refer to instumental color and magnitude respectively, outside the atmosphere; (The instrumental magnitudes are corrected for atmospheric extinction to obtain the magnitudes outside the atmosphere using: $b = b_0 - k_b X$; $v = v_0 - k_v X$; $X = airmass$; $b - v = (b - v)_0 - k_{bv}$; k_{bv} is color extinction coefficient). μ_{bv} and ϵ_v are the slopes; ζ_{bv} and ζ_v are the corresponding zero-points. Similar transformation coefficients are determined for each band-pass and color. Using these coefficients the instrumental color and magnitudes of program object are transformed to the standard system.

Determining the magnitude extinction is a difficult process; one needs to observe the standards at 3–5 positions (different airmasses) in the sky at least twice during the observing season. This requires that the sky conditions remain the same throughout the night to obtain correct extinction. However, in reality there are very few good observing sites. Alternatively, one could observe 3–5 standard fields spread from zenith to near horizon and obtain the extinction coefficients. If secondary standards are identified in the program frame itself, as in the case of rapid GRB follow-up ob-

servations, the calibrations become much simpler and accurate. Advantage of using the local standards is that one need not determine extinction coefficients as they get cancelled at the same airmass.

$$\begin{aligned} (b-r)_0^{\rm OT} &= (b-r)^{\rm OT} - k_{br}X \\ (b-r)_0^{\rm std} &= (b-r)^{\rm std} - k_{br}X \\ \Delta(b-r)_0^{\rm OT-std} &= \Delta(b-r)^{\rm OT-std} \end{aligned} \tag{2.3}$$

2.2.5 Object Identification & Astrometry

Star-galaxy Separation

Star-galaxy separation was achieved using an approach described by Woods (1995) and references therein. Fig 2.2 shows a plot of aperture magnitude v/s a shape parameter which basically gives the difference between the 'core' magnitude corresponding to the central 4 × 4 pixels of each object and the aperture magnitude. The difference between the core and aperture magnitudes can be used as a crude discriminant to separate stars and galaxies upto $I = 21$ or $V = 22$. In the plot the horizontal sequence represents objects with same PSF and these objects have a stellar appearence in the image. Therefore we can identify all the objects falling on horizontal sequence to be of stellar in origin. At the fainter end star-galaxy separation is difficult; however, the fraction of faint stars that are confused with galaxies is negligible, as the fields studied lie at high galactic latitude. Although more sophisticated software packages viz. *Faint Object Classification And Anlysis (FOCAS)* (Valdes 1993) or *Source Extractor* (Bertin 1999) are available, it was decided to use the above approach for our data set. Further, a thorough visual inspection was made to confirm the final list and discard spurious detections. Since the observed GRB fields did not have bright galaxies, aperture photometry was preferred to the isophotal/FOCAS magnitudes. For faint galaxies, aperture magnitudes are more reliable than isophotal magnitudes (Lilly 1991).

Astrometry

We have extensively used USNO-A2.0 catalog to identfy reference stars in the GRB fields. This catalog provides equatorial co-ordinates as well as crude B and R band

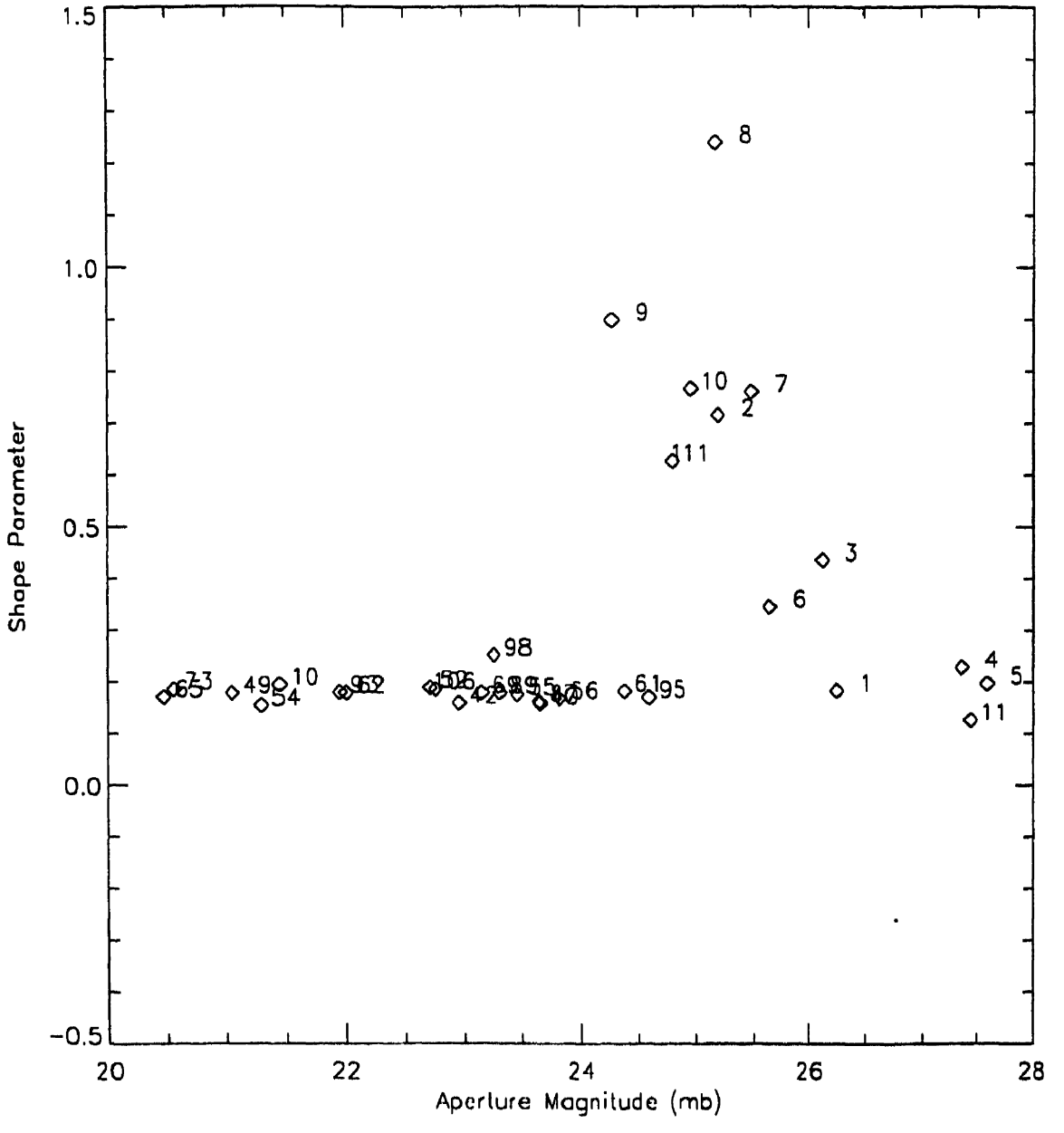

Figure 2.2: Star-Galaxy separation: The figure shows a plot of aperture magnitude v/s a shape parameter (see text for details). The horizontal sequence of objects are stellar in origin. The objects numbered 2, 3, 6–10 are identified as galaxies.

magnitudes. These reference stars are identified in the observed frames and their accurate (x,y) pixel positions are measured using the *centroid* routine. The set of points (x, y, RA) and (x, y, DEC) are used to obtain astrometric solutions. Using the parameters of the fit one could obtain precise co-ordinates of any other object in the same CCD frame. The tasks in *STSDAS* have been used for this purpose.

2.3 Afterglow Observations from VBO

We have been attempting the follow-up observations of GRBs since May 1997. Starting from GRB 970508 in 1997 May several afterglow observations were attempted. Until Mar 2000, we did not succeed in detecting any afterglow, mostly due to bad weather and quite often due to operational problems (instrument non-functioning or telescope already being allotted for other research program). These difficulties prompted us to make Target of Opportunity (ToO) proposal[3] from year 2000 onwards. In this section we present the details of observations and analysis of 7 GRB fields for which we attempted rapid follow-up observations; these include GRB 010214 and GRB 010222 observed close to the completion of this thesis. The first successful afterglow detection was for GRB 000301c - the details of which are presented in a separate chapter following this.

2.3.1 The Goal and Procedure

The Goal

The afterglow of a GRB is generally monitored down to the faintest detection limit of a telescope:

1. to study its brightness variation as a function of time since the occurence of the burst event in multi-wavelength bands.
2. to derive the decay law from the light curve.
3. to measure the precise position of OT with respect to the host galaxy (if any).
4. to measure the redshift of the transient source.

A study of all the afterglows so far detected shows a diversity of light curve properties. Therefore it is necessary to accumulate a statistically significant set of such observations for the classification of the bursts and for subsequent theoretical modelling. For instance, the offset of OT from the nucleus supports the NS-NS merger model since NS binaries are expected to have high kick velocities which would remove them from their high density birth places before they coalesce after about 10^9

[3]I am grateful to our Director and the Time Allocation Committee- particularly, to Dr A. V. Raveendran, for approving the ToO proposal.

years. On the other hand in the hypernova model a massive star is expected to collapse in the high density, star-forming, dusty regions of their host-galaxies.

Observing Procedure

- GCN circulars via e-mail provide either the central co-ordinates (*BeppoSAX*) with an error circle of a few arcseconds or corners of an irregularly shaped error box (IPN).
- Finding charts are made using the Digitized Sky Survey (DSS) available at *http://www.stsci.edu* or *http://www.eso.org*
- The error box is overlaid on the DSS image in order to correctly point the telescope and cover the area of error box.
- Once the field is observed the images are compared with those of DSS to see if there is any flaring/fading object within the uncertainties in GRB location. If the exposure is deeper than DSS, new objects may be detected. The results of analysis are posted in the GCN circular for the benefit of GRB astronomers to help them plan their subsequent observations.
- Observations are continued on subsequent nights to look for objects that varied in brightness between the 2 epochs of observations.

  In the meanwhile if there is any report on the detection of an afterglow candidate, multi-band observations are made. Whether the colors evolve in time or not has important implications for theoretical studies. Spectroscopic observations are carried out depending upon the brightness of the object and capabilities of spectrograph.
- Since ideal photometric sky conditions are not always expected at all observatories, and the optical emission fades away quite fast, observatories located at good sites normally, carry out the observations in all broad-band filters and report the field photometry. Using the photometry of field stars as secondary standards all observations can be calibrated using differential photometric techniques. So far Henden (USNO) has been providing such services to the GRB community.

2.3.2 Summary of Afterglow Observations

1. GRB 000131

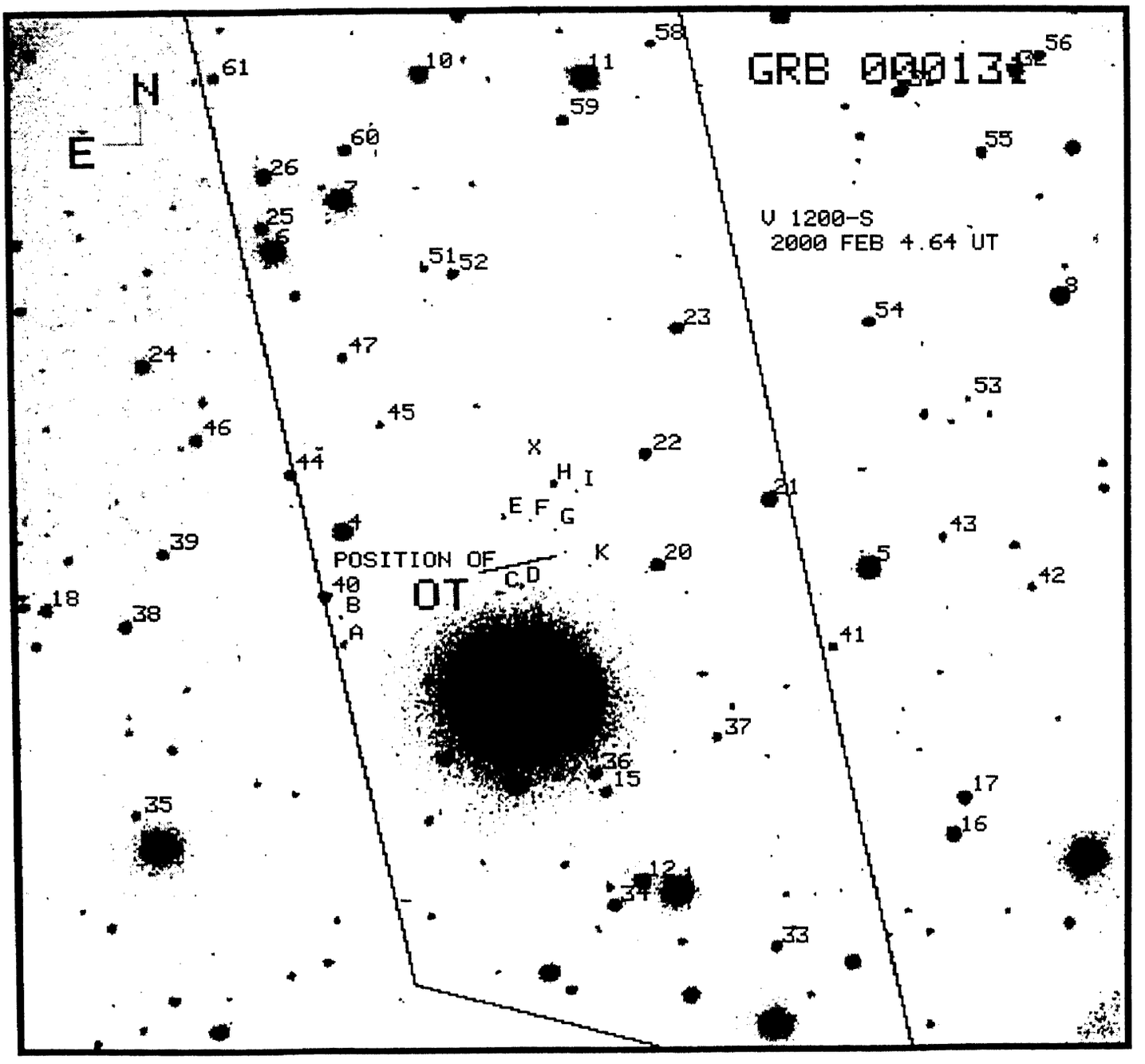

Figure 2.3: GRB 000131 observed in V-band (20 min) using 2.34 m VBT on 2000 Feb 4.64 UT. The IPN error box is overlaid on the $\sim 10'.4 \times 10'.4$ FOV of VBT. The position of the possible afterglow (Pedersen *et al.* 2000) is marked on the image.

GRB 000131 was detected by Ulysses, Konus, and NEAR on 2000 January 31.62 UT. Initial GCN notice on 2 Feb had 2 alternative error boxes of $55' \times 55'$ (Hurley *et al.* 2000a). Since BATSE also detected this burst it was possible to confirm one of

the localization (Kippen 2000a). The fading counterpart was detected by Pedersen *et al.* (2000) using 8.2 m VLT. Comparison of their images taken on Feb 4th & 6th revealed an object which faded by 0.6 magnitude from $R = 24.0$ on 4th Feb.

We observed (see Bhargavi *et al.* 2000a) the field of GRB 000131 centered at RA = 06:13:32.72, Dec = −51:55:36.77 (J2000) using VBT [4] and 1.02 m on 4th and 5th Feb. Sky conditions were non-photometric and the average seeing was $> 2''.8$. In Fig 2.3 we show V-band image taken on Feb 4.64 UT using VBT. The possible OT reported by Pedersen *et al.* (2000) is not detected in our images as, we could only reach the limit $V = 21.5$ in 1200 s integration. Several galaxies are present in this field, however we can not resolve the faint objects better than the given seeing and therefore galaxy number counts would be quite mis-leading if reported. The objects numbered in Fig 2.3 are identified from USNO-A2.0 catalog and photometric measurements are made for all the objects in the field. Assuming the magnitude of star #5 to be 14.0 we estimate that the objects marked as 'E', 'F'...etc are at the detection limit $V = 21.5$.

Whether the fading behaviour of the object at 24^{th} magnitude is associated with the GRB or not is not certain since no duplicate observations are available. Even with good weather conditions 2 m class telescopes may not be able to identify or study the fading behavior of afterglows at this faint level of 24^{th} magnitude.

2. GRB 000210

GRB 000210 was detected by WFC/SAX on Feb 10.364 UT and was localized with an error circle of $2'$ radius and initial position at (J2000) RA = 01:59:15, Dec = −40:40:07 (Stornelli *et al.* 2000; also see GCN # 538,539). The burst was also detected by Ulysses & Konus and IPN3 localization was reported by Hurley (2000b). The burst was also detected by BATSE with a strong pulse with T_{50} and T_{90} durations of 4.1 s and 12.3 s respectively. The Peak flux (50-300 keV) was 29.9 photons/cm^2/s and fluence (>20 keV) of 8.5×10^{-5}ergs/cm^2 (Kippen 2000b).

The NFI/SAX detected an X-ray afterglow inside the WFC error circle during the follow-up observations 8 hr after the burst event inside the WFC error circle (Costa *et al.* 2000). The source faded between the two epochs of observations and was located

[4] I Thank Dr A. K. Pati for observing at VBT and to Ms. S. Ambika for donating 2 hours of telescope time to observe at the 1.02 m telescope.

at RA = 01:59:15.9, Dec = −40:39:29 (J2000). The *Chandra X-ray Observatory* observed the GRB 000210 error circle 21 hours after the burst and found a source at RA = 01:59:15.5, Dec = −40:39:33.2 (J2000) consistent with the X-ray afterglow Garcia *et al.* (2000). This position coincided with the position of a faint optical source at $R \sim 23$ in the images obtained with the 1.54 m Danish Telescope on Feb 2.0 UT (Gorosabel *et al.* 2000a, 2000b). However the source was not detected in the combined image of 3000 s exposure observed on Feb 11.05 UT in R-band at the same telescope down to the limit $R \sim 23.3$. VLA observations did not reveal any radio source brighter than 0.26 mJy (Berger & Frail 2000). Similarly no radio sources were detected to the limit 55 μJy in an integration of 8.2 hr with Australia Compact Array (ATCA) on Feb 12.31 UT (McConnell *et al.* 2000).

We received the GCN notice by 12:30 UT and began our observations starting from 14 UT at 2.34 m VBT. [5] The field was 2^h40^m west of the meridian at early evening with a high background due to Moonlight. The average seeing was $3''.5$. Between Feb 10.59 UT – 10.629 UT we acquaired one V-band image of 600 s exposure and three R-band images each of 300 s exposure. On the following night between Feb 11.569 UT – 11.634 UT we acquired several short exposure R-band images. In Fig.2.4 we show the combined image with total exposure of 900 s observed on 10 Feb 2000. We did not detect any source at the position of *Chandra* source or NFI source down to the limit $R = 18.0$ (Bhargavi *et al.* 2000b). The late-time imaging observations were carried out by Gorosabel *et al.* (2000c) during 22–31 Aug 2000, in V, R and I bands. Although they detected the object at the position of *Chandra* source, it was found to be constant in brightness with $R = 23.5 \pm 0.2$.

3. GRB 010214
The first GRB follow-up from IAO, Hanle

GRB 010214 was simultaneously detected by the GRBM and WFC2 aboard BeppoSAX on Feb. 14, 08:48:11 UT (Gandolfi 2001a). The refined position was centered at RA = 17:41:0.48, Dec = 48:32:38.4 (J2000) with an error circle of radius 3′ (Gandolfi 2001b). A fading X-ray afterglow was detected in the MECS (1.6-10 keV)

[5] I Thank Ms. Geetanjali Gauba for observing on 10th Feb; although our observations began within 1.5 hr after the e-mail notification, GCN posting was delayed until feb 14th, as e-mail and internet facilities were not available till Feb 13th. We could not download DSS image to compare the field.

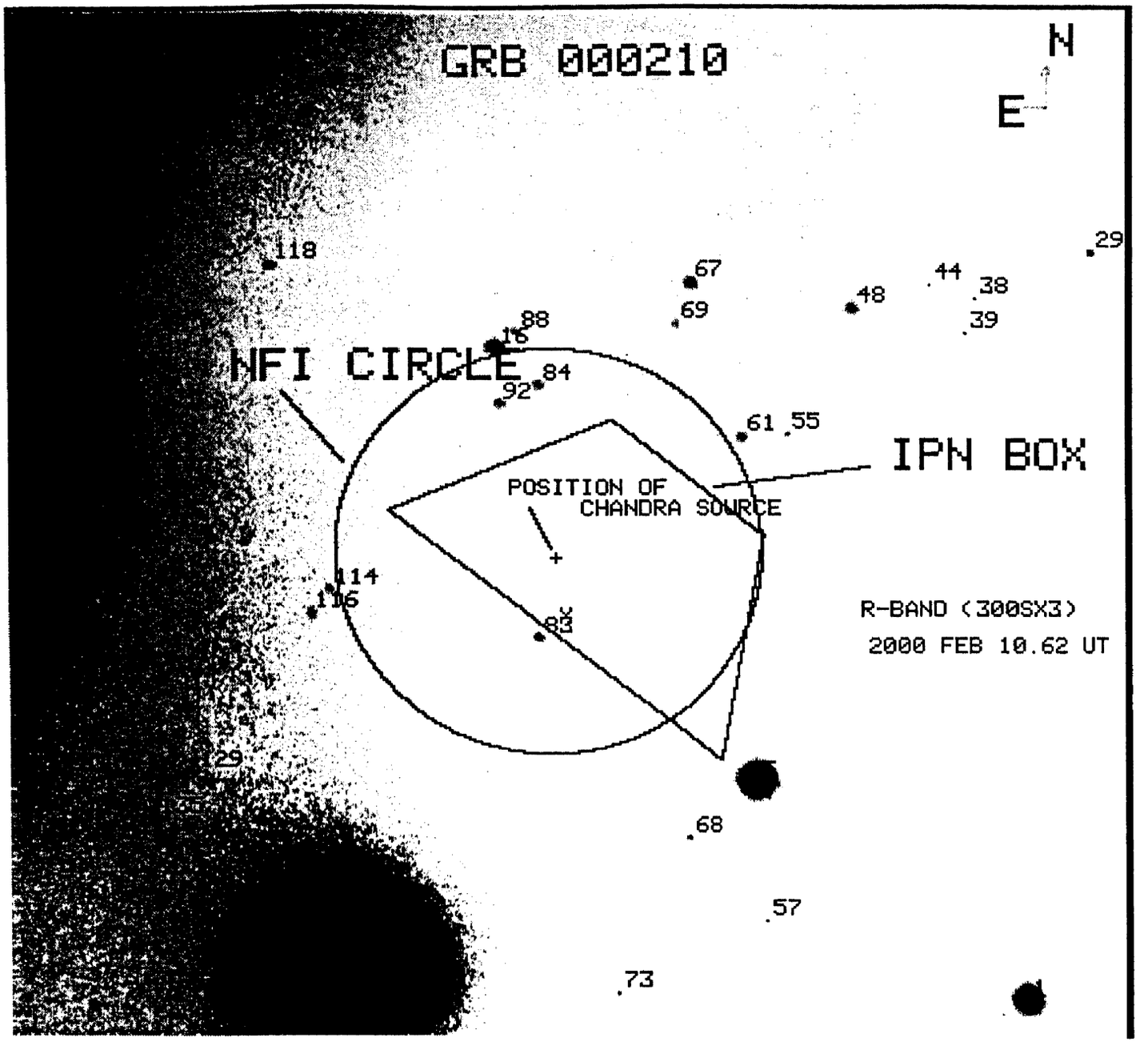

Figure 2.4: The field of GRB 000210 observed at VBT on 10 Feb 2000. In the combined $300s \times 3$ image in R-band no source is detected at the position of Chandra source down to the limit $R = 18.0$. The NFI error circle as well as the IPN error box are overlaid on the image.

image centered at RA = 17:40:56.16, Dec = 48:33:57.6 with an error radius of 1′.5 (Gandolfi 2001c; Frontera *et al.* 2001). The source faded as a power-law with index $\alpha = 1.6$. Zhu & Xue (2001) detected a faint object in one of their images at RA = 17:40:57.68, Dec = +48:33:58.3 with $R = 19.1$ and this was not detected in the other images obtained by them. A faint point-like source in Near IR was detected (Di Paola *et al.* 2001a) at RA = 17:40:54.0, Dec = +48:32:20 at $J = 19.1 \pm 0.3$ which

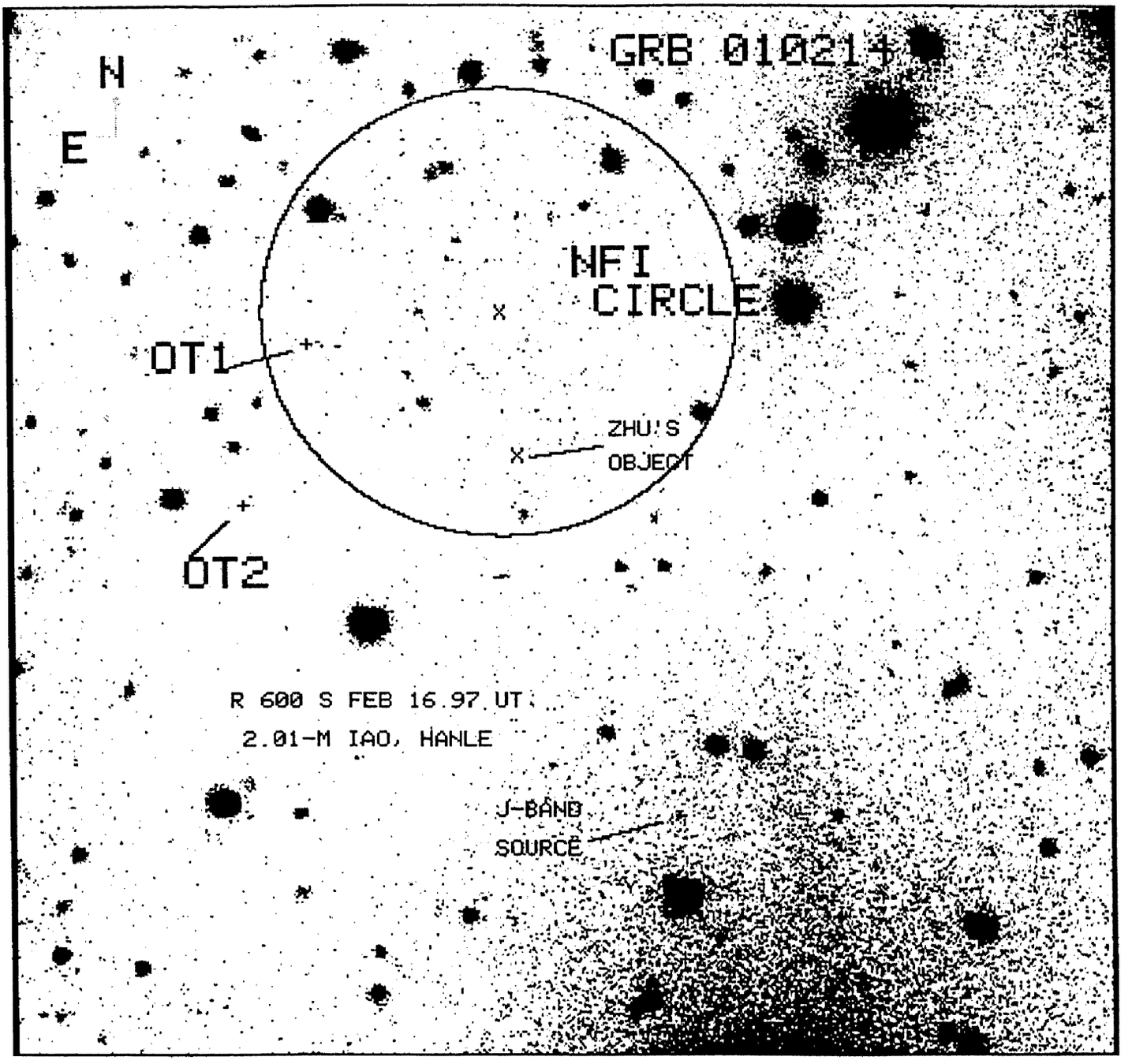

Figure 2.5: The first GRB follow-up from the new 2.01 m telescope at IAO, Hanle: CCD image of the field of GRB 010214 observed on 16 Feb 2001 in R-band. FOV is $\sim 4'.7 \times 4'.7$; The image scale is $0''.274$/pix. The NFI error circle is shown; OT1 and OT2 are positions of optical afterglow candidates reported by Rol *et al.* (2001a). The position of possible afterglow candidate reported by Zhu *et al.* (2001) and the J-band source (Di Paola *et al.* 2001a) are also shown. The faint objects inside the NFI error circle are below the DSS limit.

was not present in IR, R and B plates of DSS-2. The source had the same brightness after about 24 hr (Antonelli *et al.* 2001). The optical afterglow was reported by Rol *et al.* (2001a) within the NFI error circle at RA = 17:41:02.9, Dec= 48:34:30

(J2000). This source faded from $R = 22.9$ (Feb 15.26 UT) to $R = 24.1$ (Feb 17.25 UT). They also detected another variable source outside the NFI error circle at RA = 17:41:04.6, Dec = 48:33:47 (J2000) which faded from $R = 23.1$ to 24.0 between the two epochs of their observations. Klose *et al.* (2001) detected Rol's object at $I = 21.9 \pm 0.4$ on Feb 16, however, they claim no fading behaviour (<0.5 mag) for this candidate object after comparing its brightness against the brightness of the subsequent image observed on Feb 27 UT. Further, Rol *et al.* (2001b) obtained R-band images on 21 Feb 2001 and comparison of these images with their previous images showed no evidence for a further fading of the possible counterpart.

No radio counterpart was detected to a limit of 160 μJy (4.86 GHz) and 130 μJy (8.46 GHz) with VLA (Berger & Frail 2001a.)

We made the follow-up observations[6] of the field of GRB 010214 centered at BeppoSAX WFC error circle (Gandolfi 2001c) using the new 2.01 m telescope at Indian Astronomical Observatory (IAO), Mt. Saraswati, Hanle, India.

Two exposures of 600 s each in B and R band were acquired on 15th and 16th Feb 2001. The sky conditions were good and seeing varied from $1''.9 - 2''.5$ during the observations. The details of observations are given in Table 2.1 below:

Table 2.1: GRB 010214: Observations at Hanle

Mid-UT	Filter	Exp. time (sec)	Average seeing	Limiting Magnitude
2001 02 15.9968	R	600× 2	$2''.2$	>22.1
2001 02 16.0145	B	600× 2	$2''.2$	>23.0
2001 02 16.9728	R	600× 2	$2''.3$	>22.2
2001 02 16.9929	B	600× 2	$2''.3$	>23.0

The data reductions were carried out in the standard manner as explained in §2.2 and results have been by reported by Cowsik *et al.* (2001a). The photomertic calibration is done with respect to 12 of USNO-A2.0 stars in this field. No flaring

[6]I thank Dr T. P. Prabhu for making the telescope time available at Hanle and Dr B. C. Bhatt (IAO, Hanle) & Dr D. K. Sahu (CREST, Hoskote) for carrying out the observations.

or fading sources have been detected with respect to DSS-2 R image down to the limit R > 22.0. Several faint objects below DSS limit were measured; these have not varied more than 0.1 m between the two epochs of our observations.

The J-band source reported by Di Poala *et al.* (2001) is detected at $R = 22.2 \pm 0.22$ on Feb 15.99 UT and is found to be constant in brightness within the photometric error and consistent with the measurements of Gorosabel *et al.* (2001) and Masetti *et al.* (2001a). It is at B > 23.0 in the combined image of 1200 s on Feb 16.99 UT. The optical candidate reported by Zhu *et al.* (2001) is not detected in our images. The afterglow candidates reported by Rol *et al.* (2001a) are not detected in our images, as they are below our detection limit. The R-band image taken on 16 Feb is shown in Fig 2.5.

4. GRB 010222

GRB 010222 was detected by GRBM as well as WFC1 on board BeppoSAX on Feb 22.308 UT, 2001 and is one of the brightest among the GRBs detected by BeppoSAX (Piro 2001). The refined position from WFC was centered at RA = 14:52:12.24, Dec = 43:0:43.2 (J2000) with an error circle of radius 2′.5 (Gandolfi 2001d). The optical afterglow was first reported by Henden (2001a) at RA = 14:52:12, Dec = 43:01:06 (J2000) with $R \sim 18.3$ about 4.3 hr after the burst. The spectrum of Optical Transient (OT) was obtained by Garnavich *et al.* (2001), about 5 hr after the burst. The medium resolution spectrum covering the region 3620–7560Å showed blue continuum and two sets of absorption line systems: strong doublets of FeII (2585,2599) and MgII (2796,2803) with $z \geq 1.476$ and weaker lines of MgII (2802.7,2795.5) and FeII (2599.4, 2585.9, 2382.0) with $z = 1.157$ (Jha *et al.* 2001a, 2001b). Bloom *et al.* (2001), besides confirming these two absorption line systems, also detected an additional absorption system at $z = 0.928$. Further, Castro *et al.* (2001) reported more accurate redshifts of 3 absorption systems using high-resolution spectroscopy on Keck-II telescope. The afterglows were also detected in Near-IR (Di Paola *et al.* 2001b), radio (Berger & Frail 2001b), sub-mm (Fich *et al.* 2001; Kulkarni *et al.* 2001). The X-ray afterglow of the burst was also detected by *Chandra* observatory on Feb 22.936 UT (Garmire 2001).

We carried out the follow-up observations [7] of the afterglow of GRB 010222 as a part

[7] I Thank Ms. S. Ambika for taking observations on 24^{th} and 25^{th} Feb;
Mr. K. Jaya Kumar and team are acknowledged for observing on 28^{th} Feb and 1^{st} Mar.

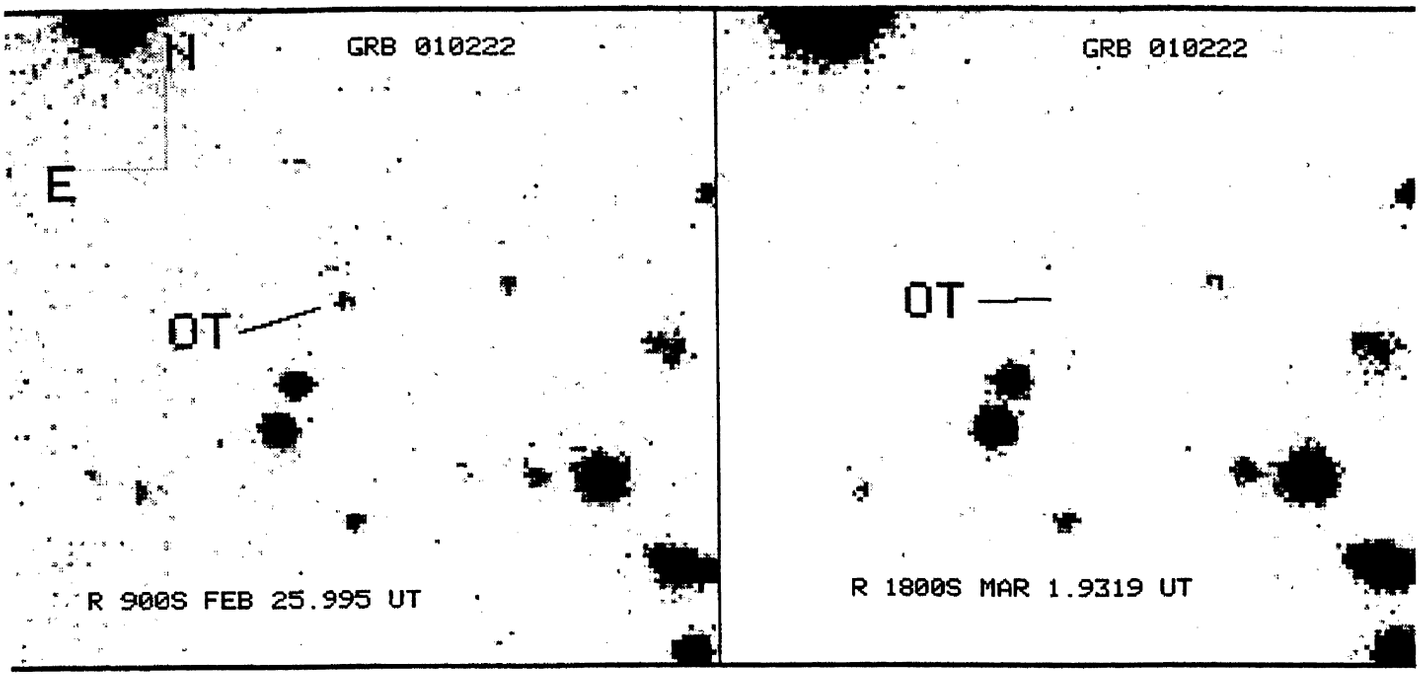

Figure 2.6: The fading behaviour of afterglow of GRB 010222 can be seen in the CCD images observed from 2.34 m VBT. The OT detected on 25th Feb 2001 (*left-panel*) has disappered in the image taken on 1st Mar, 2001 (*right-panel*). The FOV here is $1'.3 \times 1'.3$.

of our ToO proposal. Here, the analysis of follow-up observations carried out at 2.34 m VBT on 24^{th}, 25^{th}, 28^{th} Feb and 1^{st} Mar 2001 are presented. Sky conditions were good during these observations. The log of observations is as given in Table 2.2. Results were posted in GCN circular Cowsik & Bhargavi (2001).

In Fig 2.6 we show images of the afterglow of GRB 010222 in R-band observed on Feb 25.995 UT (*left-panel*) and Mar 1.932 UT (*right-panel*). The OT is detected in all frames taken on 24^{th} and 25^{th} Feb, but has disappered in those taken on 28^{th} Feb and 1^{st} Mar. The data reductions were carried out in the standard manner as explained in §2.2. We use the photometric measurements provided by Henden (2001b) for this GRB field to calibrate our magnitudes. Two of the well exposed field stars were measured at an aperture radius of 4× FWHM of seeing (i.e, at 16 pixels for 24^{th} Feb and 12 pixels for 25^{th} Feb). The OT was measured at 1.5× FWHM aperture radius (i.e, 6 pixels on Feb 24^{th} and 4 pixels on feb 25th) and then suitable aperture corrections (see §2.2) were applied to obtain its magnitude at 4× FWHM aperture radius. The magnitudes of OT given in Table 2.2 are with respect to a field star identified as Stanek 'A' (Stanek *et al.* 2001a) as measured by Henden (2001b). To check the accuracy of these measurements the magnitudes of a few more stars in

Table 2.2: GRB 010222: Observations at VBT

Mid-UT	Filter	Exp. time (sec)	Average seeing	Magnitude of OT
Feb 24.977	I	600	2.5	20.8 ± 0.2^{8}
Feb 24.9924	R	600	2.6	21.405 ± 0.172
Feb 25.9816	I	900	1.7	21.42 ± 0.182
Feb 25.9955	R	900	1.8	21.99 ± 0.162
Feb 28.9014	R	1200	2.6	> 22.0
Feb 28.9257	R	2400	3.0	> 22.1
Mar 1.9319	R	1800	2.3	> 22.1
Mar 1.95	R	600	2.3	> 22.1

the field were determined and we found them to be accurate within 0.05 magnitude with respect to Henden's values.

The observations of afterglow of GRB 010222 in R-band are combined with the other observations from literature (Cowsik *et al.* 2001b, Masetti *et al.* 2001c, Sagar *et al.* 2001, Holland *et al.* 2001, Veilett 2001) and are plotted in Figure 2.7. A break in the light curve was first reported by Masetti *et al.* (2001b, 2001c) and Holland *et al.* (2001). In the present work the light curve is fitted with the smoothly broken power-law given by Stanek *et al.* (2001b).

$$F_\nu(t) = \frac{2F_{\nu,0}}{[(t/t_b)^{\alpha_1 s} + (t/t_b)^{\alpha_2 s}]^{1/s}} \tag{2.4}$$

Here, t_b is the break-time; $F_{\nu,0}$ is the flux at t_b and $s > 1$ is the smoothness parameter with larger s implying a sharper break. This function describes a light curve falling as $t^{-\alpha_1}$ at $t \ll t_b$ and $t^{-\alpha_2}$ at $t \gg t_b$. The best fit parameters obtained using the Levenberg-Marquardt method of χ^2-minimization (Press *et al.* 1993) are given in Table 2.3.

The afterglow of GRB 010222 has displayed the earliest break than any of the known afterglows. The light curve parameters reported by various authors widely vary, this could be due to different data sets. The values obtained here are closer to those

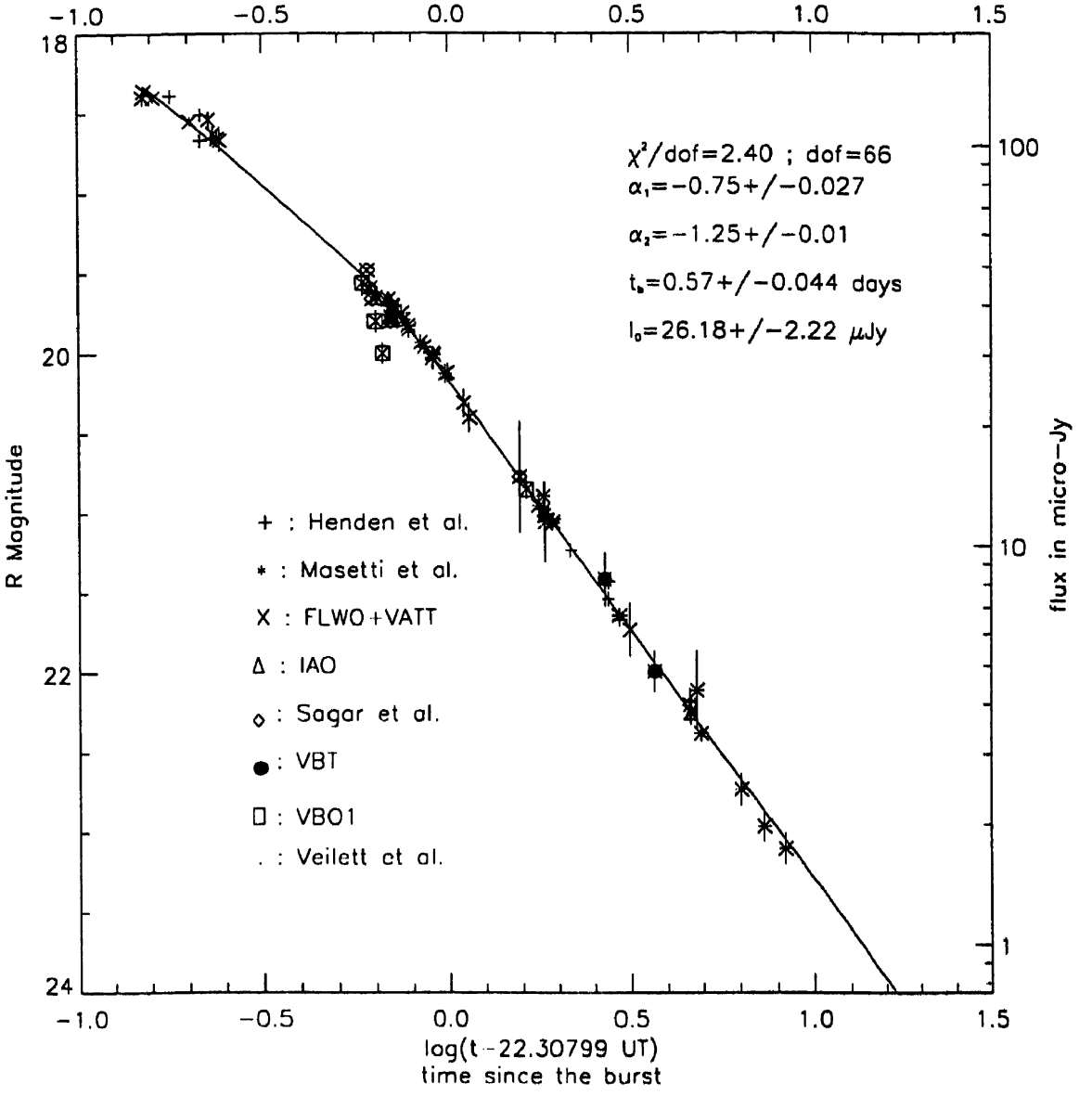

Figure 2.7: GRB 010222: R-band light curve of the afterglow.

obtained by Stanek *et al.* (2001b) and Sagar *et al.* (2001). Stanek *et al.* (2001b) find that the α and β are inconsistent with the jet model. Masetti *et al.* (2001) evaluated various cases of spectral evolution and conclude that their measurements favor a transition from relativistic to non-relativistic regime in the shock. Bhattacharya (2001) derived the afterglow behaviour for the flat electron index $1.0 < p < 2.0$. Using these expressions Sagar *et al.* (2001) derive the parameters for jet-like case, assuming $\nu_c < \nu$. Cowsik *et al.* (2001) find that the afterglow behaviour is consistent with the jet model in a uniform density medium.

Table 2.3: GRB 010222: Fit parameters

Parameter	Value	error
χ^2/dof	2.4 (d.o.f = 66)	
s	10	
F_0	26.18 μJy	2.22
R_0	20.15	
t_b	0.57 days	0.04
α_1	-0.75	0.027
α_2	-1.25	0.01

5. GRB 920620

This optical observational program was carried out in collaboration with Dr J. Greiner (AIP, Potsdam) to optically identify the X-ray sources detected in the ROSAT observations of certain GRB fields. Rapid follow-up observations of GRBs with accurate positions have been carried out with ROSAT to find their X-ray counterparts. Some of the observations detected more than one X-ray source (Greiner 1997a). In such cases it is difficult to establish the X-ray source-GRB inter relationship. If these X-ray sources are identified in optical band one could use their L_X/L_{opt} ratio to classify them. Further, the optical colors and variability if any would help to find their association with GRB. Therefore we proposed to observe these X-ray sources in broad-band filters at VBO.

Ten X-ray sources were identified in the error box of GRB 920622 (see Greiner 1995). Of these 5 were identified as likely AGN candidates. Two nights were allotted for this program in Dec 1997 which turned out to be cloudy. We observed one of the X-ray source RX J1052.5+4620 on Mar 1998 using 1.02 m telescope. Since the sky conditions were not photometric it was decided to monitor the field in a single bandpass to look for any variable object. We obtained eleven frames in V-band and 3 frames in I-band each of exposure 600 s. Seeing varied from 2".3 to 2".6 during these observations. The center of the field contained a HST guide star of V = 13 magnitude and within 10" from center are 2 faint sources suspected to be

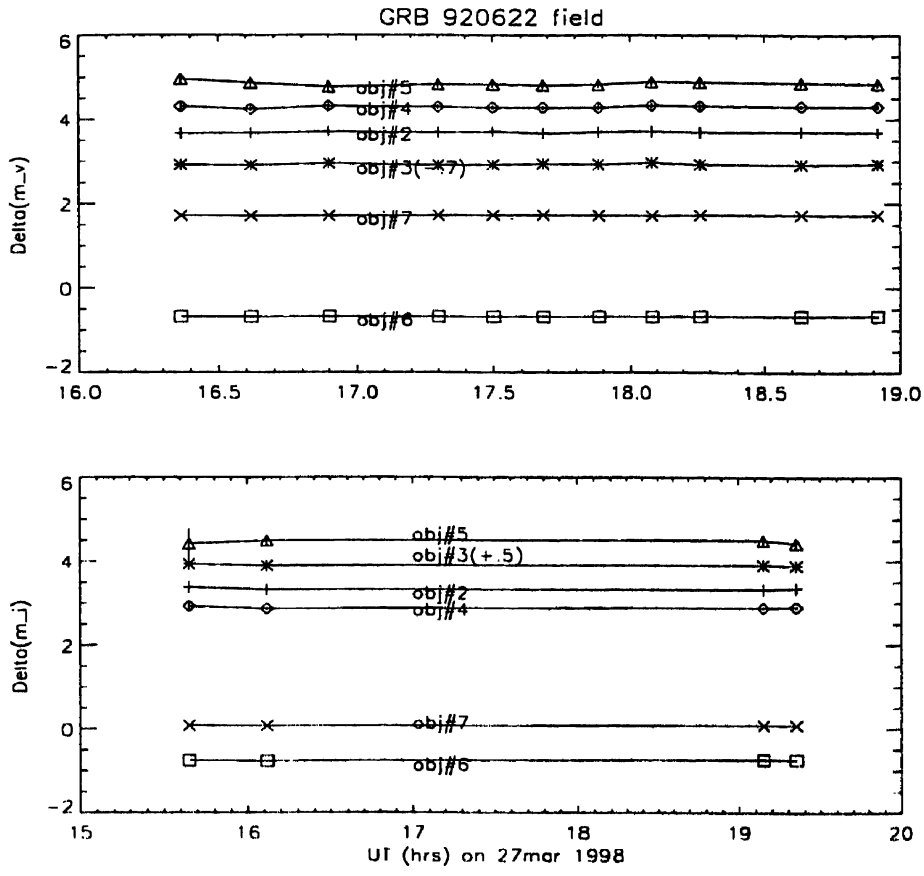

Figure 2.8: Monitoring of objects in GRB 920622 field: On the y-axis differential instrumental magnitude of 6 objects with respect to a GSC star in the field is plotted as a function of time.

variable from previous investigations (Greiner 1998; private communication). The magnitudes of these two sources along with a few objects were determined after applying suitable aperture corrections, using a reference star in the field. Fig 2.8 shows the differential magnitude of 6 objects in the field with respect to a HST guide star. The six objects remained constant in brightness within the photometric errors during $\sim$ 3 hours of observations.

6. GRB 990308

GRB 990308 was detected by the All-Sky Monitor on RXTE during a 90 s observation starting from 5.24 UT on 8 Mar 1999 and was localized by 10° × 6′.6 error box centered at RA = 12:11:2.84, Dec = 4:16:56.35 (J2000). Since it was also detected by BATSE and Ulysses, it was possible to obtain a refined localization later on.

Since the 1.02 m telescope time was allotted for our on-going program, it was possible to accomodate the observation of GRB 990308 field and we decided to take a few

frames of the central region of ASM error box on 17 Mar 1999. These observations didnot reveal any optical counterpart. However, we found 2 new asteroids in the frames, the analysis of which is presented in the next section.

7. GRB 981220

GRB 981210 was detected by RXTE/ASM on 20 Dec 1998 at 21:52 UT; the event lasted for 20 s. The burst was initially localized to an error box of $5' \times 60'.0$ centered at (J2000) RA = 03:43:01, DEC = 17:09:00 (Smith *et al.* 1998). We observed this field on 24 Dec 1998 using 2.34m VBT.[9] The sky conditions were clear with a seeing of $2''.2$. A series of 6 CCD frames, 15 min × 2 in V-band followed by 15 min × 4 in R-band were observed continuously from 16:12 UT to 17:55 UT.

In subsequent GCN notices Hurley *et al.* (1998) reported improved localization as the GRB was also detected by SAX/GRBM as well as Ulysses and KONUS. The new error box was $2'.4 \times 4'.5$ and the center was shifted by 27 s in RA. We could not intimate this change to the observatory due to non-availability of mode of communication and therefore the data observed on 24 Dec was not useful for GRB follow-up. The data analysis revealed a known asteroid. The details are presented in the next section.

[9]G. Selva Kumar and V. Ramana are acknowledged for taking these observations.

2.4 By-products of GRB Follow-up: New Asteroids

Repeated observations of GRB fields may be used to look for other interesting objects in the sky such as variable stars or moving objects. One does not strictly need photometric sky conditions to detect such objects. The brightness variation of a variable source can be measured relative to one or more local reference stars (as in the case of GRB 920622), whereas an asteroid or comet may be detected by its fast motion with respect to the background stars in successive CCD frames of the same region of the sky.

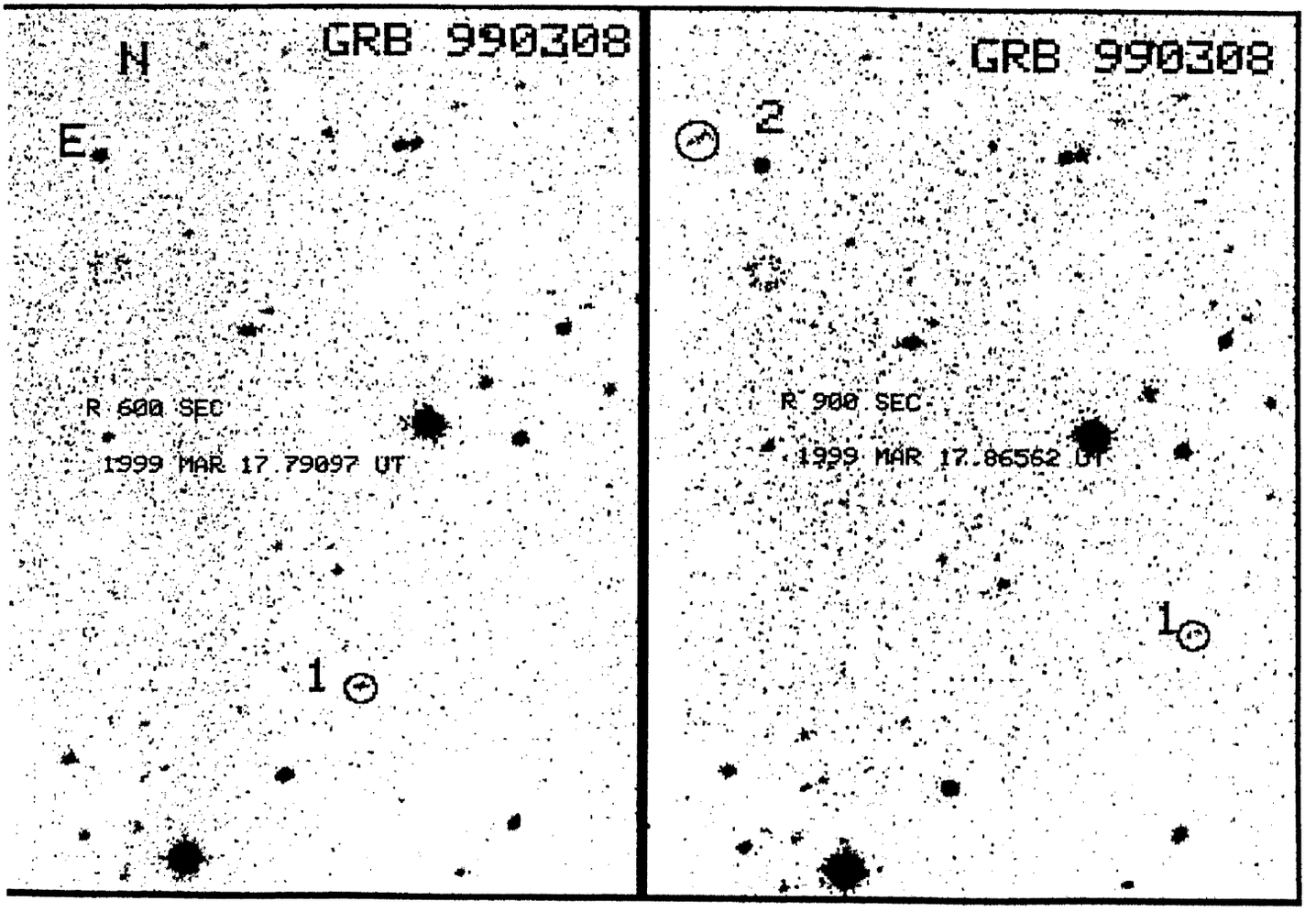

Figure 2.9: Field of GRB 990308 showing two **new asteroids:** The R-band image of 600 s (*left-panel*) observed at 18.9833 UT and R-band image of 900 s (*right-panel*) observed at 20.775 UT on 17 Mar 1999. The motion of Asteroid-1 can be clearly seen with respect to the background stars. Asteroid-2 was detected in the last two images including the one in the *right-panel*. Both the asteroids were heading in NW direction with a typical speed of main belt asteroids.

On 17th March we took several exposures of the field of GRB 990308. [10]

Table 2.4: GRB 990308: Observations & New Asteroid positions

Mid-UT	Filter	Exp. time (s)	Magnitude	RA (2000)	Dec (2000)	Asteroic
1999 03 17.79097	R	600	20.5	12:11:09.27	+04:16:30.3	1
1999 03 17.80243	V	1200	21.2	12:11:08.81	+04:16:34.4	1
1999 03 17.83785	R	900	20.3	12:11:07.39	+04:16:46.2	1
1999 03 17.85312	R	900	20.5	12:11:06.89	+04:16:50.8	1
				12:11:19.47	+04:19:17.8	2
1999 03 17.86562	R	900	20.5	12:11:06.33	+04:16:55.2	1
			20.6	12:11:18.88	+04:19:24.14	2

Between 18:54 UT and 20:54 UT we obtained a series of images in R and V-band filters. A quick-look analysis revealed a faint object moving in NW direction in all the frames and yet another faint streak in the last 2 frames. A search run using 'Minor Planet Checker' at MPC web-site *http://cfa-www.harvard.edu/iau/mpc.html* did not reveal any object in the observed frames at the time of our observations. This confirmed that the moving objects were new asteroids not reported so far. It is customary to report the detection of any new or catalogued minor planets to MPC by measuring their astrometric positions. As a first-hand information the offset of the asteroid from CCD center in every frame, approximate speed (in RA and Dec) as well as it's direction of motion were reported to MPC. Determination of precise

[10]It was worth arguing with the technical division to provide me the desired instrument - as the hard work rewards at times! On 18th evening I began to examine the images of the previous night after receiving the data. A faint asteroid showed up in all the images and yet another one in just 2 images of GRB 990308. I was desperate to check the Minor Planet Center (MPC) web site, if any known asteroid is expected to be in the field at the time of observation. Since VBO has no internet facility I could only think of phoning Dr R. Srikanth (who is generally at CC all through the night) at IIA, Bangalore and ask him to run the search programs at the MPC site. The telephone connection was extremely bad and I must say I was exhausted when I finished giving him all the instructions on how to run the search program. We tried VSET next and Srik said that the search came out with 'no objects fou.....' and then the connection broke. I could confidently conclude that I found 2 new asteroids and retire from work by 4 am. I did not feel the slightest of excitement but had the most peaceful, and un-interrupted 6 hours of sleep I could ever get during all my Kavalur trips over years!!

positions requires the co-ordinates of reference stars in the field and it had to wait until getting back to home institute at Bangalore.

Three stars were identified from HST-GSC within the frame and were chosen as reference stars to measure the precise position of asteroids in every frame. In Table 2.4 the measured positions in each frame along with the details of observations are tabulated. The magnitude of the asteroids were determined and calibrated with respect to seven Landolt's standard stars in SA-98 field observed on the same night.

Follow-up:

Table 2.5: Asteroid follow-up: Observations & Astrometry

Mid-UT	Filter	Exp.time (s)	Magnitude	RA(2000)	Dec (2000)	Asteroid
1999 04 11.6663	R	900	21.55	11:55:04.35	06:00:34.00	1
			21.07	11:55:07.00	06:03:21.63	2
1999 04 11.7135	R	900	21.55	11:55:01.86	06:00:36.36	1
			21.07	11:55:04.68	06:03:36.04	2
1999 04 11.7270	R	900	21.5	11:55:01.11	06:00:36.61	1
			21.18	11:55:04.01	06:03:40.46	2
1999 04 11.7440	R	900	21.48	11:55:00.57	06:00:37.18	1
			21.2	11:55:03.38	06:03:44.13	2
1999 04 11.7610	R	1200	22.08	11:54:59.08	06:00:38.24	1
			20.9	11:55:02.24	06:03:51.15	2

Following the confirmation of the asteroid discovery[11] and upon receiving a temporary designation (Marsden 1999; email communication) it's future positions were predicted using a software available at MPC. The follow-up observations were planned for 11 Apr 1999 at the same telescope. Five frames were observed in R-band under non-photometric sky conditions. Data analysis revealed both the asteroids. They were confirmed to be the same objects as their brightness, speed and direction of

[11] Asteroid discovery was the memorable incidence during my Ph D program that revealed the real world around me. I am grateful to prof R. Cowsik for the moral support and encouragement.

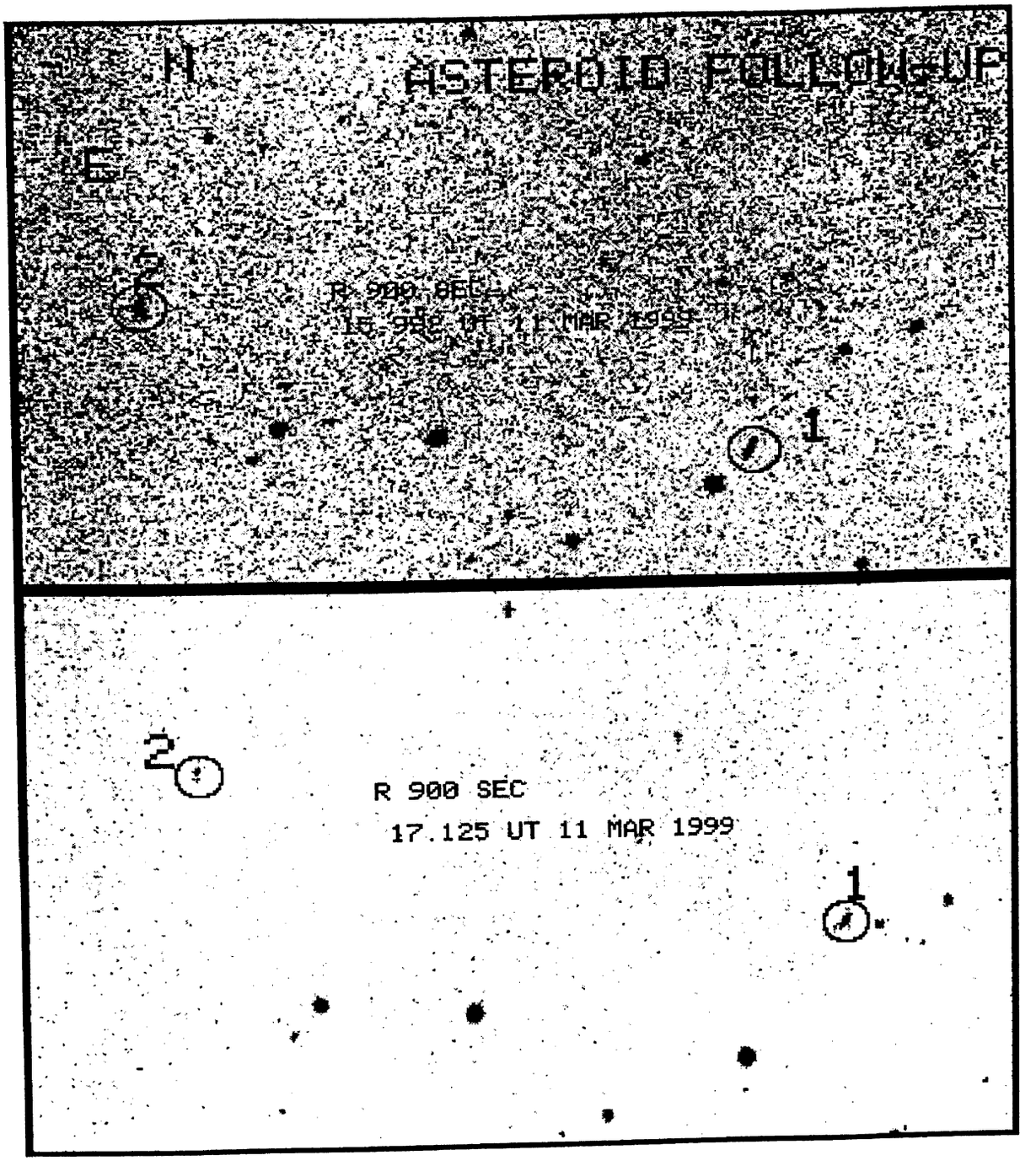

Figure 2.10: Follow-up of Asteroids: Region of the sky with predicted positions of asteroids was observed on 11 Mar 1999. In a series of 5 images both the asteroids were recovered. Asteroid motion in NW direction can be clearly seen with respect to the background stars in above images.

were confirmed to be the same objects as their brightness, speed and direction of motion were consistent with the expectations. The log of observations and new astrometric positions are as shown in Table 2.5. Photometric calibrations were carried out w.r.t Landolt's standard field PG0942-029 containing 5 standard stars observed

on that night. The astrometric positions were determined with respect to three HST-guide stars within the asteroid field.

Table 2.6: GRB 981220: Astrometry of 1618dawn

object	mid-UT	RA (2000) DEC
(1618)	1998 24 16.00833	03 43 06.10 +17 04 22.4
(1618)	1998 24 16.325	03 43 05.78 +17 04 22.15
(1618)	1998 24 16.79166	03 43 05.19 +17 04 21.88
(1618)	1998 24 17.125	03 43 04.64 +17 04 21.50
(1618)	1998 24 17.475	03 43 04.23 +17 04 21.23
(1618)	1998 24 17.79166	03 43 03.77 +17 04 21.01

A moving object of $\sim 16^{th}$ magnitude was identified among the 6 frames of the field of GRB 981220 observed on 24 Dec 1998. The object was suspected to be an asteroid. Further, Minor Planet Catalog was searched using the 'Minor Planet Checker' at http://cfa-www.harvard.edu/iau/mpc.html to see if any object is present at the time of our observation.[12] This revealed an object designated as '1618dawn'.

Astrometric positions of the asteroid in each frame were calculated with respect to 7 HST-Guide stars in the field and were then reported to the MPC (see Table 2.6). Such observational reports are useful in monitoring these objects and improving their orbital parameters.

At the time of our observation the asteroid was heading in South-West direction with a speed, $\Delta\alpha = 0'.326/\text{hr}$; $\Delta\delta = 0'.789/\text{hr}$ consistent with the speed of 1618 dawn.

[12] I Thank Dr A. K. Pati for his help in running the search program at MPC site.

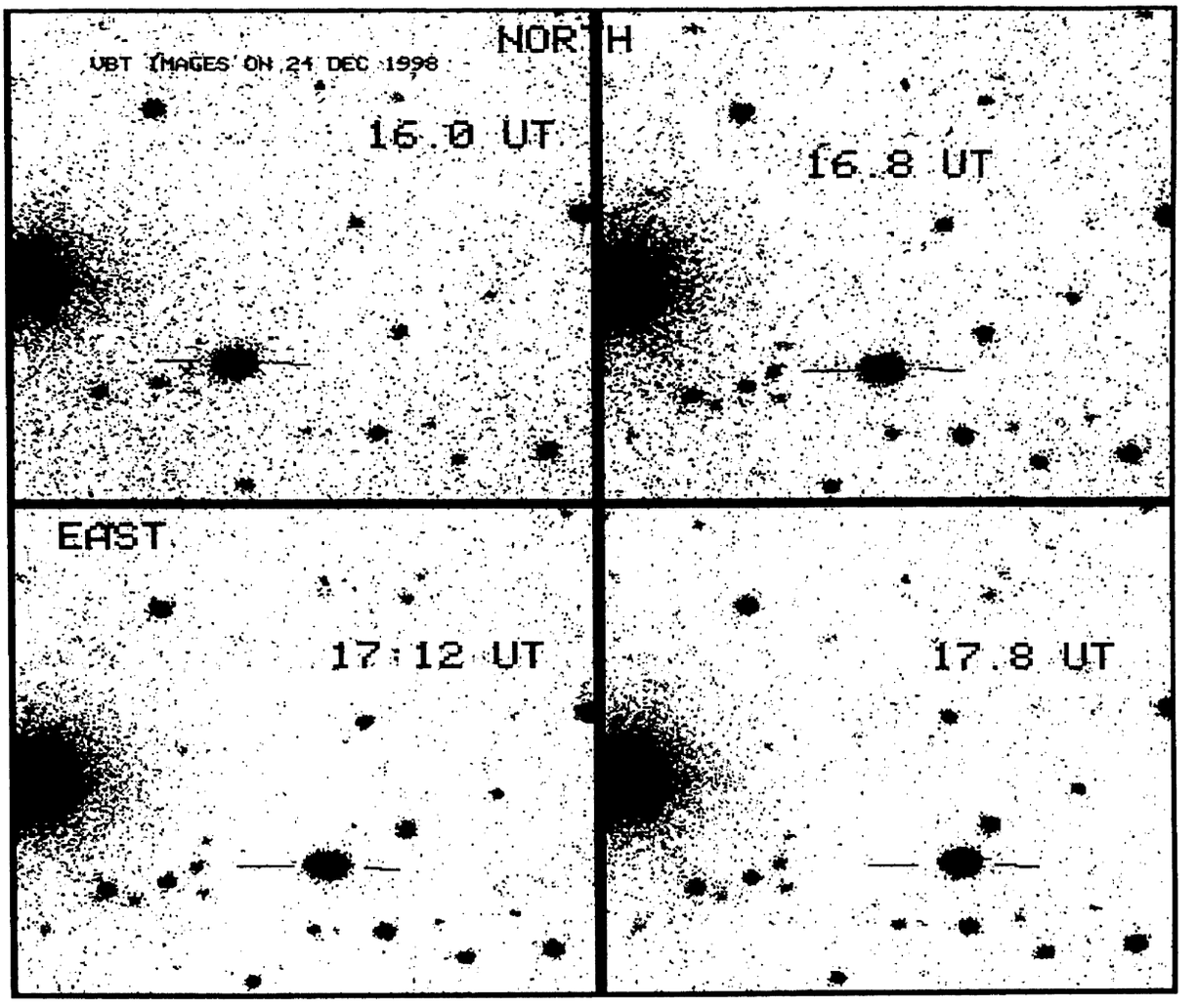

Figure 2.11: FOV of GRB 981220: Figure shows the motion of asteroid '1618 dawn' towards South-West direction with respect to the background stars in 4 successive CCD frames. North is top and East is to the left. Each frame is of size $2'.5 \times 2'.5$.

Appendix

Telescope Parameters

Two parameters are important in determining the FOV of a telescope: Plate or Image scale and size of the CCD.

Traditionally, the term 'plate scale' in units of arcsec/mm was in use when photographic plates were used for astronomical imaging. These days photographic plates are replaced by CCDs and therefore it is convenient to use the term 'Image scale' in units of arcsec/pixel.

An object with angular extension $\Delta\theta$ has a linear extension of $\Delta x = f \times \Delta\theta$ at the plane of the mirror. Then, the image scale (arcsec/mm) $\equiv \Delta\theta/\Delta x = 1/f$

The image scales (arcsec/pix) for 2.34 m VBT and 1.02 m telescopes using various CCDs and the corresponding FOVs are tabulated below:

Telescope	f-ratio	CCD#1 astromed 576×385 (22μ) (1995-96)	CCD#2 TEK 1024 (24μ) (1996)	CCD#3 TEK 1024 (24μ) (1997 - present)
VBT (FOV)	f/3.25	0″.55/pix (5′.3 × 3′.5)	0″.609/pix (10′.4 × 10′.4)	0″.609/pix (10′.4 × 10′.4)
1.02 m (FOV)	f/13	- n/a	0″.37/pix (6′.4 × 6′.4) (1998-99)	- n/a

The 2.01 m telescope at Hanle yields 0″.274/pix and with the TEK 1k CCD of $24\mu^2$ pixel the FOV is $\sim 4'.7 \times 4'.7$.

- f-ratio : is the ratio of focal length to the diameter of mirror; generally quoted as f/3.25, f/13 and so on.
- Cassegrain: is an arrangement to effectively increase the focal length, by introducing a secondary mirror into the light beam and reflect it to a focus behind the main mirror through a hole in the center of the main mirror.

Bibliography

[1] Antonelli, L. A. *et al.* 2001, GCN Circular. 944

[2] Berger, E. & Frail, D. A. 2001a, GCN Circular. 943

[3] Berger, E. & Frail, D. A. 2001b, GCN Circular. 968

[4] Berger, E. & Frail, D. A. 2000, GCN Circular. 546

[5] Berry, R. 1995, *'CCD Astronomy'*, vol. 2. No. 4. p.14

[6] Bhargavi, S. G. *et al.* 2000a, GCN Circular. 537

[7] Bhargavi, S. G., Gauba, G. & Cowsik, R. 2000b, GCN Circular. 554

[8] Bhattacharya, D. 2001, astro-ph/0104250

[9] Bloom, J. S. *et al.* 2001, GCN Circular. 989

[10] Castro, S. *et al.* 2001, GCN Circular. 999

[11] Costa, E. *et al.* 1997, 387, 783

[12] Costa, E. *et al.* 2000, GCN Circular. 542, 553

[13] Cowsik, R. *et al.* 2001a, GCN Circular. 978

[14] Cowsik, R. *et al.* 2001b, astro-ph/0104363

[15] Cowsik, R. & Bhargavi, S. G. 2001, GCN Circular 1051

[16] Di Paola, A. *et al.* 2001a, GCN Circular. 939

[17] Di Paola, A. *et al.* 2001b, GCN Circular. 977

[18] Fich, M. *et al.* 2001, GCN Circular. 971

[19] Frontera, F. *et al.* 2001, GCN Circular. 950

[20] Gandolfi, G. 2001a, GCN Circular. 932

[21] Gandolfi, G. 2001b, GCN Circular. 933

[22] Gandolfi, G. 2001c, GCN Circular. 937

[23] Gandolfi, G. 2001d, GCN Circular. 960

[24] Garcia, M. 2000, GCN Circular. 544, 548

[25] Garmire, G. P. *et al.* 2001, GCN Circular. 1005

[26] Garnavich, P. M. *et al.* 2001, GCN Circular. 965

[27] Gorosabel, J. *et al.* 2000a, GCN Circular. 545

[28] Gorosabel, J. *et al.* 2000b, GCN Circular. 547

[29] Gorosabel, J. *et al.* 2000c, GCN Circular. 783

[30] Gorosabel, J. *et al.* 2001, GCN Circular. 972

[31] Greiner, J. 1995, A & A 302, 121

[32] Greiner, J. 1997a, In proc. of the conf. *'All Sky X-ray observations in the next decade'* held at Tokyo, Mar 1997 (eds) M. Matsuoka & N. Kawai, p. 155; astroph/9704010

[33] Henden, A. 2001a, GCN Circular. 961

[34] Henden, A. 2001b, GCN Circular. 987

[35] Holland, S. 2001, GCN Circular. 1002

[36] Howell, S. B. 1992, *Astonomical CCD observing and reduction techniques*, ASP. Conf. Ser, Vol 23

[37] Howell, S. B. 2000, *Handbook of CCD Astronomy*, Cambridge University Press.

[38] Hurley, K. *et al.* 1988, GCN Circular. 160

[39] Hurley, K. *et al.* 2000a, GCN Circular. 529

[40] Hurley, K. *et al.* 2000b, GCN Circular. 543

[41] Jacoby, G. H. 1990, *CCDs in Astronomy*, Asp. Conf. Ser, Vol 8

[42] Jha, S. *et al.* 2001a, GCN Circular. 974

[43] Jha, S. *et al.* 2001b, astro-ph/0103081

[44] Kippen, M. R. 2000a, GCN Circular. 530

[45] Kippen, M. R. 2000b, GCN Circular. 549

[46] Klose, S. *et al.* 2001, GCN Circular. 997

[47] Kulkarni, S. R. *et al.* 2001, GCN Circular. 996

[48] Landolt, A. U. 1992, AJ, 104, 340

[49] Mackay, Craig, D. 1986, Ann. Rev. Astron. Astrophys., 24, 255

[50] Masetti, N. *et al.* 2001a, GCN Circular. 954

[51] Masetti, N. *et al.* 2001b, GCN Circular. 985

[52] Masetti, N. *et al.* 2001c, astro-ph/0103296

[53] McConnel, D. *et al.* 2000, GCN Circular. 560

[54] McLean, I. S. 1997, *Electronic Imaging in Astronomy*, Wiley.

[55] Pedersen, H. 2000, GCN Circular. 534

[56] Piro, L. 2001, GCN Circular. 959

[57] Press, W. H., et al. 1993, *'Numerical Recipes'*, Cambridge University Press

[58] Rol, E. *et al.* 2001a, GCN Circular. 955

[59] Rol, E. *et al.* 2001b, GCN Circular. 1059

[60] Sagar, R. *et al.* 2001, astro-ph/0104249

[61] Smith, D. A. *et al.* 1998, GCN Circular. 159

[62] Stanek, S. *et al.* 2001a, GCN Circular. 970

[63] Stanek, S. *et al.* 2001b, astroph/0104329

[64] Stetson, P. B. 1987, PASP, 99, 191

[65] Stornelli, M. 2000, GCN Circular. 540 (538,539)

[66] Van Paradijs, J. *et al.* 1997, Nature, 386, 686

[67] Veilett, C. 2001, GCN Circular. 1000, 1003

[68] Woods, D. 1995, ApJ, 454, 32

[69] Zhu, J. & Xue, S. J. 2001, GCN Circular. 938

GCN circulars may be found at *http://gcn.gsfc.nasa.gov/gcn/gcn3/*

Chapter 3

GRB000301c - First Afterglow detection from VBO

Abstract

We report multiband observations of the Optical Transient (OT) associated with GRB000301c carried out between 2-4 March 2000 using the 2.34-m Vainu Bappu Telescope (VBT) at Kavalur, India. When combined with other reported data, the initial decline in the R-band magnitude with log $(t - t_0)$, the time since the burst is fit with a slope α_1 = -0.70 ± 0.07 which steepens after about 6.0 days to a slope of α_2 = -2.44 ± 0.29. This change in slope does not occur smoothly but there is an indication for a bimodal distribution. The available measurements of the evolution of (B-R) color do not show any discernible evolution in the first 12 days.

3.1 The Burst

GRB000301c was detected by All Sky Monitor (ASM) on board *Rossi X-Ray Timing Explorer (RXTE)* on 2000, March 1.4108UT and also by two other spacecrafts *Ulysses* and *NEAR*. The burst had a single peak with slow decay structure lasting 10 seconds and was localized by an error box of area 50 sq. arcmin centred at (J2000.) RA=$16^h20^m21^s.5$, DEC=+29°24′56″.37 (Smith, Hurley & Cline 2000). The Optical counterpart was first reported by Fynbo *et al.* (2000a) and the redshift has been measured to be z=1.95 ± 0.1 by Smette *et al.* (2000) using HST and to be z=2.03 ± 0.003 by Castro *et al.* (2000) using the Keck-II telescope. The R-band magnitude of the OT has been estimated to be R = 27.9 ± 0.15 from the HST imaging on 19 Apr,

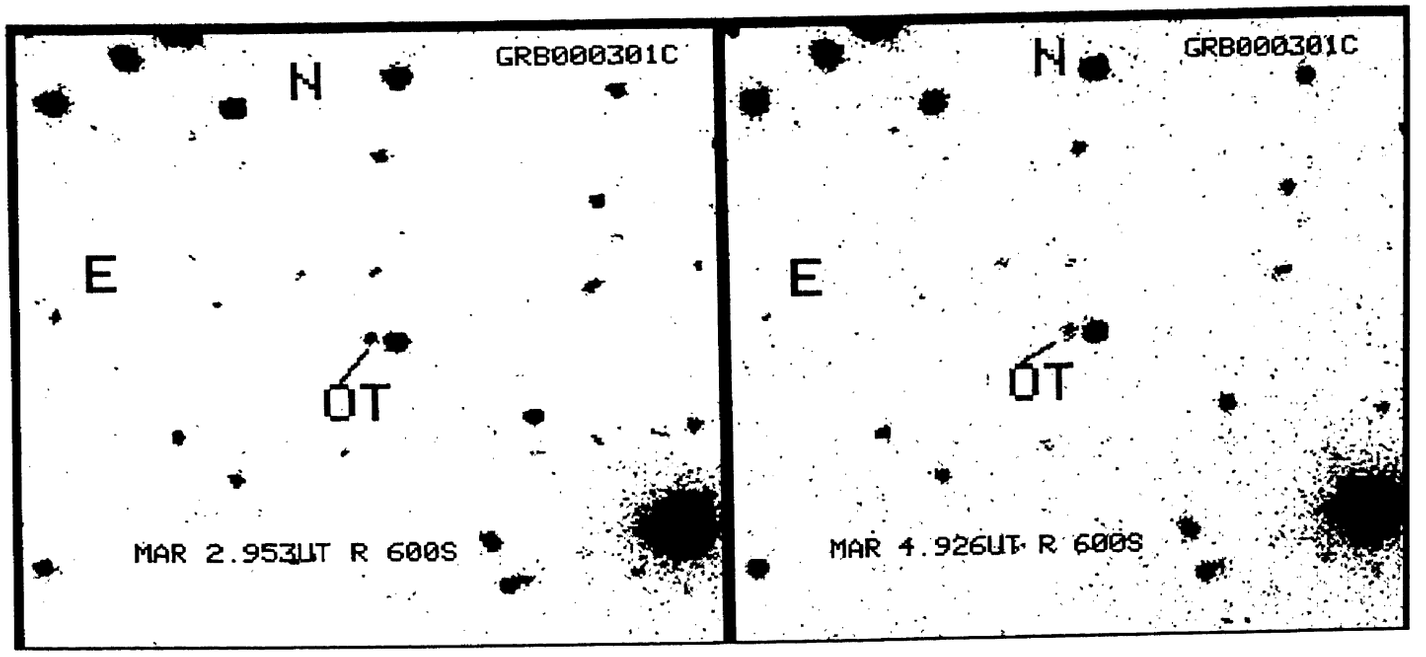

Figure 3.1: The R-band images of GRB000301c field of exposure 600 s each taken on Mar 2.9953UT and Mar 4.9257UT where the fading of OT is clearly seen. The image portions shown here are of size $2'.6 \times 2'.6$; North is up and East is to the left.

2000, but no evidence of a host galaxy was found to a magnitude of 28.5 (Fruchter *et al.* 2000a). Late-time HST observations were carried out on 25 Feb 2001, nearly one year after the burst and a tentative detection of host galaxy has been reported by Fruchter & Vreeswijk (2001). The estimated magnitude of the host is $R = 28.0 \pm 0.3$ and it lies within $0''.1$ of the position of OT.

3.2 Optical Observations, Data Reductions and Analysis

At the Vainu Bappu Telescope (VBT), the follow-up observations in the B, R and I bands of GRB000301c began 3 hours after the e-mail notification of the burst event on March 2, 2000. We could continue the observations on March 3 and 4 also as the telescope time was already allocated for our ongoing program on GRBs. Our observations were carried out with a Tek 1024 CCD with $24\mu \times 24\mu$ pixels positioned at the f/3.25 prime focus of the telescope covering a FOV of $10'.4 \times 10'.4$ with an image scale of $0.''61$/pixel. The sky conditions were clear with an average seeing of $2.''5$; however, the quality of the acquired data was found to be better on March 2 and 4 compared to those obtained on March 3. We show in Fig 3.1 two R-band

images each of 600s exposure taken on March 2.953UT and 4.9257UT where the fading of the OT is seen clearly. The details of the observations along with the magnitudes are summarized in Table 3.1.

Table 3.1: GRB 000301c: Observations at VBT

UT(days)	Filter	Total exp (sec)	Magnitude of OT	Mag error	Remarks
Mar 2.9618	R	2400	20.02	0.028	4 x 600s summed
Mar 2.9986	B	1200	20.99	0.17	single frame
Mar 3.9323	R	1800	20.45	0.12	3 x 600s summed
Mar 3.9976[1]	R	1200	20.49	0.10	2 x 600s summed
Mar 3.9694	I	3000	20.09	0.10	2 x 600s + 2 x 900s
Mar 4.9087	R	3600	20.57	0.05	6 x 600s summed
Mar 4.9799	B	1800	21.29	0.12	single frame
Mar 4.9517	I	1800	19.96	0.05	3 x 600s summed

The pre-processing of CCD frames viz. de-biasing, flat-fielding and removal of cosmic rays were accomplished in a standard manner using the *IRAF* software package as described in chapter 2. Thereafter the images taken with the same filters were aligned and co-added.

About 40 isolated stars were chosen as secondary standards for which photometry were made available by Henden (2000). Instrumental magnitudes of these along with four stars marked as A, B, C, D by Garnavich (2000) and of OT were determined at an aperture of 7″.2. Aperture corrections were applied for fainter objects including the OT. The sky background has been estimated using an annulus of 10″ width at a distance of 16″ from each object that is measured. Since the average seeing was 2.″5 in some of our R-band exposures the OT is blended with the nearby star 'A' of Garnavich(2000) at a distance of about 6″. In such instances we have also estimated the magnitude of OT by masking the nearby bright star after fitting a circularly symmetrical Gaussian profile and obtained consistent results. The calibration solutions (Fig 3.2) are derived by fitting the transformation equations (Eq. 3.1) to

the select stars in the field and from these the magnitudes of OT and the refernce stars of Garnavich (2000) are derived. The magnitudes as well as the colors of select stars obtained in this manner were in good agreement with the values provided by Henden (2000) and had residuals in the range 0.001 mag to 0.01 mag indicating the degree of reliability of our photometric measurements. As an example we show the fit for the March 4 data: (The transformation coefficients derived for 2 & 3 Mar are close to the ones obtained for 4 Mar).

$$\begin{aligned} B-R &= (0.9672 \pm 0.02) \times (b-r) - (1.4341 \pm 0.06) \\ B &= m_b + (0.0308 \pm 0.01) \times (B-R) - (5.4849 \pm 0.01) \\ R-I &= (1.0095 \pm 0.02) \times (r-i) - (0.1731 \pm 0.02) \\ R &= m_r + (0.0581 \pm 0.036) \times (R-I) - (3.9659 \pm 0.017) \\ B-I &= (0.9928 \pm 0.02) \times (b-i) - (1.6431 \pm 0.10) \\ I &= m_i + (0.0132 \pm 0.01) \times (B-I) - (3.7833 \pm 0.02) \end{aligned} \tag{3.1}$$

With such a fit, difference between the colors given by Henden and those measured by us for the 3 reference stars A, B & D are as shown in Table 3.2. (The corresponding values for reference star 'C' are not given because it's R-I color was not available in Henden's catalog).

Table 3.2: Residual magnitudes and colors

Star	δ(B–R)	δ(B)	δ(R–I)	δR	δ(B–I)	δ(I)
A	0.0505	0.0144	-0.0199	0.0043	-0.0042	0.011
	± 0.09	± 0.039	±0.026	±0.028	±0.01	±0.03
B	-0.1013	-0.135	-0.0397	0.0326	-0.1902	0.065
	±0.13	±0.096	±0.038	±0.045	±0.02	±0.04
D	0.010	-0.0075	0.0079	-0.0056	-0.0032	-0.026
	±0.08	±0.025	±0.023	±0.022	±0.01	±0.02

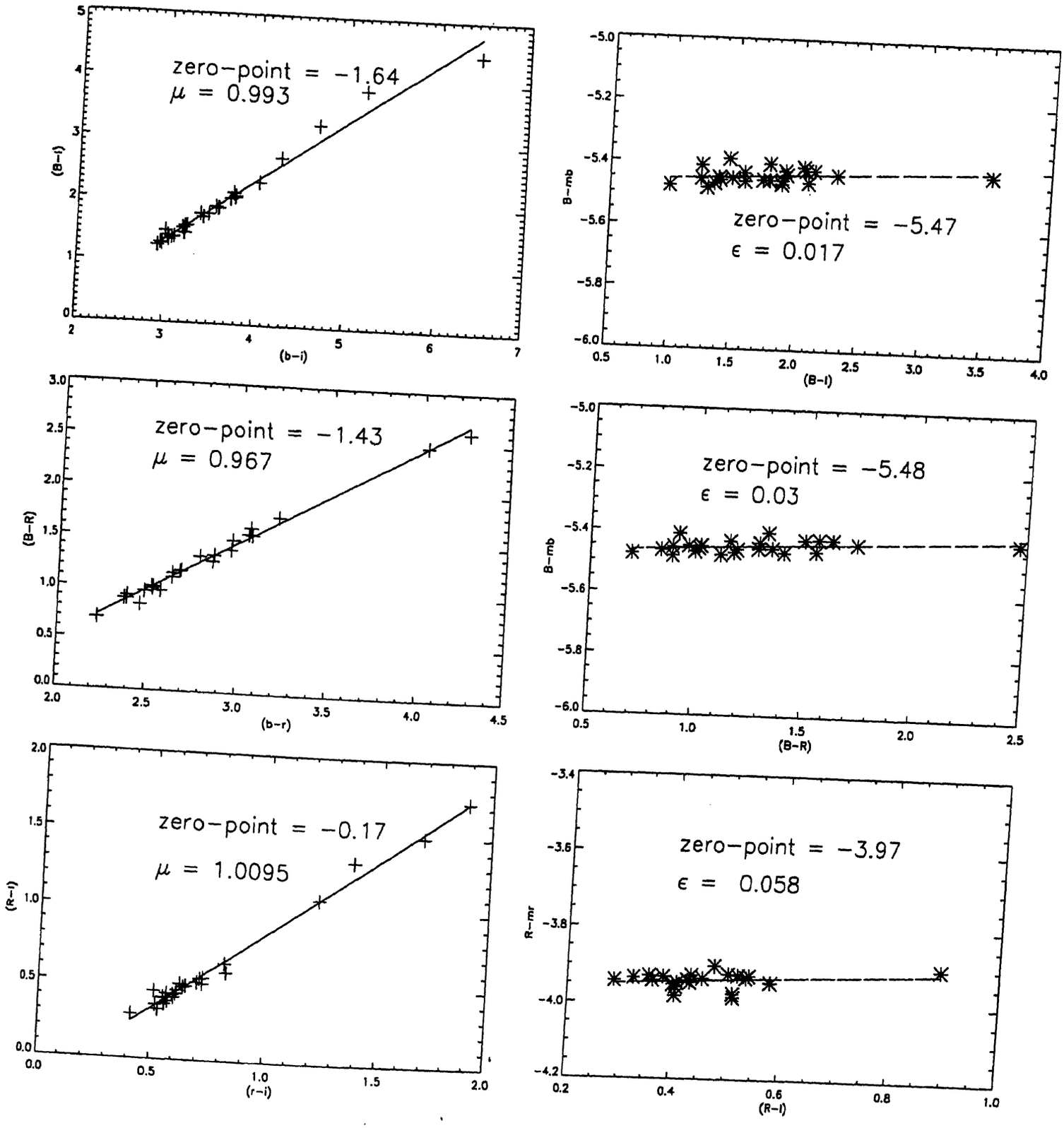

Figure 3.2: Calibration solutions for 4 Mar 2000 data. The notations B, R, I, B–R, B–I and B–R refer to standards from Henden's photometry.

3.3 Light curve fit

In order to place our observations in the context of other observations in the R-band we have collected the data available through GCN circulars and those given by Jensen *et al.* (2000) (in thier Table 2) who have perhaps the most extensive coverage of the event. Following the standard practice in combining the photometric data obtained by different groups and different instruments, we renormalize all measurements to that of Jensen *et al.* (2000). The corrections applied to various data sets is shown in Table 3.4. Notice the correction for our observations at VBT is < 0.01m and falls within the uncertainty in the observations.

We attempt to fit the data on intensities in R-band to a time evolution defined by Eq. 3.2.

$$\begin{aligned} I(t) &= I(t_1)(t/t_1)^{\alpha_1} \qquad \text{for } t < t_1 \\ I(t) &= gI(t_1)(t/t_1)^{\alpha_1} + (1-g)I(t_1)(t/t_1)^{\alpha_2} \text{ for } t_1 \leq t < t_2 \\ I(t) &= \{g(t_2/t_1)^{\alpha_1} + (1-g)(t_2/t_1)^{\alpha_2}\}I(t_1)(t/t_2)^{\alpha_2} \text{ for } t \geq t_2 \end{aligned} \tag{3.2}$$

This form is motivated by the feature observed in the R-band light curve at $t - t_0 \approx 4.5$ days. This might have been generated by a major burst and followed after a short interval by a minor burst, each being represented by a powerlaw form with a slope α_1 which at later times steepens to a slope α_2. The function given in Eq. 3.2 is designed to test this hypothesis. Notice that this function has 6 parameters $I(t_1)$, g, t_1, t_2, α_1 and α_2, two more than than the functional form adopted by Jensen *et al.* (2000).

Table 3.3: R-band data from literature

UT(days)	R	σ(R)	Authors
2.930	20.42	0.06	Sagar *et al.*
2.962	20.02	0.028	Bhargavi & Cowsik
3.140	20.09	0.04	Jensen *et al.*
3.144	20.25	0.05	Masetti et al.
3.170	19.94	0.04	Fynbo et al. (2000b)
3.170	20.15	0.04	Jensen et al.
3.190	20.11	0.04	Jensen et al.
3.191	20.11	0.05	Bernabei et al.
3.200	20.14	0.05	Jensen et al.
3.205	20.25	0.05	Masetti et al.
3.210	20.14	0.04	Jensen et al.
3.220	20.11	0.05	Jensen et al.
3.240	20.12	0.06	Jensen et al.
3.250	20.16	0.04	Jensen et al.
3.260	20.09	0.08	Jensen et al.
3.270	20.08	0.07	Jensen et al.
3.510	20.28	0.05	Garnavich et al.
3.510	20.27	0.04	Veilet & Boer
3.510	20.24	0.05	Halpern et al.
3.930	20.53	0.05	Mohan et al.
3.998	20.49	0.1	Bhargavi & Cowsik
4.038	20.53	0.06	Masetti et al.
4.052	20.46	0.09	Castro-Tirado et al.
4.079	20.57	0.06	Gal-Yam et al.
4.140	20.59	0.11	Jensen et al.
4.178	20.22	0.20	Bernabei et al.
4.380	20.56	0.05	Garnavich et al.
4.390	20.53	0.12	Jensen et al.
4.410	20.44	0.06	Jensen et al.
4.420	20.61	0.06	Jensen et al.
4.430	20.42	0.12	Jensen et al.
4.458	20.54	0.06	Mujica et al.
4.480	20.58	0.04	Jensen et al.
4.490	20.54	0.04	Jensen et al.
4.500	20.61	0.04	Halpern et al.
4.500	20.60	0.04	Jensen et al.
4.520	20.51	0.05	Jensen et al.
4.909	20.58	0.048	Bhargavi & Cowsik
5.135	20.47	0.07	Masetti et al.
5.230	20.73	0.13	Jensen et al.
5.390	20.61	0.05	Jensen et al.
5.630	20.86	0.04	Veilet & Boer
5.960	21.18	0.05	Mohan et al.
6.145	21.60	0.20	Bernabei et al.
6.220	21.50	0.15	Fruchter et al. (2000b)
6.390	21.43	0.26	Jensen et al.
6.968	21.70	0.13	Masetti et al.
7.135	21.63	0.15	Bernabei et al.
7.220	21.59	0.07	Jensen et al.
7.230	21.62	0.155	Jensen et al.
7.240	21.52	0.08	Jensen et al.
7.650	21.74	0.07	Veilet & Boer
7.930	21.95	0.1	Sagar et al.
8.157	21.63	0.1	Bernabei et al.
8.180	21.80	0.05	Jensen et al.
8.200	21.88	0.09	Jensen et al.
8.210	21.98	0.08	Jensen et al.
8.250	22.09	0.13	Jensen et al.
8.950	22.13	0.1	Sagar et al.
9.150	22.11	0.15	Jensen et al.
9.200	22.29	0.21	Jensen et al.
9.240	22.10	0.11	Jensen et al.
9.260	22.21	0.155	Jensen et al.
9.520	22.28	0.09	Halpern et al.
10.050	22.34	0.20	Jensen et al.
10.400	22.49	0.30	Jensen et al.
11.21	23.12	0.27	Jensen et al.
11.39	23.12	0.18	Jensen et al.
11.63	23.02	0.1	Veillet & Boer
12.44	23.10	0.22	Jensen et al.
14.60	23.82	0.1	Veillet & Boer

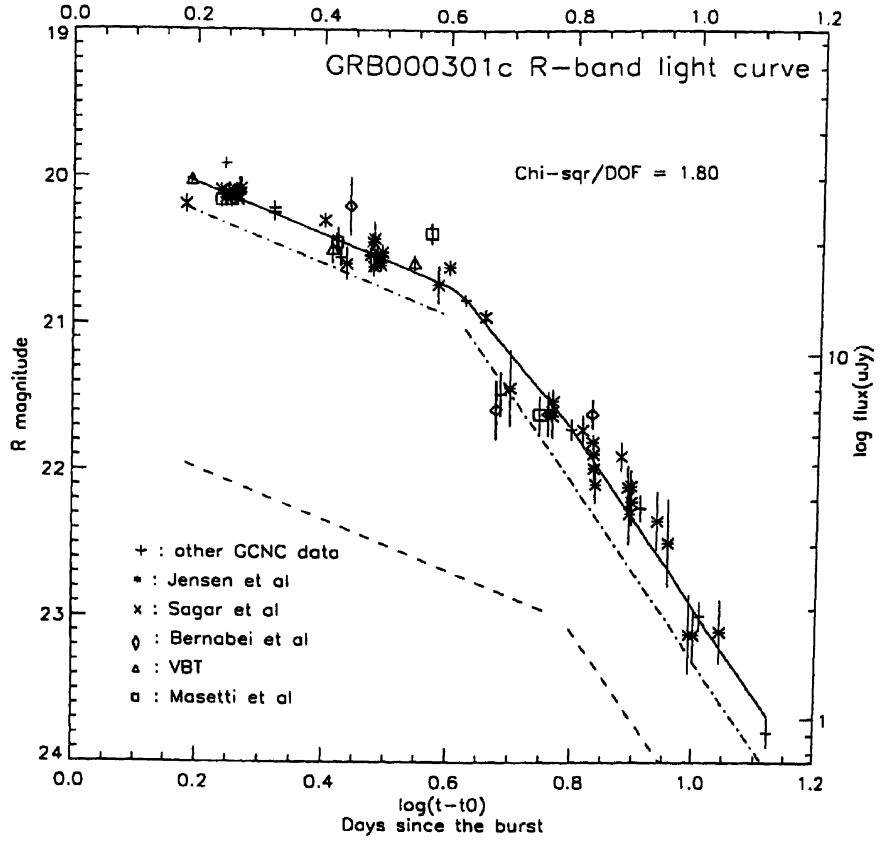

Figure 3.3: GRB000301c R-band light curve: The dotted and dashed lines represent the major and minor burst which add up to give the light curve shown as a solid line.

Table 3.4: Magnitude corrections

Data set	Magnitude shift
vbt	-0.009
Masetti	0.088
Bernabei	-0.02
Sagar	0.232
Other GCN data	0.03

The values of the parameters and their 1σ errors which provide the best fit to the data along with the normalized χ^2 are computed using 'Levenberg-Marquardt method' (Press 1992) and are listed in Table 3.5. Notice that our fit for very early and very late times coincides quite closely with the fit obtained by Jensen *et al.*

(2000) and has a normalized $\chi^2 = 1.80$ (d.o.f=65). Even though Jensen *et al.* (2000) obtain with a single break an excellent fit to their own data, the single-break form fails to reproduce the collection of world data which have a slightly closer coverage around the break point at 4–5 days after the burst; the χ^2 they quote for the fit to the world data is 3.687 for $\nu = 88$. After applying the corrections given in Table 3.4 to the data in Table 3.3, we fit the single-break form in equation (1) of Jensen *et al.* (2000) and find that the χ^2_{64} reduces to 1.95 from its value of 2.85 for the same data points when no magnitude corrections are applied. Thus, with suitable corrections for normalizing different photometric data the χ^2 reduces to 1.8 ($\nu = 65$) for the two-break form and to 1.95 ($\nu = 64$) for the single-break form. The improvement on the χ^2 with double break is significant at the 38% level as seen from the F-distribution test, although we can not rule out the fact that the high chi^2 may be due due to genuine variations due to inhomogeneities in the medium surrounding the GRB host.

The motivation for the function given in Eq. 3.2 is clearly seen in Fig 3.3 The OT is fit with two events each of the type where a power-law decay sharply steepens into another power-law several days after the burst. The light curve in the K-band reported by Rhoads & Fruchter (2000) agrees broadly with the fit we have obtained here for the first break (Eq 3.2). If their curve is simply extrapolated and compared with the data obtained by Jensen et al. (2000) in the later and fainter epochs then one may find an apparent color evolution. More accurate photometry with better coverage is needed to confirm and characterize the possible existence of secondary events which may be expected in some refreshed-shock models (Mészáros, Rees and Weijers 1998). In the case of GRB980228 the re-brightening of the afterglow ~3 weeks after the burst event and the reddening of the spectrum have been hypothesized (Bloom et al. 1999) to be due to an underlying SN explosion which triggered from the energy released by a 'Collapsar' (MacFadyen & Woosely 1999) that gave rise to the initial GRB event. Reichart(1999) also explained the color evolution in case of GRB980228 using the supernova hypothesis.

3.4 Discussions & Conclusions

To check if there are any color changes during the evolution we display in Fig 3.4 the behaviour of the light curve both in the B and in the R bands using the B–R

Table 3.5: Fit parameters

Parameter	Value	Error
$I(t_1)$	14.88 μJy	1.28 μJy
g	0.169	0.30
t_1	4.12 days	0.30 days
t_2	6.07 days	0.44 days
α_1	-0.70	0.07
α_2	-2.44	0.29
χ^2/DOF	1.80	-
goodness-of-fit	2.65×10^{-4}	-

data tabulated in Table 3.6. It is seen that the evolution of R and B magnitudes are nearly the same within the photometric uncertainties. This result has been reported by Jensen et al. (2000) and Masetti et al. (2000) with a smaller sample, although Rhoads & Fruchter (2000) finds shift in R–K' color towards blue. Running a F-test (Press et al. 1992) gives 90% probability that the two distributions are equal. The color B–R can be fit with a function $(B-R) = a(t-t_0)^n$ where, a and n are the two fitted parameters. Our best fit values are: $a = 0.793 \pm 0.073$ and the slope $n = 0.073 \pm 0.074$ with a reduced $\chi^2 = 1.3$. This is consistent with the achromatic behaviour of the B–R evolution. Hence chromatic behaviour is not established on the basis of B–R data and the suggestions of color variations are based on comparison of R-evolution with the K data by Rhoads & Fruchter (2000).

The steepening in the light curve of afterglow of GRB 000301c was attributed to jet geometry by Berger *et al.* (2000), while Rhoads & Fruchter (2000) argued that jet collimation is not responsible for the sharp break. The fluctuations of short time scale seen in the light curve were interpreted as due to the the irregularities in the medium by Masetti *et al.* (2000b), while Garnavich *et al.* (2000) interpreted it as an evidence for gravitational microlensing due to an intervening star. In a detailed analysis Panitescu (2000) showed that microlensing by a star in an intervening galaxy can only produce flattening in the light curve and can not explain the brightening seen $\sim$ 4 days.

Table 3.6: B–R color

UT(days)	B–R	σ(B–R)	Authors
2.975	0.9686	0.207	Bhargavi & Cowsik
3.162	0.82	0.07	Masetti *et al.*
3.51	0.84	0.06	Veillet & Boer
4.52	0.77	0.06	Halpern *et al.*
4.9375	0.734	0.14	Bhargavi & Cowsik
5.1435	1.13	0.21	Masetti *et al.*
6.149	0.80	0.25	Masetti *et al.*
7.137	0.75	0.212	Masetti *et al.*
14.6	1.01	0.12	Veillet & Boer

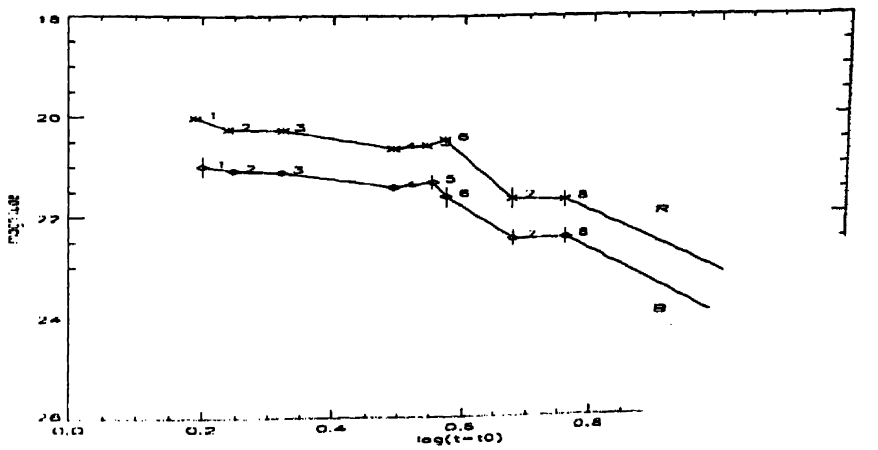

Figure 3.4: GRB000301c B-

Bibliography

[1] Bernabei, S., Bartolini, C., Di Fabrizio, L., Guarnieri, A., Pic cioni, A., Masetti, N. 2000, GCN Circular 599

[2] Bhargavi, S. G. & Cowsik, R. 2000c, GCN Circular 591, 630

[3] Castro, S. M., Diercks, A., Djorgovski, S. G., Kulkarni, S. R., Galama, T. J., Bool, J. S., Harrison, F. A., Frail, D. A. 2000, GCN Circular 605

[4] Castro-Tirado, J. A., Bock, H., Greiner, J., Klose, S., Gorosabel, J. 2000, GCN Circular 579

[5] Costa, E. *et al.* 1997, Nature, 387, 783

[6] Fruchter, A. S. & Vreeswijk, P. 2001, GCN Circular. 1063

[7] Fruchter, A. S., Metzer M. and Petro L. 2000a, GCN Circular 701.

[8] Fruchter, A. S., Smette, A., Gull, T., Gibbons, R., Ferguson, H ., Petro, L., Sahu, K. 2000b, GCN Circular 602

[9] Fynbo, J. P. U., Jensen, B.L., Pedersen, H., Gorosabel, J. 2000a, GCN Circular 570

[10] Fynbo, J. P. U., Jensen, B.L., Pedersen, H., Gorosabel, J. 2000b, GCN Circular 576

[11] Gal-Yam, A., Ofek, E., Maoz, D., Leibowitz, E. M. 2000, GCN circular 593

[12] Garnavich, P., Barmby, P., Jha, S., Stanek, K. 2000, GCN Circular 573

[13] Halpern, J. P., Mirabal, N., Lawrence, S. 2000a, GCN Circular 578

[14] Halpern, J. P., Mirabal, N., Lawrence, S. 2000b, GCN Circular 582

[15] Halpern, J. P., Kemp, J. 2000c, GCN Circular 604

[16] Henden, A. A. 2000, GCN Circular 583

[17] Jensen, B. L. 2000, astroph/0005609

[18] Kulkarni, S. R. *et al.* 2000, astroph/0002168

[19] Masetti, N. *et al.* 2000, astroph/0004186

[20] Mészáros, P., Rees, M. J., Wijers, R. A. M. J. 1998, ApJ, 499, 301

[21] Mohan, V., Pandey, A. K., Pandey, S. B., Sagar, R. 2000, GCN Circular 595

[22] Musica, R., Chavushyan, V., Zharikov, S., Tovmassian, G. 2000, GCN Circular 597

[23] Piran, T. 1999, Physics Reports, 314, 575 (astroph/9810256)

[24] Press, W. H., *et al.* 1992, 'Numerical Recipes', (2d ed.; Cambridge: Cambridge University press).

[25] Sagar, R., Mohan, V., Pandey, S. B., Pandey, A. K., Castro-Tirado, A. J. 2000, astroph/0004223

[26] Smette, A., Fruchter, A. S., Gull, T., Sahu, K., Ferguson, H., Petroa, L., Lindler, D. 2000, GCN Circular 603

[27] Smith, D. A., Hurley, K., Cline, T. 2000, GCN Circular 568

[28] Van Paradijs, J. *et al.* 1997, Nature, 386, 686

[29] Veillet, C., Boer, M. 2000, GCN Circular 588, 598, 610, 611

GCN circulars may be found at *http://gcn.gsfc.nasa.gov/gcn/gcn3/*

Chapter 4

Luminosity Function of GRBs

Abstract

We attempt to constrain the luminosity function of Gamma Ray Bursts (GRBs) from (a) the observed number count–flux relation and (b) the afterglow redshift data. We consider three classes of luminosity functions for our analysis: Log-normal distribution, Schechter distribution, and Scale-free distribution with several models of the evolution of the GRB population. Our analysis shows that: log-normal is the only luminosity function that is compatible with both (a) and (b). This result is independent of the GRB evolution model; for log-normal function, the average photon luminosity L_0 and the width of the luminosity function σ that are compatible with both (a) and (b) fall in the range: $10^{55}\,\mathrm{sec}^{-1} \lesssim L_0 \lesssim 10^{56}\,\mathrm{sec}^{-1}$ *and* $2 \lesssim \sigma \lesssim 3$*; the agreement of observations with other luminosity functions requires the GRB population to evolve more strongly than the evolution of the star-formation rate of the universe.*

4.1 Introduction

The afterglow observations of GRBs have firmly established their cosmological origin (Kulkarni *et al.* 2000). The afterglow database (Greiner 2001) is sufficiently large that one could now think of using these data for other studies in astronomy. For instance, one could address the issue concerning the luminosity distribution of GRBs using the redshift measurements available in this database. The luminosity distribution of GRBs was hitherto obtainable only from the number count-flux relationship (see next section).

We take two approaches to estimate the luminosity functions of GRBs: (a.) using the redshift measurements for a sample of $\sim$ 16 GRBs from afterglow observations; (b.) using the number-count v/s flux (i.e, log $\mathcal{N}$ - log $\mathcal{F}$) relation for GRBs in the current BATSE catalog. We assume a cosmological model (with $\Omega_m = 0.3\,, \Omega_\lambda = 0.7\,, H_0 = 65$Km/s/Mpc) that is most favoured by recent observations to fit the log $\mathcal{N}$ - log $\mathcal{F}$ curve theoretically. In doing so, we consider various luminosity functions of galaxies (viz. Schecter, scale-free and log-normal) each with 'no-evolution' and some of the evolutionary models consistent with star-formation histories. We check if the luminosity functions obtained from log $\mathcal{N}$ - log$\mathcal{F}$ relation for BATSE GRBs is consistent with the one determined for a sample of GRBs where redshift measurements are available from afterglow observations.

In the next section a brief review on earlier work in the literature is presented. In §3 we describe the number–count method and models we used for luminosity function and GRB number density evolution. In §4 we discuss the Likelihood method used for extracting information about the luminosity function parameters from the afterglow redshift data. The results are presented and discussed in §5. Throughout this paper we assume a cosmological model with $\Omega_m = 0.3\,, \Omega_\Lambda = 0.7\,, H_0 = 65\,$Km/s/Mpc; this model is favoured by recent observations (Perlmutter *et al.* 1998, de Bernardis *et al.* 2000).

4.2 Previous work: A brief Review

Luminosity function of a population of sources, $\phi(L)$ is the number of sources/unit volume having luminosity in range (L, L+dL) with the normalization $\int \phi(L)dL = 1$. The galaxy LF is well studied (see Bingelli *et al.* 1988). However the LF of GRBs is not established since the redshifts were not available until recently. Hence the studies on luminosity function of GRBs depended on statistical approaches (mainly number count–flux relation). This indirect method requires additional knowledge about the evolution of sources and their redshift distribution. In their earliest studies, Mao & Paczyński (1992) assumed GRBs to be standard candles (all GRBs have the same luminosity) with identical power-law spectra. They also assumed that GRBs do not evolve in number density (rate of bursts is constant/comoving volume/unit comoving time). In later analyses (see e.g. Woods & Loeb 1995) several of these assumptions were dropped. In many of these analyses (Piran 1992, 1999; Mao & Paczyński

1992; Woods & Loeb 1995, Lubin & Wijers 1993; Ulmer & Wijers 1995; Ulmer *et al.* 1995; Cohen & Piran 1995; Hogg & Fruchter 1998) it was shown that the number count–flux relation is consistent with a wide variety of GRB evolution histories and LF widths. We confirm this result for the full BATSE sample and compute allowed parameters for several assumed luminosity functions and for several evolution models of GRB population.

4.3 The $\mathcal{N}(>F)$–F of BATSE GRBs

For calculating the number of bursts exceeding a given flux F, $\mathcal{N}(>F)$, from BATSE sources we first need to define the 'flux' of a GRB. The current BATSE catalog (Paciesas 2000) provides fluence (in erg/cm^2) and the peak flux (in photons/cm^2/s) values for 2093 burst events. The peak fluxes in the energy range 50 kev to 300 kev are available for three integration times: 64, 256 and 1024ms. We use the BATSE peak photon flux F, averaged over the trigger time of 1.024 seconds as being representative of GRB flux. This is related to the photon luminosity L in photons sec^{-1} (see **Appendix A** for a derivation):

$$F = \frac{L(1+z)^{2-\alpha}}{4\pi D_L^2} \tag{4.1}$$

Here, F is in units cm^{-2}sec^{-1}; α is the spectral index of intrinsic photon luminosity. We take $\alpha = 2$ following Band *et al.* (1993) as it provides a reasonable fit to the burst spectra. The luminosity distance $D_L = r(1+z)$, r is the coordinate distance to the GRB at a redshift z, for flat cosmologies i.e. $\Omega_{\rm Total} = 1$, is given by:

$$r = H_0^{-1} \int_0^z \frac{dz'}{(\Omega_m(1+z')^3 + \Omega_\Lambda)^{1/2}} \tag{4.2}$$

Here the Hubble length $H_0^{-1} = 9.1 \times 10^{27} h^{-1}$ cm. Ω_m and Ω_Λ are the present energy densities (in units of the critical density) of the non-relativistic matter and the cosmological constant, respectively.

For comparing the observed $\mathcal{N}(>F)$–F with theoretical fit we consider only the events with $F \geq 0.4\,{\rm cm}^{-2}$ sec^{-1} following Loredo & Wasserman (1998). This requirement leaves us with $\simeq$ 1790 events for our analysis. These are divided into 170 flux bins for computing the number count–flux relation. In Figure 1.3 we show the $\mathcal{N}(>F) - F$ curve. The dotted lines (merged with solid lines) represents our theoretical curve.

The theoretical number count $\mathcal{N}(>F)$ can be expressed as:

$$\mathcal{N}(>F) = 4\pi \int_0^{z_{max}} dr\, r^2 \int_{4\pi D_L^2 F}^{\infty} dL\, n(L,z)(1+z)^{-\alpha}. \tag{4.3}$$

Here we assume pure density evolution (see Hartwick & Schade 1990).

$$n(L,z) = \phi_*(z)\phi(L)dL \tag{4.4}$$

is the comoving number density of GRBs in a given luminosity range L to $L+dL$ at a given redshift. Luminosity function, $\phi(L)$ is expressed as probability density, defined such that $\int_0^\infty \phi(L)dL = 1$. We assume a simple power-law for the evolution of the number density of sources with redshifts with a possible sharp cut-off at z_{max}. $\phi_*(z) = \phi_*(0) \times (1+z)^\gamma$ is the total comoving number density of GRBs at redshift z. The factor of $(1+z)^{-\alpha}$ in Eq. (4.3) gives the 'k-correction' which corrects for the difference between the emitted and the observed wavelength.

We assume several different luminosity functions, $\phi(L)$, for our study:

Log-Normal distribution function:[1]

$$\phi(L) = \frac{\exp(-\sigma^2/2)}{\sqrt{2\pi\sigma^2}} \exp\left[-(\ln(L/L_0))^2/2\sigma^2\right] \frac{1}{L_0} \tag{4.5}$$

σ and L_0 are the width and the average luminosity of the luminosity function, respectively. The log-normal distribution is representative of the luminosity function of spiral galaxies (for details see Bingelli *et al.* 1988).

Schechter distribution:

$$\phi(L) = A\left(\frac{L}{L_*}\right)^{-\beta} \exp\left(-L/L_*\right) \frac{1}{L_*} \tag{4.6}$$

A is a normalizing constant. The entire galaxy population can be roughly represented by this function (for details see Bingelli *et al.* 1988). We restrict ourselves to $\beta \leq 1$ in this paper. L_* is known as characteristic luminosity.

Scale-free luminosity function:

$$\phi(L) = A\left(\frac{L}{L_*}\right)^{-\beta} \frac{1}{L_*} \quad \text{for } L_{\min} \leq L \leq L_{\max} \tag{4.7}$$

A is a normalizing constant.

[1] One often encounters in literature, especially in probability theory, a different definition for the log-normal distribution viz. $\phi(L)dL = \frac{1}{\sqrt{2\pi\sigma^2}} \exp\left[-(\ln(L/L_0))^2/2\sigma^2\right] \frac{dL}{L_0}$

$\mathcal{N}(>F)$ depends on a number of parameters: (a) cosmological parameters through D_L and r. (b) $z_{\rm max}$, the maximum redshift of GRBs, (c) $\phi_*(z)$, which gives the redshift dependence of the GRB population, (d) the parameters of the luminosity function. We fix the cosmological parameters to their most favoured values. Our aim is to obtain the values of the parameters of the luminosity function that best fit the observation. After fixing the cosmological model and the spectral index, the most important remaining uncertainty comes from the evolution of GRB population. One obvious choice is the 'no evolution' model. In this model, $\phi_*(z)$ is a constant independent of z. However afterglow observations give circumstantial evidence that GRBs might be associated with star-forming regions (Kulkarni *et al.* 2000 and references therein). Such an association might mean that GRB population trace the star-formation history of the universe. Therefore we also consider several other models, which are consistent with the star-formation history of the universe:

Model I: No Evolution model

Model II: The GRB population evolves as the luminosity density at 1600 Å, which is a good tracer of star-formation history (Madau *et al.* 1998, Madau *et al.* 1996). In this case the comoving number density of GRBs increases by a factor of $\simeq 10$ from $z \simeq 0$ to $z \simeq 1.5$ (Lilly *et al.* 1996) and then decreases approximately $\propto (1+z)^{-1}$ at higher redshifts (Figure 3 of Madau *et al.* 1998).

Model III: To account for the possible dust-extinction in the the star-forming regions for $z \geq 1.5$ (Conolly *et al.* 1997), we assume that the star-formation rate grows for $z \leq 1.5$ as in the previous model, but remains constant at the value of $z = 1.5$ till $z \simeq 3$, and then declines as $\propto (1+z)^{-1}$ at larger redshifts.

Model IV: We consider an extreme model that, is barely consistent with the star-formation history of the universe but within the uncertainty in the evolution of the star-formation rate at $z \geq 1.5$. In this model, the comoving number density of GRB population evolves $\propto (1+z)^{3.5}$ for $z \lesssim 1.5$ (Lilly *et al.* 1996). The comoving number density remains at the value of $z = 1.5$ for $z \leq 5$

and then it gradually declines at $\propto (1+z)^{-0.5}$. In this model much of star-formation at redshifts $\gtrsim 1.5$ occurs in regions highly shrouded by dust which allows a high star-formation rate to be compatible with the star-formation rate observed in HDF UV drop-out galaxies. However, further increase in the star-formation rate, which must be accompanied by a suitable increase in the dust content, might be incompatible with the observation of Far Infra-red background (Puget *et al.* 1996, Guiderdoni *et al. 1997*).

4.4 Observed GRB redshifts

In Table 4.1 we list the redshifts of GRBs used to calculate the luminosity distribution of GRBs. The GRB at $z = 0.008$ (GRB 980425) has been excluded from this list, as it is probably associated with a supernova (Galama *et al.* 1998) and therefore corresponds to a different population of GRBs (Kulkarni *et al.* 2000). Three GRBs whose redshifts are not certain (GRB 980326 $z \simeq 1$; GRB 980329 $z \leq 3.5$; GRB 990507 $z \simeq 0.25$) are also excluded.

Gamma-ray fluxes (photons $\mathrm{cm}^{-2}\,\mathrm{sec}^{-1}$) corresponding to these 16 GRBs are listed in Table 4.1: Eight of these are taken from BATSE flux table (integrated over 1024 milliseconds). Gamma-ray fluxes of the remaining GRBs, triggered either by BeppoSAX or IPN satellites are in different energy band and therefore had to be estimated through extrapolation to the energy range of BATSE. The band-pass conversion is achieved using a spectral index, $\alpha = 2$ (see appendix B) for the photon luminosity. We adopt the values of the gamma-ray fluxes given by Schaefer (2000) for three of the GRBs.

From the measured redshifts and observed $\gamma-$ray fluxes, the total energies of GRBs, assuming isotropic emission, is estimated to be in the range 10^{51-54} erg. The channeling of such large amount of energy into gamma rays pose serious problems in theoretical modelling. One of the proposal to resolve the energy crisis was to have the emission collimated into jets, which would lower the total energies by a factor of few hundreds (Rhoads 1999; Piran 1999). The GRB afterglow observations have shown evidences for beaming via break in the light curves in 5 cases : GRB990123 (Holland 2000; Kulkarni 1999), GRB990510(Holland 2000, Harrison 1999), GRB 991216(Halpern 2000), GRB 000301c (Sagar *et al.* 2000, Berger *et al.* 2000) and GRB 000926 (Price *et al.* 2000). The opening angle $\theta_\circ$ of the jet may be calculated

Table 4.1: Parameters of GRB Afterglows

GRB	BATSE tr#	Redshift z	Photon flux ph/cm^2/s	Luminosity ph/s	Beaming factor*	Ref. for photon flux**
GRB970228	–	0.695	10.0	2.34×10^{58}	-	1
GRB970508	6225	0.835	0.969	3.56×10^{57}	-	2
GRB970828	6350	0.958	1.5	7.74×10^{57}	-	1
GRB971214	6533	3.418	1.955	2.27×10^{59}	-	2
GRB980613	–	1.096	0.5	3.60×10^{57}	-	1
GRB980703	6891	0.966	2.398	1.26×10^{58}	-	2
GRB990123	7343	1.6	16.41	3.0×10^{59}	300	2
GRB990506	7549	1.31	18.56	2.08×10^{59}	-	2
GRB990510	7560	1.619	8.16	1.54×10^{59}	300	2
GRB990712	7647	0.434	11.64	8.56×10^{57}	-	2
GRB991208	–	0.706	11.2	2.72×10^{58}	-	3
GRB991216	7906	1.02	67.5	4.06×10^{59}	200	2
GRB000131	-	4.5	1.5	3.35×10^{59}	-	3
GRB000301c	-	2.03	1.32	4.34×10^{58}	90	3
GRB000418	-	1.118	3.3	2.5×10^{58}	-	3
GRB000926	-	2.066	10.0	3.45×10^{59}	120	3

*References for beaming factor follow: GRB 990123: Holland *et al.* 2000; GRB 990510: Holland *et al.* 2000, Harrison *et al.* 1999; GRB 991216: Halpern *et al.* 2000; GRB 000301c: calculated for t_b=4.1 days from Bhargavi & Cowsik (2000) using Eq 1. of Sari *et al.* 1999; GRB 000926: Price *et al.* 2000

The references for fluxes are as follows: 1. Schaefer(2000); 2. BATSE catalog; 3. conversion made by applying band-pass corrections as explained in **Appendix B.

from Eq 1. of Sari *et al.* (1999) knowing the break-time t_b in the light curve. The beaming factor in Table 4.1. is $\approx 2/\theta_\circ^2$ and has been used to apply the corrections

[2] to luminosities in 5 cases.

The probability that burst of a given flux will occur in a redshift range z to $z+dz$ is given by (Woods & Loeb 1995),

$$p(z)dz = \phi(L) \times \frac{dL}{dz}dz \tag{4.8}$$

$\phi(L)$ is given by Eqs. (4.5), (4.6), or (4.7), and L for a given flux F and redshift is determined by Eq. (4.1). The likelihood that the observed set of GRB luminosities were drawn from a given luminosity function is:

$$\mathcal{L}(a_k) = \prod_{i=1}^{16} p(z_i, F_i) \tag{4.9}$$

where a_k are the set of parameters describing the luminosity function. We maximize the likelihood function with respect to $a_k = \{L_0, \sigma\}$ for the Log-normal luminosity function. It should be noted that parameters estimated using this method do not depend on the number density $\phi_*(z)$ of the GRBs.

4.5 Results and conclusions

We show our results for the log-normal luminosity function in Figure 4.1. We plot the allowed region in the L_0–σ plane from both the observed $\mathcal{N}(>F)$–F from BATSE catalog and the afterglow redshift data. The allowed region from requiring consistency between the observed $\mathcal{N}(>F)$–F relation and the theoretical number counts (Eq. 4.3) corresponds to the area in which the K-S probability $P_{\rm ks} \geq 0.01$ (see e.g. Press *et al.* 1992 for details on the K-S test).

The best fit value of σ and L_0 from the afterglow redshift data are: $\sigma = 1.7$ and $L_0 = 3 \times 10^{57}$ ph sec^{-1} without the beaming corrections and $\sigma = 2$ and $L_0 = 2 \times 10^{56}$ ph sec^{-1} with the beaming corrections. We show in Figure 4.1 the region within which the value of the likelihood function is $\geq 10^{-4}$ times the value at the maximum. This correspond roughly to 99% confidence level for a two-parameter fit (Press *et al.* 1992). (We do not calculate the joint confidence levels using the usual Fisher matrix approach because the Likelihood function is not a joint Gaussian distribution and also because the Likelihood function is very broad near the maximum).

[2]Thanks to A. Loeb for suggesting to apply the beaming corrections in our analysis during a brief discussion at GRB winter school (Dec27, 2000–Jan5, 2001) at Hebrew university, Jerusalem.

Results for other assumed luminosity functions are shown in Figure 4.2, 4.3 and 4.4, using the same criteria for showing the allowed regions as given in the preceding paragraph. The results are shown for only two representative scale-free models. The best-fit values of parameters from GRB redshift data are: $\beta = 0.6$, $L_* = 3 \times 10^{59}\,\mathrm{sec}^{-1}$ without beaming correction and $\beta = 0.6$, $L_* = 2 \times 10^{59}\,\mathrm{sec}^{-1}$ with beaming correction (Schechter luminosity function); $\beta = 0.65$, $L_* = 5 \times 10^{56}\,\mathrm{sec}^{-1}$ without beaming corrections and $\beta = 1.05$, $L_* = 3.8 \times 10^{56}\,\mathrm{sec}^{-1}$ (scale-free model with $L_{\rm min} \simeq L_*$ and $L_{\rm max} \simeq 10^3 L_*$); $\beta = 0.65$, $L_* = 6 \times 10^{57}\,\mathrm{sec}^{-1}$ without beaming correction and $\beta = 1.15$, $L_* = 1.2 \times 10^{58}\,\mathrm{sec}^{-1}$ with beaming correction (scale-free model with $L_{\rm min} \simeq 3 \times 10^{-2} L_*$ and $L_{\rm max} \simeq 10^2 L_*$).

As seen in the Figures, it is possible to explain the observed $\mathcal{N}(>F)$–F relation using any of the luminosity functions we assume. Further the allowed regions do not strongly constrain either the luminosity of the GRB or the width of the luminosity function (Loredo & Wasserman 1998, Schmidt 2000). For any luminosity function the allowed range of luminosities span atleast a decade depending on the evolution of GRB population (Figure 4.1). It can be noticed that stronger evolution in the GRB population results in a higher average luminosity (Schaefer 2000). $z_{\rm max}$, the maximum redshift of GRBs is not an important parameter so long as $z_{\rm max} \gtrsim 5$. It is because even the faintest bursts we consider in our analysis ($F \simeq 0.4\,\mathrm{cm}^{-2}\,\mathrm{sec}^{-1}$) come from $z \lesssim 5$ for much of the allowed luminosity range.

The GRB redshift data give a large range of photon luminosities ($10^{57}\,\mathrm{sec}^{-1} \lesssim L \lesssim 10^{59}\,\mathrm{sec}^{-1}$ in photons sec^{-1}). Therefore it is natural to expect that the underlying luminosity function is broad. It is clearly seen in the figures. It should be noted that the GRB luminosities implied by the $\mathcal{N}(>F)$–F relation are not at variance with the observed GRB luminosities. However, as seen in the figures, these two observations imply two different set of luminosity function parameters in most cases.

The log-normal is the only luminosity function that is compatible with both BATSE number count and the afterglow redshift data. This agreement is independent of the GRB evolution model. The agreement between the two data sets requires $10^{55}\,\mathrm{sec}^{-1} \lesssim L_0 \lesssim 10^{56}\,\mathrm{sec}^{-1}$ and $2 \lesssim \sigma \lesssim 3$. For other luminosity functions the agreement between the two observations becomes better as GRB evolution becomes stronger (Figures 4.2, 4.3 and 4.4). However the requirement that the two regions overlap can be fulfilled only if the GRBs evolve at a rate much stronger than the star-formation rate of the universe.

It is seen in Figures 4.1, 4.2, 4.3 and 4.4 that the beaming correction does not make any quantitative difference to our results. In almost all the cases the 99% region from the afterglow data becomes smaller after the beaming correction, but it is difficult to draw any conclusions from it. A particularly interesting case is one of the scale-free models (Figure 4.4) in which the beaming correction reduces the area of the 99% region quite dramatically. However this is owing to the fact that the beaming correction increases the luminosity width of the observed GRB afterglows, and the model in question has a luminosity width of 1000 which matches the luminosity width of the GRBs. Therefore only of a very small range of L_* is compatible with observations.

One possible reason for the discrepancy/agreement between the number count–flux and GRB redshift data results could be selection effects. Most of the redshift determinations have been possible owing to the detection of X-ray counterpart of the GRB by BeppoSAX. This results in two types of selection effects: (a) BeppoSAX is not sensitive to burst duration ≤ 1 sec (Feroci *et al.* 1999), (b) the GRBs detected by BeppoSAX might be X-ray selected though Feroci *et al.* (1999) emphasize it is unlikely.

The burst-duration selection effect might mean the GRBs for which the redshifts have been determined belong to a different population of GRBs. The burst duration distribution for the BATSE bursts is observed to be bi-modal (Fishman & Meegan 1995), which strongly suggest that long- and short-duration bursts are different populations of GRBs. In light of this it is usual to expect that these two might have different luminosity functions. To check for this effect we make a sub-catalog of GRB bursts with duration ≥ 2 sec (measured in $T90$). The best fit luminosity function parameters from the $\mathcal{N}(>F)$–F relation of this sub-catalog are very similar to those for the entire catalog (Sethi & Bhargavi 2001) indicating that results are not sensitive to this selection bias.

If the BeppoSAX GRBs are X-ray selected in addition to being long-duration then the GRB redshift sample may not be representative of the luminosity function at $z \geq 1$. The X-ray selection may mean that the average GRB luminosities are far in excess of the average luminosities. The long-duration selection will tend to pick out bursts which are systematically at larger redshifts because of the cosmological stretching of the GRB time-duration.

To sum up: of the four luminosity functions considered here, log-normal is the only luminosity function that is consistent with both the BATSE number count–flux relation and afterglow redshift data, independent of the evolution of the GRB population. Notwithstanding the selection effects, the other luminosity function can be consistent with both observations only if the GRBs evolution far exceeds the evolution of star-formation rate in the universe.

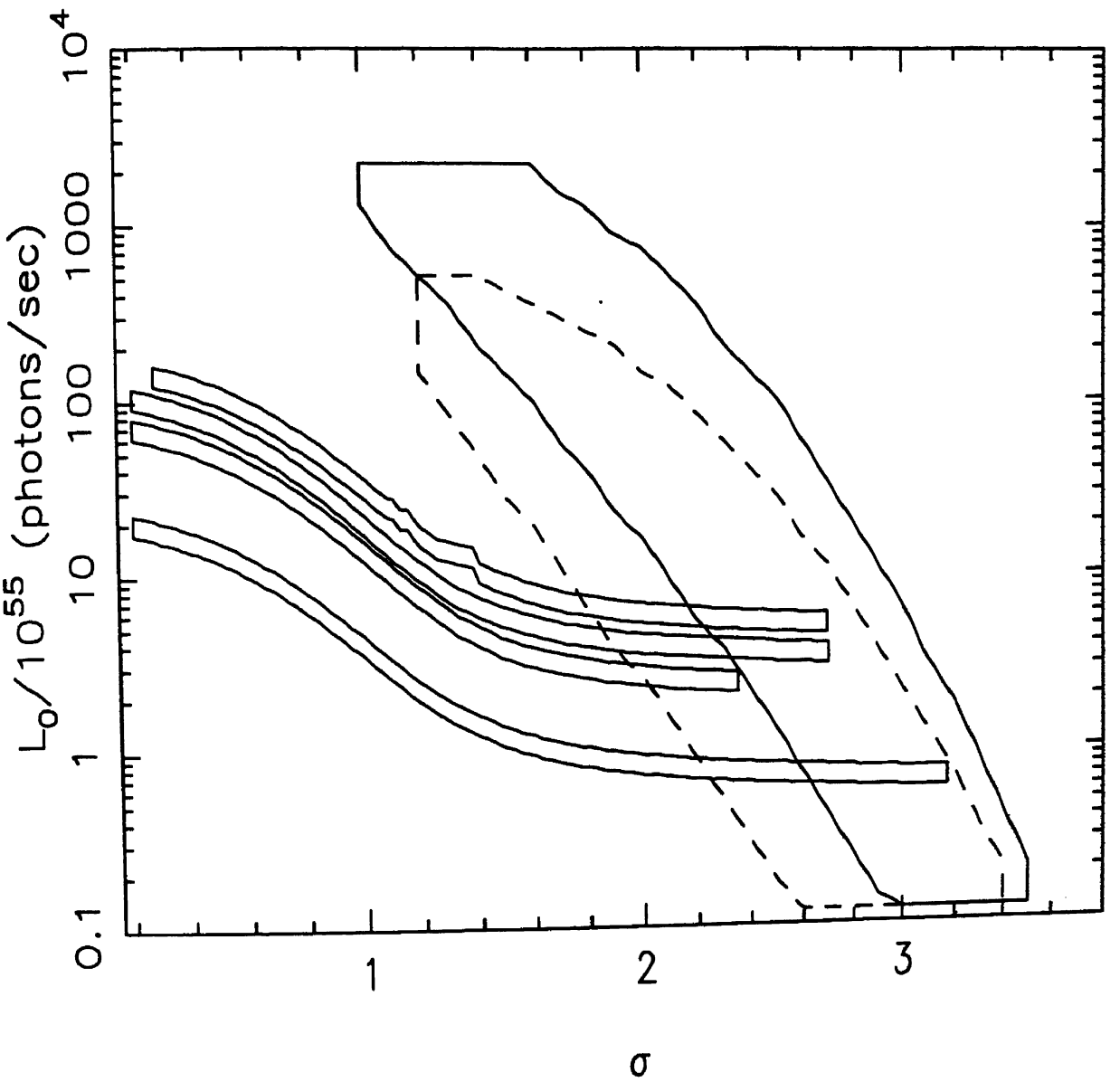

Figure 4.1: The results for the Log-normal luminosity function are shown: The bigger regions in the center enclose the allowed region of likelihood function (i.e $\mathcal{L} > 10^{-4}$ of maximum likelihood)in $L_0 - \sigma$ plane for afterglow observations. The region with dotted lines corresponds to a run where beaming corrections are applied. The 4 contours on the left side represent the region of K-S probability $P_{ks} > 0.01$ for the consistency between observed and theoretical number count-flux relation. They correspond, from bottom to top (with increasing luminosity) to four models 1-4 respectively of GRB evolution described in the text.

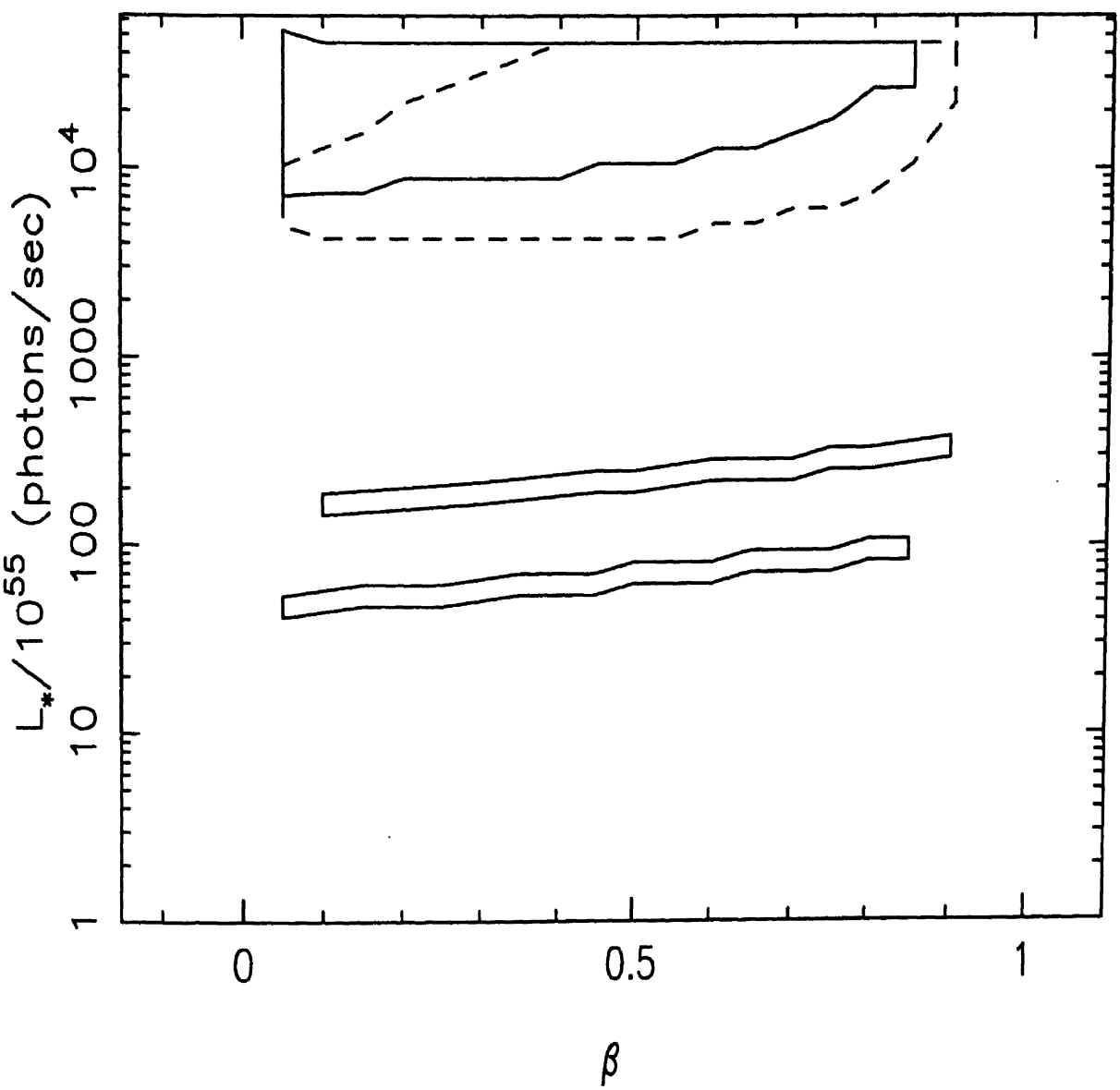

Figure 4.2: The results for the Schechter luminosity function are shown: The bigger regions at the top of the figure enclose the allowed region of likelihood function (i.e $\mathcal{L} > 10^{-4}$ of maximum likelihood) in $L_0 - \sigma$ plane for afterglow observations. The region with dotted lines corresponds to a run where beaming corrections are applied. The smaller regions at the center represent the region of K-S probability $P_{\rm ks} > 0.01$ for the consistency between observed and theoretical number count-flux relation. These correspond, with increasing photon luminosity, to GRB evolution models III and IV discussed in the text. The allowed regions for models I and II fall below the allowed regions for the models shown.

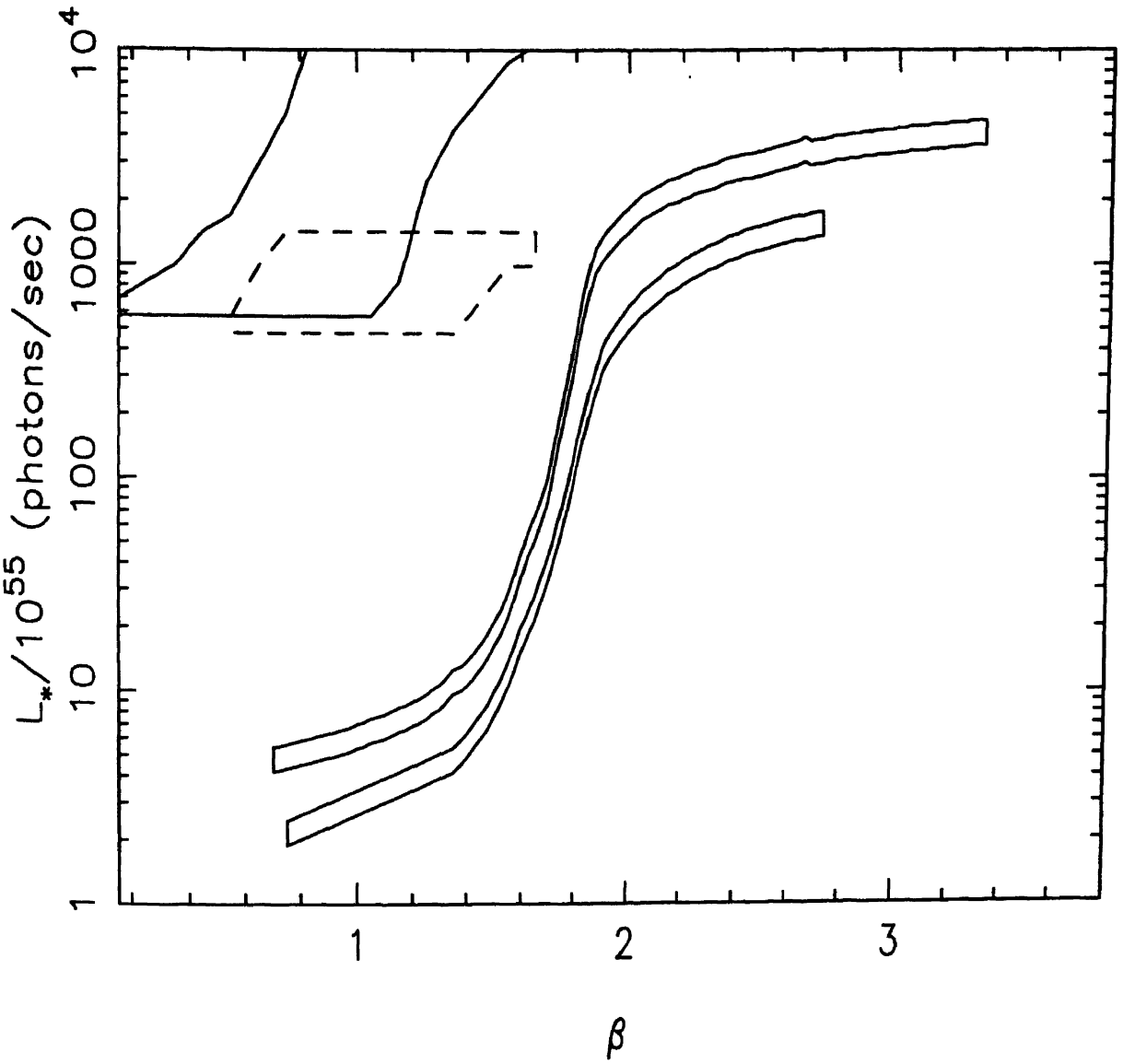

Figure 4.3: The results for the scale-free luminosity function are shown. In this model $L_{\rm min} = 3 \times 10^{-2} L_*$ and $L_{\rm max} = 100 L_*$. The regions at the top left of the figure represent the allowed region of likelihood function (i.e $\mathcal{L} > 10^{-4}$ of maximum likelihood) in $L_0 - \sigma$ plane for afterglow observations. The region with dotted lines corresponds to a run where beaming corrections are applied. The thin regions represent the region of K-S probability $P_{\rm ks} > 0.01$ for the consistency between observed and theoretical number count-flux relation. These correspond, with increasing photon luminosity, to GRB evolution models III and IV discussed in the text. The allowed regions for models I and II fall below the allowed regions for the models shown.

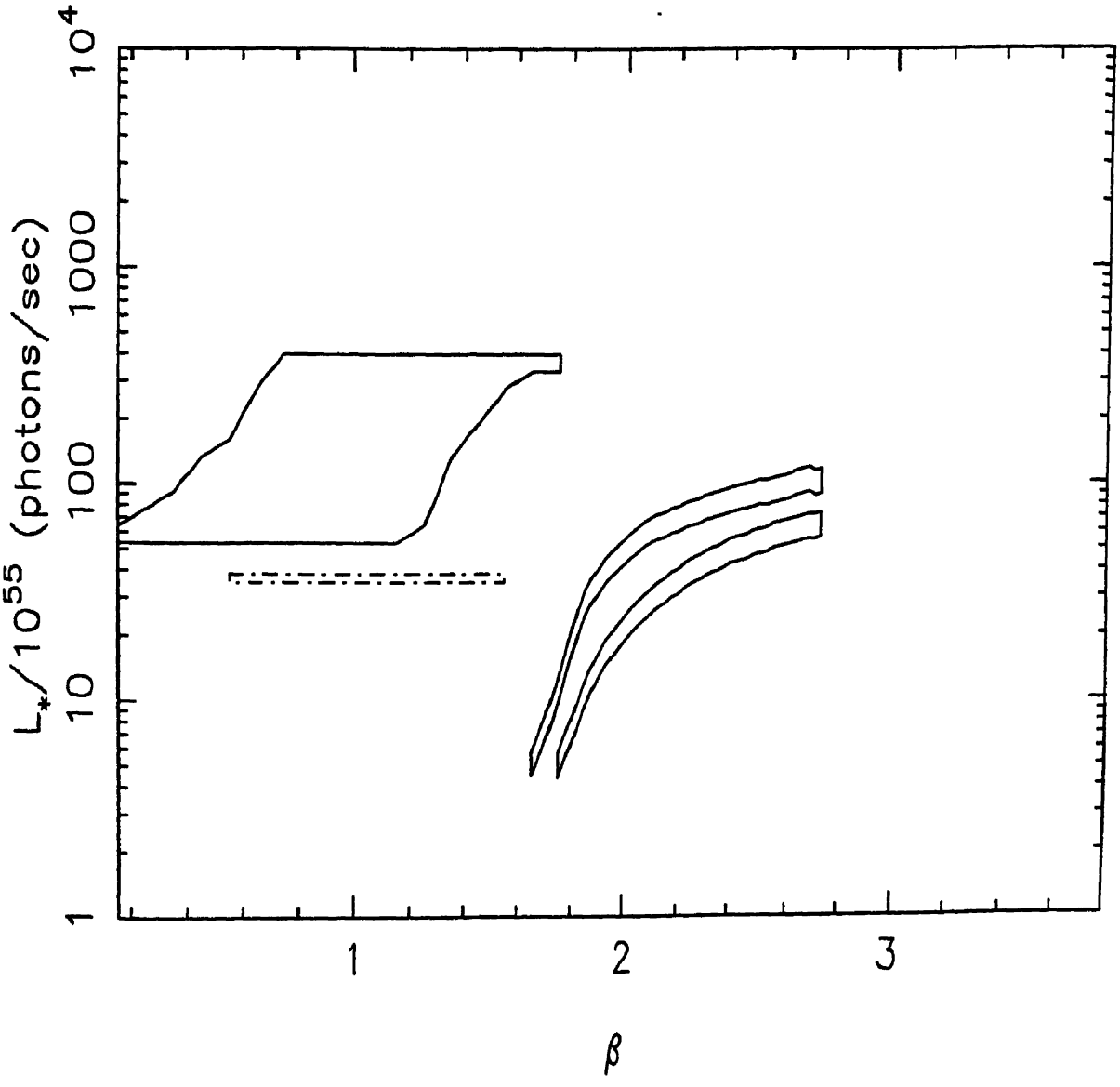

Figure 4.4: The results for the scale-free luminosity function are shown. In this model $L_{\min} = L_*$ and $L_{\max} = 1000L_*$. The bigger region on the left represent the allowed region of likelihood function (i.e $\mathcal{L} > 10^{-4}$ of maximum likelihood) in $L_0 - \sigma$ plane for afterglow observations. The dotted region corresponds to a run where beaming corrections are applied. Thin regions in the center of the figure represent the region of K-S probability $P_{\rm ks} > 0.01$ for the consistency between observed and theoretical number count-flux relation. These correspond, with increasing photon luminosity, to GRB evolution model III and IV discussed in the text. The allowed regions for models I and II fall below the allowed regions for the models shown.

Appendix A

Here we give a brief derivation of Eq. (4.1). Assume that a source at a redshift z is emitting with photon luminosity L_ν (photons $\sec^{-1}\,\mathrm{Hz}^{-1}$), with intrinsic spectrum:

$$L_\nu = L_f \left(\frac{\nu}{\nu_f}\right)^{-\alpha} \tag{4.10}$$

Here ν_f is some fiducial frequency. The received photon flux (photons $\sec^{-1}\,\mathrm{Hz}^{-1}\,\mathrm{cm}^{-2}$) is:

$$F_{\nu_0} = \frac{L_\nu}{4\pi r^2} \tag{4.11}$$

Here r, defined in Eq. (4.2), is the coordinate distance to the source from the observer at the present epoch and ν_0 is the observed frequency. Note that there are no factors of (1+z) in the denominator of Eq. (4.11). Integrating the flux over the observed band-pass (50 kev to 300 kev for BATSE), and using $\nu/\nu_0 = (1+z)$, we get:

$$F \equiv \int F_{\nu_0} d\nu_0 = \frac{L_f (1+z)^{-\alpha}}{4\pi r^2} \int \left(\frac{\nu_0}{\nu_f}\right)^{-\alpha} d\nu_0 \tag{4.12}$$

Defining

$$L = L_f \int \left(\frac{\nu_0}{\nu_f}\right)^{-\alpha} d\nu_0, \tag{4.13}$$

and using $D_L = (1+z)r$, we obtain Eq. (4.1).

Appendix B

Throughout this paper 'flux' refers to photon flux averaged over 1.024 sec BATSE trigger, in the energy range 50–300 kev. Out of 16 afterglows whose redshifts have been determined, only 7 have known BATSE fluxes. In the other cases, the gamma-ray fluxes are available in other frequency bands by either BeppoSAX or IPN satellites. To be consistent with our definition of flux, we extrapolate the observed fluxes from the observed band to the BATSE band. We briefly describe the method of this extrapolation in this appendix. It should be pointed out that the difference of trigger time between BATSE and other instruments must also be taken into account for extrapolating fluxes. However, we apply only band-pass corrections.

Assume that a source at redshift z is emitting with a luminosity L_ν (erg sec^{-1} cm^{-2}) and spectrum:

$$L_\nu = L_f \left(\frac{\nu}{\nu_f}\right)^{-\beta} \tag{4.14}$$

ν_f is some fiducial frequency. The observed flux at the frequency $\nu_0 = \nu/(1+z)$ is:

$$F_{\nu_0} = \frac{L_\nu}{4\pi r^2(1+z)} \tag{4.15}$$

The flux integrated over a band-pass between frequencies ν_1 and ν_2 is given by:

$$F(\nu_1, \nu_2) \equiv \int_{\nu_1}^{\nu_2} F_{\nu_0} d\nu_0 = \frac{F(z)}{\nu_f^{-\beta}} \int_{\nu_1}^{\nu_2} \left(\frac{\nu_0}{\nu_f}\right)^{-\beta} d\nu_0, \tag{4.16}$$

with the definition $F(z) = L_f(1+z)^{-\beta-1}/(4\pi r^2)$. We assume $\beta = 1$ in this paper (the spectral index α for the photon luminosity is related to β as $\alpha = \beta + 1$). This gives:

$$F(\nu_1, \nu_2) = \frac{F(z)}{\nu_f^{-1}} \log(\nu_2/\nu_1). \tag{4.17}$$

Eq. (4.17) can be used to convert flux observed in any band-pass to the BATSE band-pass.

The photon luminosity (L_ν^p) is related to the energy luminosity as: $L_\nu^p = L_\nu/(h\nu)$. h being the Planck's constant. This relation and the methods described above as well as in the previous appendix can be used to get the conversion between the band-pass integrated photon flux (F) and the energy flux ($F(\nu_1, \nu_2)$). The relation is (for $\beta = 1$):

$$F = F(\nu_1, \nu_2) \frac{\nu_1^{-1} - \nu_2^{-2}}{h \log(\nu_2/\nu_1)}. \tag{4.18}$$

Bibliography

[1] Band, D. *et al.* 1993, ApJ, 413, 281

[2] Berger, E. *et al.* 2000, astro-ph/0005465

[3] Bhargavi, S. G. & Cowsik, R. 2000, ApJ 545, L77

[4] Bingelli, B., Sandage,A., & Tamman, G. A. 1988, ARA & A, 26, 509

[5] Connolly, A. J., Szalay, A. S., Dickinson, M., SubbaRao, M. U. & Brunner, R. J. 1997, ApJ, 486, L11

[6] Cohen, E. & Piran, T. 1995, ApJ 444, L25

[7] de Bernardis, P. *et al.* 2000, Nature, 404, 995

[8] Feroci, M. *et al.* 1999, A&AS, 138, 407

[9] Fishman, G. J. & Meegan, C. A. 1995, ARA & A, 33, 415

[10] Galama, T. J., *et al.* 1998, Nature, 395, 670

[11] Greiner, J. 2001, *http://www.aip.de/People/JGreiner*

[12] Guiderdoni, B. *et al.* 1997, Nature, 390, 257

[13] Halpern, J. P. *et al.* 2000, astro-ph/0006206

[14] Harrison, F. A. *et al.* 1999, ApJ 523, L121

[15] Hartwick, F. D. A. & Schade, D. 1990, ARAA, 28, 437

[16] Hogg, D. W. & Fruchter, A. S. 1998, astro-ph/9807262

[17] Holland, S. *et al.* 2000, astro-ph/0010196

[18] Kulkarni, S. R. *et al.* 2000, In *Cosmic Explosions: Tenth Astrophysical Conference*, (ed). Holt, S. S. & Zhang, W. W., Am. Inst. Phys., AIP-522; astro-ph/0002168

[19] Kulkarni, S. R. *et al.* 1999, Nature, 398, 389

[20] Lilly, S., Le Fèvre, O. Hammer, F, Crampton, D. 1996, ApJ, 460, L1

[21] Loredo, T. J. & Wasserman, I. 1998, ApJ 502, 75

[22] Lubin, L. M. & Wijers, R. A. M. J. 1993, ApJ 418, L9

[23] Madau, P., Pozzetti, L., & Dickinson, M. 1998, ApJ, 498, 106

[24] Madau, P., Ferguson, H. C., Dickinson, M., Giavalisco, M., Steidel, C., & Fruchter, A. 1996, MNRAS, 283, 1388

[25] Mao, S. & Paczyński, B. 1992, ApJ 388, L45

[26] Paciesas, W. S. 2000, http://gammaray.msfc.nasa.gov/batse/data/

[27] Perlmutter, S. *et al.* 1999, ApJ, 517, 565

[28] Piran, T. 1992, ApJ 389, L45

[29] Piran, T. 1999, Phys. Rep., 314, 575

[30] Press, W. H., Teukolsky, S., Vellering, W. T., & Flannery, B. P. 1992, *Numerical Recipes in Fortran*, Cambridge university Press

[31] Price, P. A. *et al.* 2000, astro-ph/0012303

[32] Puget, J-. L. *et al.* 1996, A&A, 308, L5

[33] Rhoads, J. E. 1999, ApJ, 525, 737

[34] Sagar, R. *et al.* 2000, BASI, 28, 499

[35] Sari, R. *et al.* 1999, ApJ, 519, L17

[36] Schmidt, M. 2000, astro-ph/0001121

[37] Schaefer, B. 2000, ApJ, 532, L21

[38] Sethi, S. & Bhargavi, S. G. 2001, A & A (accepted for publication).

[39] Ulmer, A. & Wijers, R. A. M. J. 1995, ApJ 439, 303

[40] Ulmer, A., Wijers, R. A. M. J. & Fenimore, E. E. 1995, ApJ 440, L9

[41] Woods, E. & Loeb, A. 1995, ApJ, 453, 583

Chapter 5

CCD Imaging of IPN-GRB Fields

Abstract

We present the observations and analysis of four of the IPN[3] GRB fields studied before the afterglow of GRBs had been detected in the optical band. Using the best fit parameters of the luminosity function that is compatible with both the afterglow redshift data and number-count v/s flux relation for GRBs we estimate the most probable range of redshifts for the GRB hosts. We check to see if the observed fields contain suitable galaxies within the estimated redshift range.

5.1 Introduction

We had undertaken a program in 1994-95 to make an optical survey of a few GRB fields chosen from third Inter-Planetary Network (IPN[3]) catalog (Hurley 1995, private communication; Laros *et al.* 1998; Hurley *et al.* 2000). Deep CCD imaging of these fields was carried out at the 2.34 m and 1.02 m telescopes of VBO, until 1998. It was an attempt to identify the transient/quiescent counterparts of GRBs on the basis of photometric studies. The recent afterglow studies of GRBs have shown that fading Optical Transient (OT) is observable over a period of a couple of months from ground-based optical telescopes (although with HST and in radio band the observations may be extended upto $\sim$ year) and therefore one can safely rule out the possiblity of detecting any possible transient counterpart associated with IPN[3] GRBs in the CCD frames observed several years after the burst. Afterglow studies have also shown that GRBs are hosted by faint galaxies at cosmological distances. In any given field of $\sim 10' \times 10'$ area one may find several faint galaxies and the

number would increase as one observes deeper and deeper. But, it is not possible to pinpoint to any of these objects and say that it gave rise to GRB a few years ago. This is because the host galaxies neither show any evidence of burst in their quiescent state (i.e, OT does not leave behind any signature identifiable by optical observations after several years), nor exhibit any 'unusal' properties. *In other words GRB-host galaxy relation is quite subtle.*

However, one could use the number count-flux relation of BATSE GRBs and the afterglow data to estimate the average redshift of host galaxies. This may be compared with the average redshift estimated for a given depth of a photometric survey. Thus one could check if galaxies in the observed field are potential candidates for GRB hosts. These aspects are discussed in section §4. In §2 previous attempts are briefly reviewed and in §3 the details of our observations and data analysis are presented.

5.2 A Brief Review on Optical Counterpart Searches

The earliest efforts in searching for the optical counterparts of GRBs were by looking for, flaring objects in the archival photographic plates containing the GRB positions. About a dozen possible optical transient objects were identified (see Hudec 1993 and references therein). Deep searches of these OT fields to investigate the reality of their association with GRBs were conducted and discussed by several authors (Greiner & Wenzel 1990; Hudec 1990; Schaefer 1987, 1989, 1990).

Triangulation technique (see section §1.2) applied to some of the GRBs, where multi-satellite data was available, yielded precise localizations less than $10' \times 10'$. Such GRB fields from both first and third IPN catalogs (Atteia *et al.* 1987; Hurley *et al.* 2000; Laros *et al.* 1998) were thoroughly searched in optical band (Schaefer 1992, 1998; Vrba 1995, 1998) for counterparts.

Indeed, the searches were biased by the theoretical models, as it can be seen that the earliest searches focussed on looking for galactic objects while those performed after the 90's (i.e, after *BATSE* discovered the isotropic and inhomogeneous distribution of GRBs) began to look for extra-galactic objects as the possible sources of GRBs. Schaefer (1992) studied 13 IPN[1] fields in various broad-band filters and reported the lack of bright host-galaxies inside the error boxes. This result, which basically opened up the so called "no-host" problem, was often used in the literature to argue

against cosmological models.

Larson *et al.* (1996, 1997a, 1997b) made a deep imaging survey of small error boxes of IPN[3] GRBs in JHK' bands to examine the extragalactic content of these fields and found bright galaxies in the fields. They concluded that "no-host" problem does not exist and on the contrary, there is an overabundance of galaxies in these fields. Vrba *et al.* (1995) carried out a deep photometric survey of 7 IPN^1 fields containing repeated observations over a period of 5 years. While the survey did not reveal any obvious counterpart to the limit $V \approx 24$, they detected several interesting objects of unusual color including QSOs and blue galaxies. The strategy they adopted to identify a counterpart in their 'non-real time' search is that the objects of any known class should have special characteristics to pass as a candidate. They concluded saying that either the underlying source is a normal galaxy in its quiescent state or is fainter than 24^{th} magnitude. In their survey of 5 IPN^3 fields (Vrba *et al.* 1998) several galaxies ranging from $V \sim 18$ to $V \sim 23$ were detected. Without imposing model-dependent assumptions about GRB distances they proposed these galaxies as potential GRB hosts.

5.3 The Sample

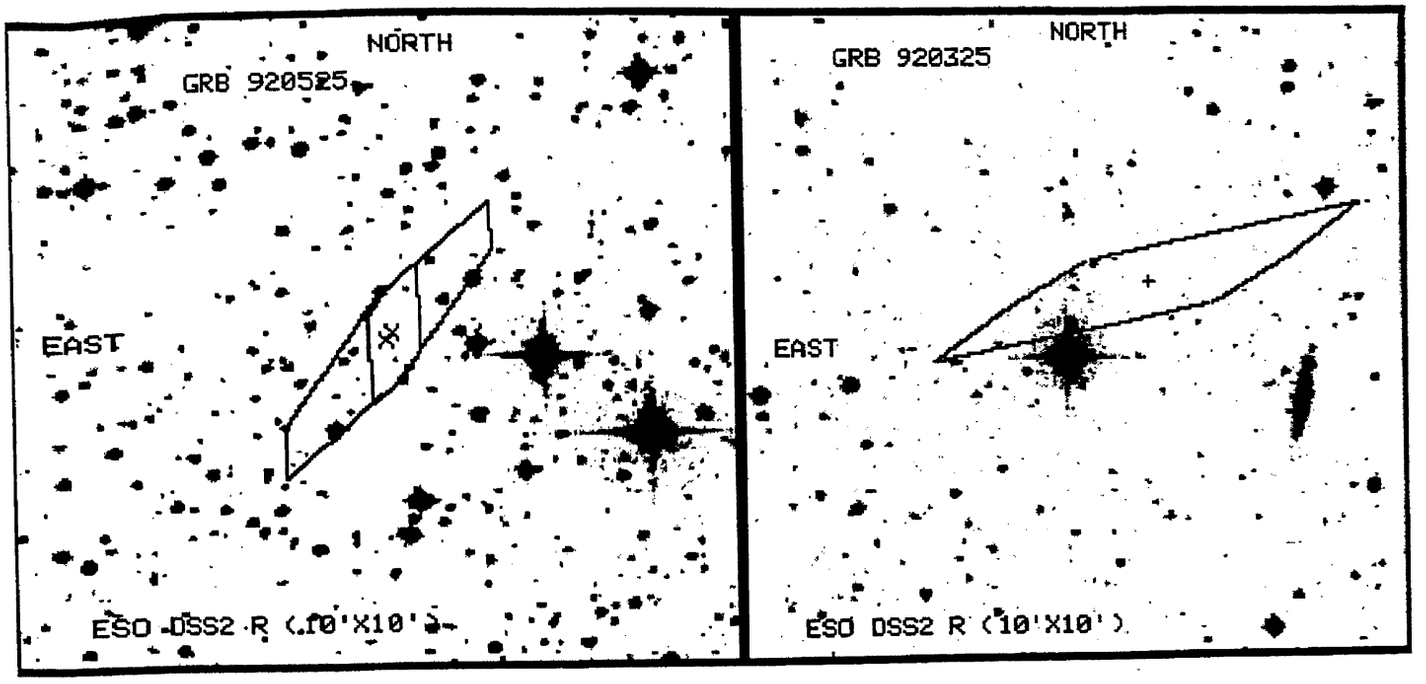

Figure 5.1: DSS2 R-band images : *left-panel*: The field of GRB 920525; The revised (central) and initial (outer) rectangles are drawn using the co-ordinates of the corners of IPN^3 error box from Laros *et al.* (1998) and Vrba (e-mail communication) respectively. *right-panel*: The field of GRB 920325 with IPN^3 error box drawn from Laros *et al.* (1998).

The unpublished co-ordinates of GRBs localized by third Inter-Planetary Network (IPN^3) were initially distributed to observers over e-mail (Hurley 1994, Hudec 1994; private communication). However, the initial centers as well as the size of the error boxes were subsequently revised (Laros *et al.* 1998; Hurley *et al.* 2000). The observations we made on some of those GRB fields became unusable, as the revised error boxes fell outside our observed FOV: e.g. GRB 920311, GRB 910522, GRB 911118, GRB 911104 and GRB 910717. In this section we present the details of observations and results of analysis of of four IPN^3 fields: GRB 920720, GRB 920517, GRB 920525 and GRB 920325, centered at the initial co-ordinates given in Table 5.1. The offset from the revised center and the area in arcmin^2 of the revised error box are given in the last two columns. In case of GRB 920325, a small portion of the revised error box is outside the observed field of view as shown in Fig 5.11 (see Fig 5.1 with complete error box overlaid on the DSS image). In the case of GRB 920720, GRB 920517 & GRB 920525, the revised error box remains within the observed FOV because the shift is small. As the observations of GRB 920517

field were made using a bigger (1k) CCD, the revised error box remained within the observed FOV. The observed image sections along with the overlay of IPN error boxes are shown in respective sections below. We show in Fig 5.1 the R-band DSS-2 images of the fields of GRB 920525 (*left-panel*) and GRB 920325 (*right-panel*). The rectangles represent the error boxes.

Table 5.1: IPN[3] GRB Sample

GRB	RA(2000)	DEC(2000)	Δ RA	Δ Dec	Area (arcmin^2)
GRB 920720	13:29:26.0	+37:14:13.2	3.24s	-4′.36	0.87
GRB 920517	13:33:16.3	-16:41:13.2	-4.39s	-2′.85	3.1
GRB 920525	20:03:28.6	-42:34:22.8	0.424s	-6″.12	1.02
GRB 920325	23:22:18.5	+13:03:11.0	4.32s	-49″.84	4.8

[1] Offset is w.r.t Laros *et al.* 1998

It may be noted that the observations presented below are not uniformly sampled in each bandpass. Due to varying seeing, high humidity or bad weather conditions it was difficult to achieve complete coverage over all band-passes or to achieve equal depths in all the observed band-passes. The magnitudes of the objects inside the error boxes and the limiting magnitudes have been presented in each observed band-pass. The photometric calibration of the objects in the fields of GRB 920720 and GRB 920525 were done using the field photometry provided by Vrba (2000; e-mail communication) and that of GRB 920517 using the field photometry provided by Henden (2001; email communication). In the case of GRB 920325, we used one of the Landolt standard field observed on the same night for calibrating the objects. The calibration solutions and color–magnitude diagrams are presented below. Since the data are taken under non-photometric sky conditions we do not intend to present the galaxy number-counts from these observations since there might be several objects at the position of a given unresolved object, observed with better seeing.

5.4 Deep CCD Imaging of GRB Fields.

1. GRB 920720

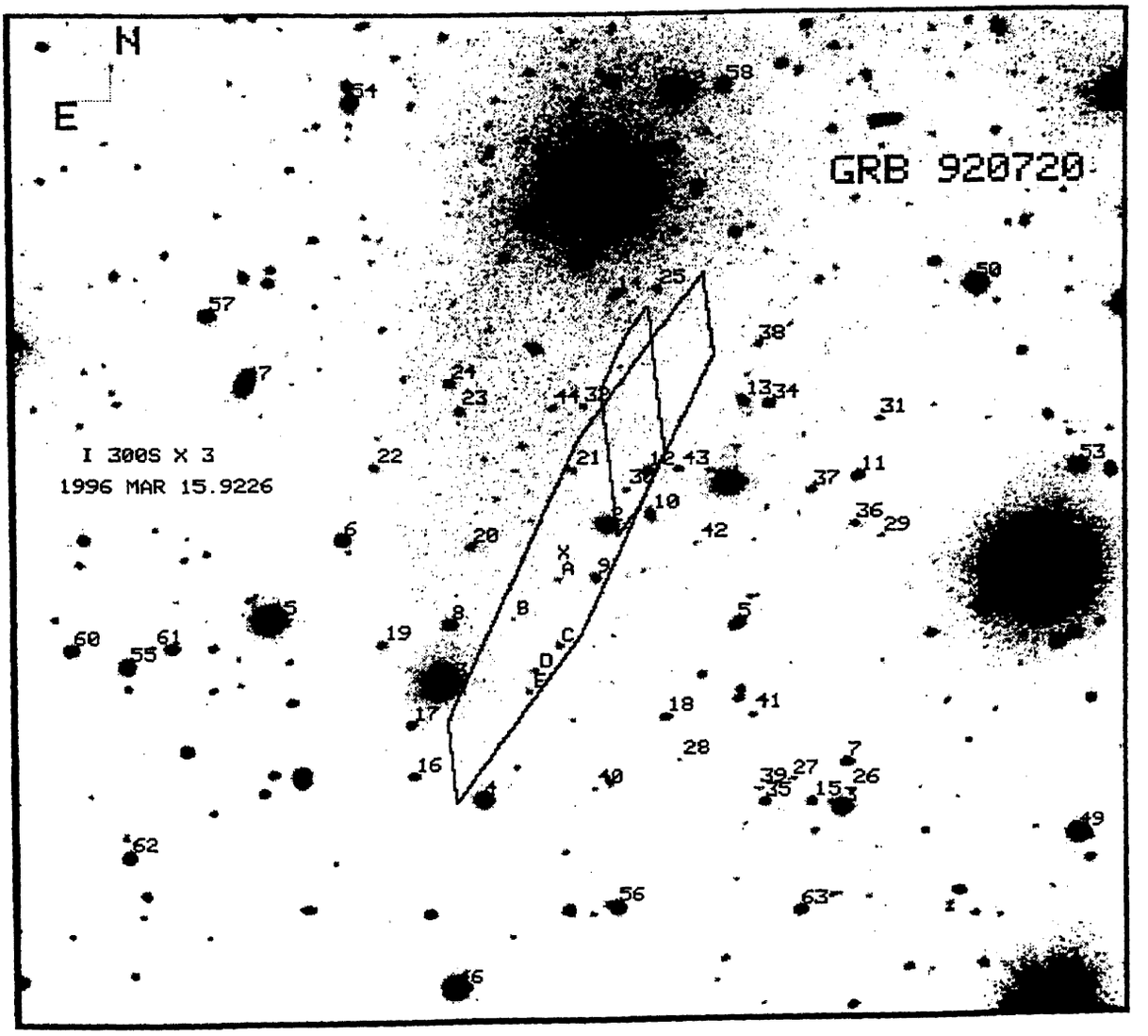

Figure 5.2: GRB 920720: I band image of 300 s × 3 exposure observed at VBT. The revised (*smaller*) and initial (*larger*) IPN error boxes are shown. The initial center is marked by 'X'. The image scale is 0″.609/ pix and total FOV is 10′.4 × 10′.4.

We present the details of observations and data analysis of GRB 920720 field observed on 15 Mar 1996 using 1k CCD (CCD #2 VBT; see Appendix 2.1) and broad-band filters at 2.34 m VBT. Two exposures of 600 s in B-band and three exposures of 300 s in I-band were obtained.

Following the pre-processing of the frames as detailed in Chapter 2 the images were summed in each filter. Fig 5.2 shows the summed I-band image with an overlay of initial (*larger*) and revised (*smaller*) error boxes. A total of 177 objects both

Table 5.2: GRB 920720: Observations

Mid-UT	Filter	Exp. time (sec)	Average Seeing	Limiting Magnitude
1996 03 15.8983	B	600 × 2	3″.5	22.8
1996 03 15.9226	I	300 × 3	3″.2	21.5

in B and I-band images and 54 faint objects only in I-band image are detected within the observed FOV. However, we donot present the analysis of all the objects, but restrict ourselves to the objects inside the error box and secondary standards. Aperture corrections to the magnitudes were applied using 2 to 3 well exposed stars in the field.

About 20 isolated stars were chosen as secondary standards for which Vrba *et al.*

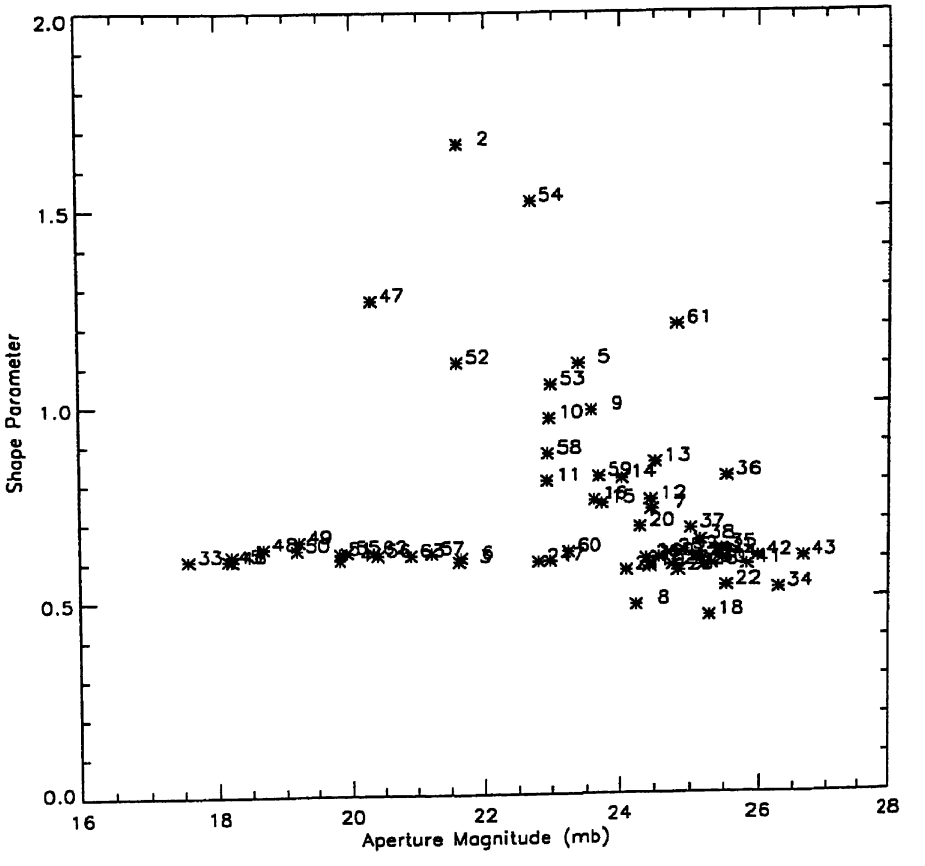

Figure 5.3: GRB 920720: Star-galaxy separation using the shape parameter (see §2.2.5 for details).

(2000; private communication) provided UBVRI field photometry. Fig 5.4 (a) and (b) shows the calibration solutions and (c) shows residual (i.e, computed - standard) B magnitude plotted against the standard B magnitude. In (d) we show the computed B–I color v/s B magnitude plot. In Fig 5.3 we display the crude shape parameter used to separate the objects into stars and galaxies. It may be seen that this field being at high Galactic latitude, virtually all objects are galaxies. The horizontal sequence identifies the stellar objects and the objects falling diagonally are galaxies. The object marked as #2 at the center of the field is a galaxy with B=18.87±0.01 and lies outside the revised error box. Only two objects have been detected inside the revised error box and these are at B=22±0.13 and B=21.25±0.065. The objects marked A, B, C, D and E are detected only in I-band and their magnitudes are 20.617±0.09, 21.44±0.19, 19.643±0.04, 20.23±0.07 and 20.108±0.06, respectively. The limiting magnitudes are measured to be B > 22.8 and I > 21.5.

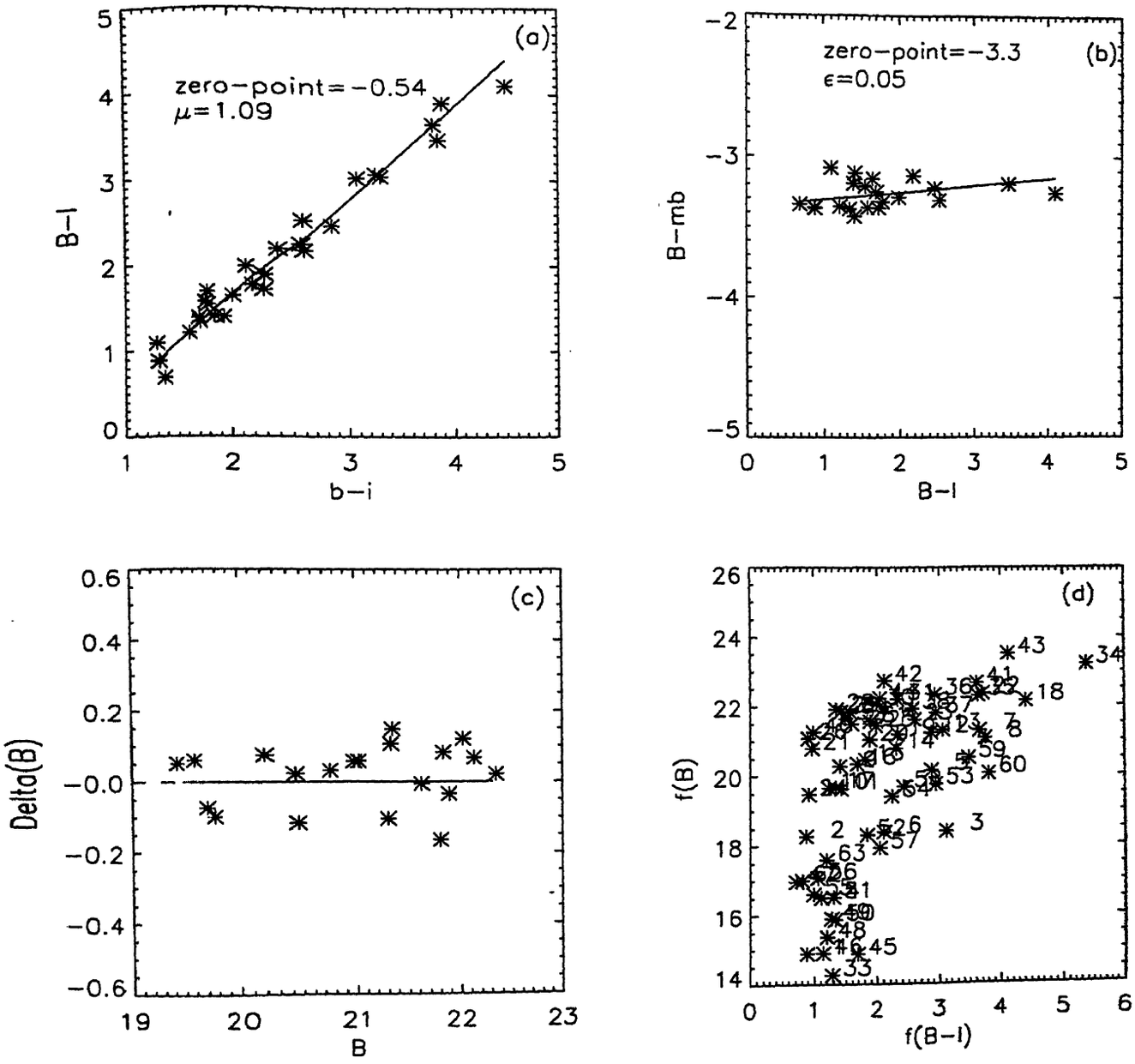

Figure 5.4: GRB 920720: (a)&(b) Calibration solutions (c) residual B (i.e, computed — standard) v/s B (d) color–magnitude diagram. Here, B and (B-I) represent the standard values (taken from Vrba *et al.*); fB and f(B-I) represent the computed values.

2. GRB 920517

The field of GRB 920517 was observed on 12 Mar 1997 using 1k CCD (CCD #3 VBT; see Appendix 2.1) in combination with new 2-in filters procured for the use at 1.02 m telescope. The details of observations are as in Table 5.3. Following the basic CCD reductions, individual frames in each band-pass were aligned and combined to

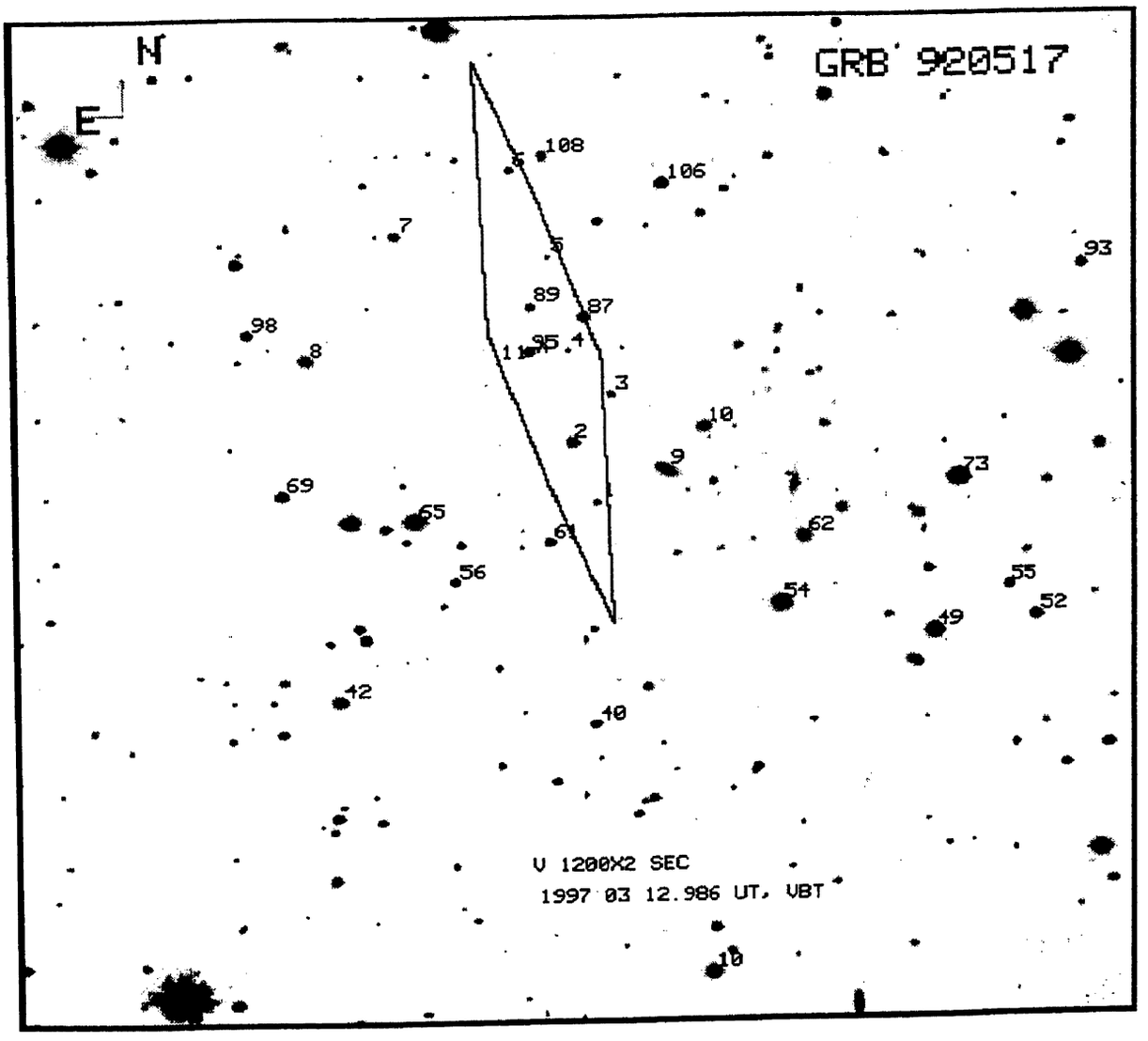

Figure 5.5: GRB 920517: V-band image observed with VBT. The objects marked outside the error box are local standards chosen from the field photometry provided by Henden (2001) and are used to calibrate the objects inside the error box. The total FOV is $10'.4 \times 10'.4$.

form an average image as explained in Chapter 2. In Fig 5.5 we show the combined V-band image along with the overlay of revised IPN[3] error box. A total of 193 objects were detected common to B, V & I frames; 164 objects in V & I-band , but not present in B-band and 110 objects present only in I-band. However, we do not intend to present the analysis of all these, but restrict ourselves to objects contained within the error box.

Twenty field stars were chosen as local standards for which astrometric positions as well as B, V, R and I photometry were provided by Henden (2001; private communication). These were identified after determining the astrometric solutions for our observed frame. Following this, we determined aperture magnitudes for local

Table 5.3: GRB 920517: Observations

Mid-UT	Filter	Exp. time (sec)	Average Seeing	Limiting Magnitude
1997 03 12.8281	I	900 × 2	2″.1	20.5
1997 03 12.9146	B	1800× 2	2″.3	22.0
1997 03 12.9861	V	1200× 2	2″.1	21.8

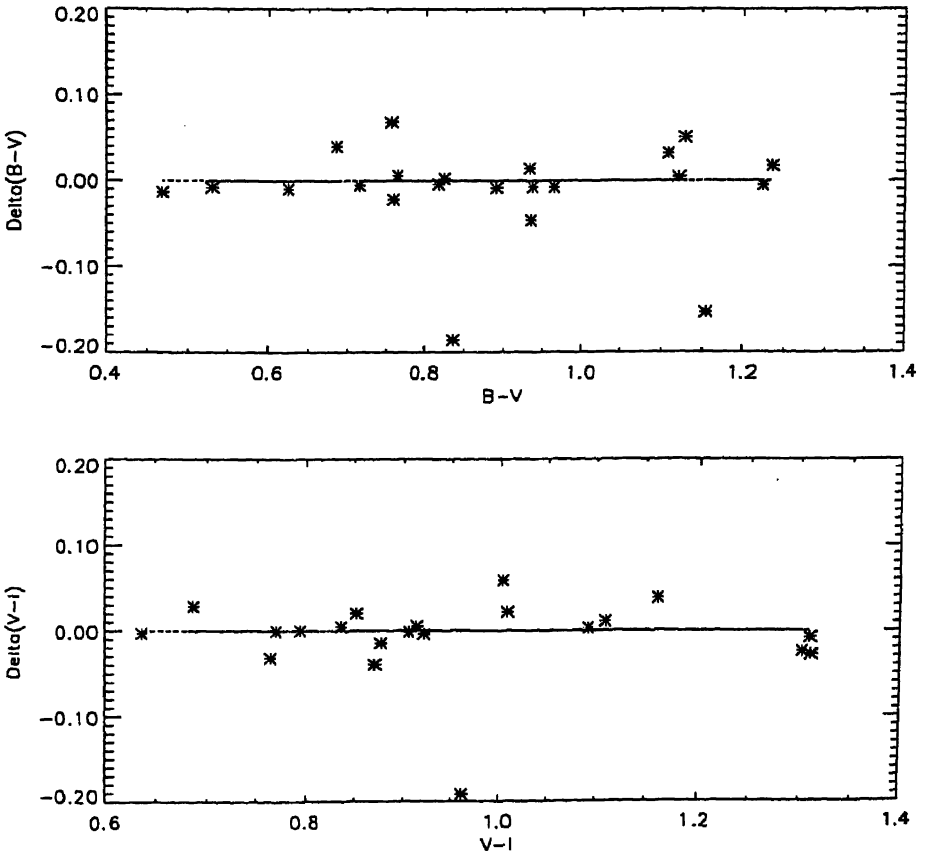

Figure 5.6: GRB 920517: The residual (computed – standard) colors B–V (*upper panel*) and V–I (*lower panel*) are plotted against the respective standard colors.

reference stars as well as all the objects inside the error box. The calibration solutions were obtained as detailed in Chapter 2. and are shown in Fig 5.7. Using the calibration solutions we obtained B, V and I magnitudes as well as colors B–V and V–I for the objects of interest. The residual values of B–V and V–I color are plotted against standard colors (Fig 5.6). The color–magnitude as well as color-color plots

are shown in (e) and (f) respectively. From the color-color plot and Fig 2.2 separating the objects into stars and galaxies using the shape parameter the galaxies were identified. Further, visual examination was used to confirm the detection. Table 5.4 tabulates the computed B, B–V, V–I and the photometric errors for objects inside the error box.

Table 5.4: GRB 920517: Photometry

id	fB	e(fB)	f(B-V)	e(fBV)	f(V-I)	e(fVI)
1	19.4031	0.014	1.21752	0.050	1.28285	0.017
2	18.5587	0.011	1.00039	0.031	1.48326	0.016
3	19.3467	0.018	1.14071	0.065	1.58140	0.021
4	20.2417	0.029	1.51044	0.13	1.41921	0.035
5	20.6083	0.040	1.36193	0.16	2.59587	0.041
6	18.8510	0.011	1.16938	0.039	1.32107	0.013
7	18.6412	0.010	1.22162	0.040	1.33450	0.012
8	18.3169	0.010	1.23800	0.038	1.21983	0.012
9	17.3105	0.0060	1.34350	0.027	1.37066	0.0072
10	18.0969	0.0090	1.23800	0.033	1.34277	0.010

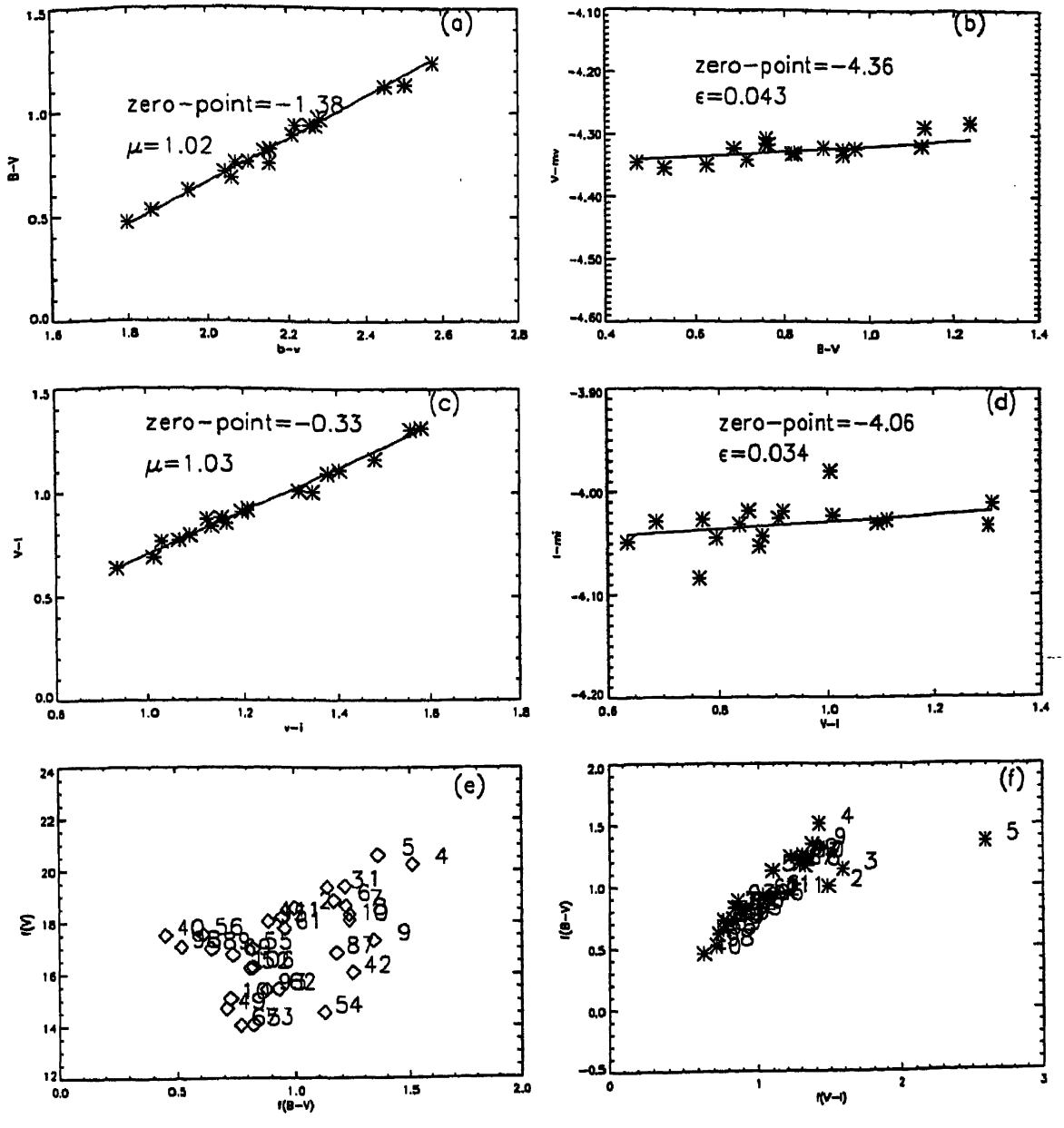

Figure 5.7: GRB 920517: (a)–(d) shows the calibration solutions using Henden photometry. Solid lines are least square fits to the local reference stars; (e) shows the color-magnitude diagram, and (f) the color-color diagram.

3. GRB 920525

The field of GRB 920525 was observed on 24 Sept, 1995 using 2.34 m VBT equipped with astromed CCD chip GEC P8603 - one of the rare occasion for sky to clear in this season. Seeing varied from 2″.2–2″.8 during our observations. The log of observations is shown in Tabel 5.5.

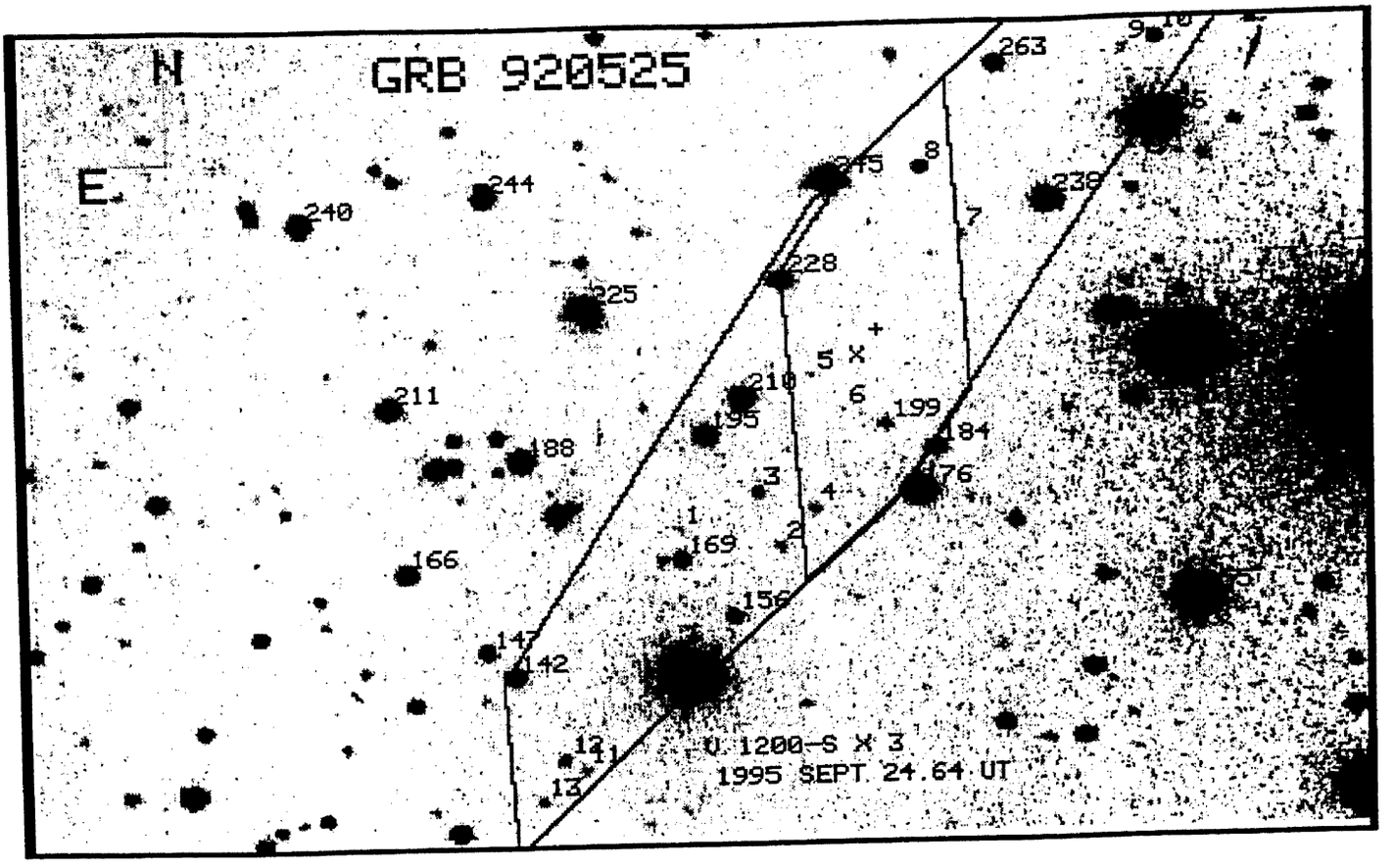

Figure 5.8: GRB 920525: The CCD image in V-band of 20 min × 3 exposure taken with Astromed CCD 578 × 385 at VBT. The FOV is ∼ 5′.3 × 3′.5. The revised (inner) and initial (outer) error boxes are drawn using the box co-ordinates from Laros *et al.* (1998) and Vrba (2000; e-mail communication) respectively. The object marked as #225 is a bright galaxy ∼ 30″ from the box center.

Table 5.5: GRB 920525: Observations

Mid-UT	Filter	Exp. time (sec)	Average Seeing	Limiting Magnitude
1995 08 24.638	V	1200 × 3	2″.1	22.7
1995 08 24.646	I	900 ×3	2″.2	21.3
1995 08 24.748	R	900 × 3	2″.3	–

CCD reductions were carried out in standard manner as explained in Chapter 2. Three frames in each bandpass were aligned w.r.t. the astrometric positions of a few USNO-A2.0 stars in the field (marked as 240, 244, 245, 256, 238, 223, 155, 176, 141,

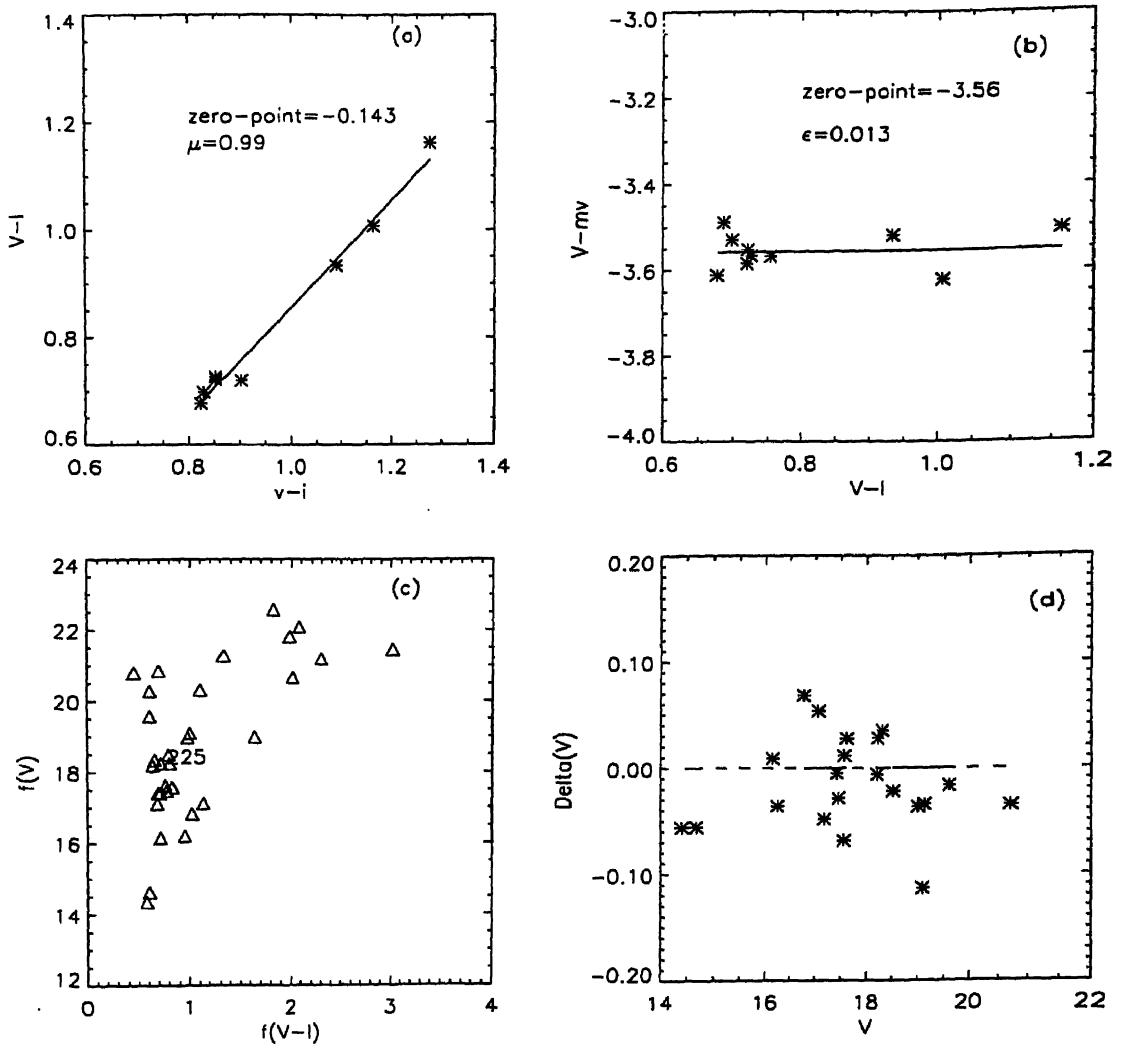

Figure 5.9: GRB 920525: (a) & (b) show the calibration solutions, (c) the color–magnitude diagram and (d) the residual (computed - standard) V magnitude plotted v/s standard V magnitude. (V-I), V and f(V-I), fV represent standard (from Vrba *et al.*) and computed color and magnitudes, respectively.

188) and then combined to obtain an average image (Fig 5.8). Aperture magnitudes were determined for all the objects inside the error box. Suitable aperture corrections were applied and magnitudes were determined at $\sim 9''$ aperture radius. Using the field photometry provided by Vrba *et al.* (2000; e-mail communication) in U, B, V & I bands we calibrated V, I and V-I. The calibration solutions are shown in Fig 5.9. The brigtest galaxy (# 225) in the field has $V = 18.2$ and color $V - I = 0.8$ and it is outside the IPN error box.

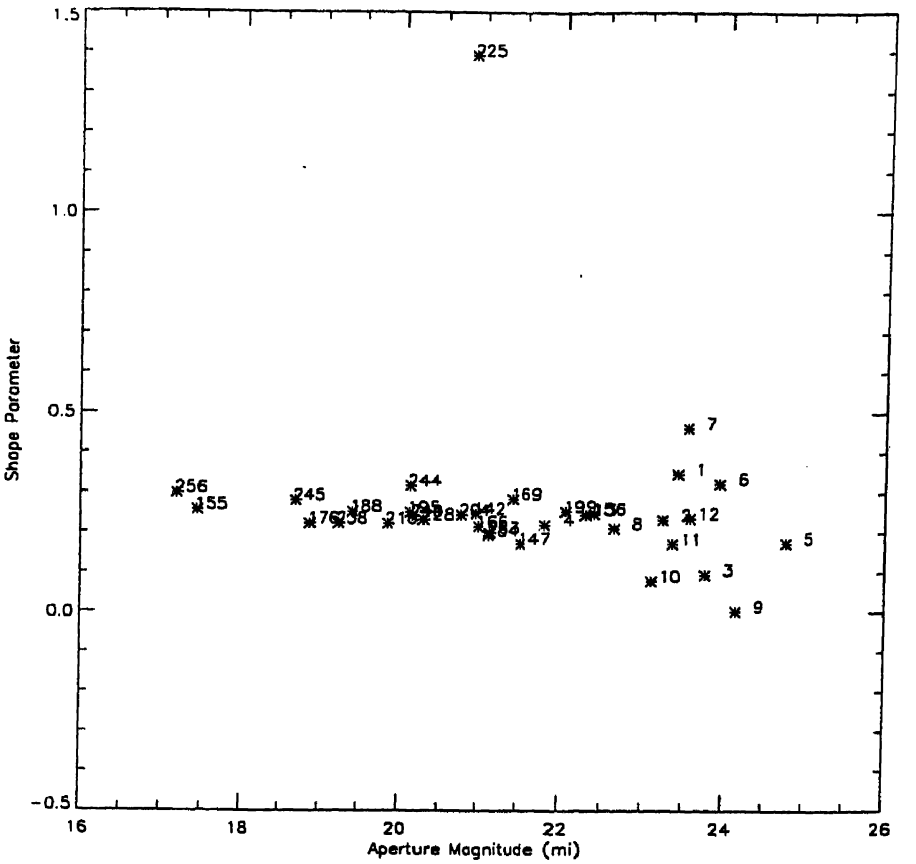

Figure 5.10: GRB 920325: Star-galaxy separation using the shape parameter (see §2.2.5 for details).

4. GRB 920325

Observations and data analysis

The field of GRB 920325 was observed on 29 June, 1995 using 2.34 m VBT equipped with astromed CCD chip GEC P8603. We observed three frames of 600 s each in R-band under non-photometric sky conditions. The typical seeing was 3″.3. The position of this field in the sky make it available (at reasonable hour-angles) for observations during the monsoon period in India and therefore complete coverage in all filters or even coverage of complete IPN error box using a single filter could not be achieved. Our observations were centered at initial co-ordinates (J2000) RA=23:22:18.5, DEC=+13:03:11 (Hurley 1995; private communication). The revised IPN[3] error box ($7' \times 2'$) is overlaid on the DSS image shown in Figure 5.1 (*right-panel*).

CCD reductions were carried out in the standard manner as explained in Chapter 2. Three R-band images were aligned using the astrometric positions of a few

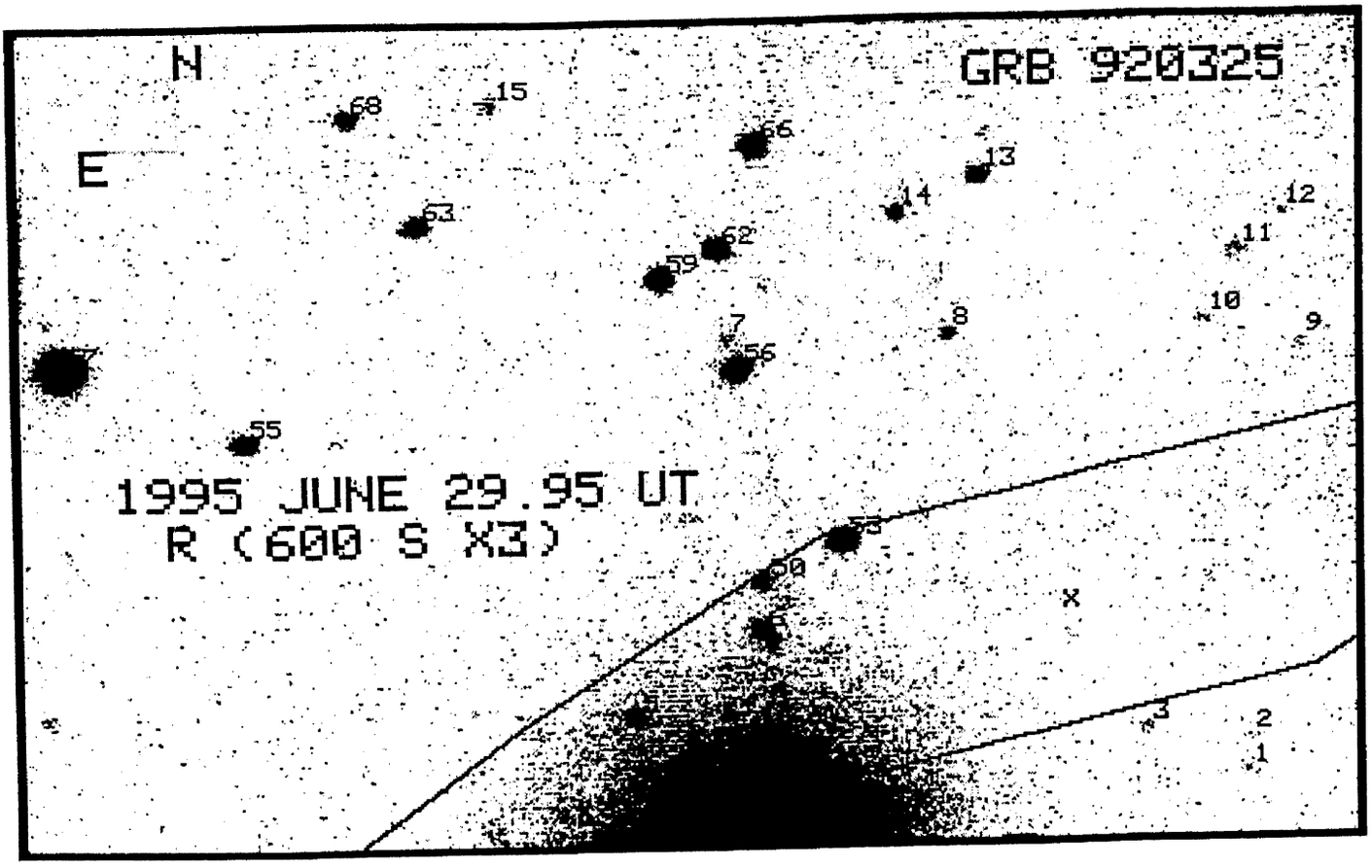

Figure 5.11: GRB 920325: The combined R-band image of 600×3 sec exposure observed with VBT on 29 June 1995. The FOV is $\sim 5'.3 \times 3'.5$. The revised IPN[3] error box (Laros *et al.* 1998) is shown.

USNO-A2.0 stars in the field and then an average combined image was formed (Fig 5.11). Aperture magnitudes were determined for all the 26 objects in this frame. In Fig 5.12(a) we show the growth curve (see §2.2.4) for standard stars. Suitable aperture corrections were applied and magnitudes were determined at 9″ aperture radius. Since the magnitudes of USNO-A2.0 are not recommended for calibration, (see *http://www.nofs.navy.mil*) we used Landolt's standard field PG2213-006 observed an hour before the GRB 920325 field on the same night to calibrate the magnitudes of objects in GRB field. We obtained zero-point constant= -4.1 and slope = 0.99 from the standard star measurement. The residual (computed - Landolt) for four stars is $\langle 0.026 \pm 0.005 \rangle$. In Fig 5.12 (b)and (d) we show the calibration solutions; The magnitudes calibrated using USNO stars systematically differ by $\langle 0.5 \pm 0.02 \rangle$ from those calibrated using the standard star and are fainter by ~ 0.3 mag as compared to USNO catalog itself.

It may be seen from both Fig 5.12 (c) as well as Fig 5.11 that there is just one

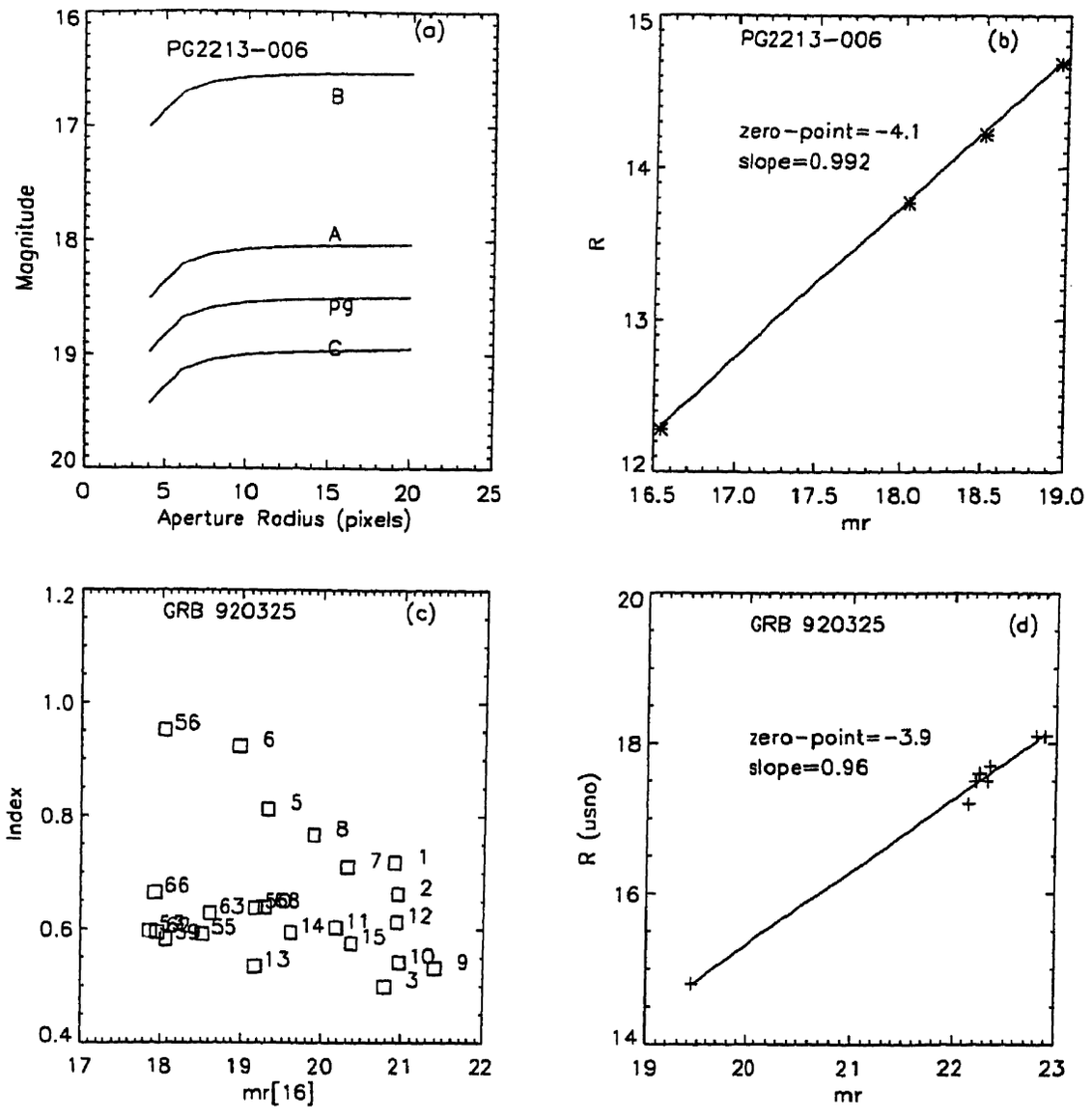

Figure 5.12: GRB 920325: Growth curve (a) and calibration plot (b) using the nightly standard star observation; star-galaxy separation using the shape parameter (see §2.2.5 for details) (c). The instrumental v/s R magnitude (USNO-A2.0) is also shown in (d).

stellar object (# 53) and four unresolved objects within the error box. The objects numbered #6 and #50 are definitely galaxies and their R magnitudes are 18.97 ± 0.05 and 19.17 ±0.05 respectively. The objects #1, 2, 10, & 12 are at the detection limit R=20.9 ±0.1 With the given seeing and sky conditions it is hard to make any statements about the variability of the objects in the frame; however, among the three frames each of exposure 600 s taken continuously in R-band, these objects have not shown any obvious variability.

5.5 Estimation of Host-galaxy Redshifts & Discussion

In an attempt to ask 'what can be derived from the old IPN data' we use the results on LF of GRBs presented in Chapter 4 and determine the redshift range of host-galaxies from which these GRBs could have come from. We assume the GRBs to have a log-normal luminosity function with $10^{55}\,\mathrm{sec}^{-1} \leq L_0 \leq 10^{56}$ and $\sigma = 2$, in agreement with the afterglow data and BATSE N–F relation that is independent of the evolution of GRBs with redshift (Chapter 4). This allows us to calculate the redshift range from which the GRB with a given flux originates.

Table 5.6: Probable Redshift range: IPN GRBs

GRB	Peak Flux	$\langle z \rangle$ for $L_0(\mathrm{sec}^{-1})$	
	ph/cm^2/s	10^{55}	10^{56}
GRB 920720	15.437	0.16	0.42
GRB 920517	38.757	0.11	0.29
GRB 920525	22.64	0.14	0.36
GRB 920325	13.75	0.17	0.44

Fluxes of 4 IPN GRBs and the range of their redshift is given in Table 5.6. Since the BATSE flux was not available for GRB 920325, it is converted from the observed 25–100 keV range (Hurley 2000; private communication) to the BATSE range (50–300 keV) using the method discussed in Appendix B of Chapter 4. The durations of these 4 GRBs are > 2 sec and they belong to the class of long duration bursts. For a given flux, L is determined using the Eq. 4.1 and using Eq. 4.8 the average redshift of the GRB of a given flux can be calculated to be:

$$\langle z \rangle = \int_0^\infty dz\, z p(z) \tag{5.1}$$

The variance of the the expected redshift is:

$$\sigma = \int_0^\infty dz\, (z - \langle z \rangle)^2 p(z) dz \tag{5.2}$$

From Table 5.6 it is seen that the redshifts lie in the range 0.1–0.4 when L_0 is varied between 1–10 in units of $10^{55}\,\mathrm{sec}^{-1}$. The variances are close to the mean value.

Similarly, we estimate the the average redshift and variance for a sample of galaxies in a magnitude-limited sample. The relation between apparent magnitude m and absolute magnitude M is:

$$M = m - 25\log_{10}(r/1\,\mathrm{Mpc}) - 2.5\log_{10}(1+z) - m_K(z,\lambda) \tag{5.3}$$

m_K is the K-correction for galaxies and is a function of the redshift and the wavelength λ of the observed band. Given the absolute magnitude, the luminosity ($\mathrm{erg\,sec}^{-1}$) in different wave bands can be calculated using:

$$\begin{aligned} L_B &= L_\odot \times 10^{[0.4\times(5.41-M_B)]} \\ L_V &= L_\odot \times 10^{[0.4\times(4.79-M_V)]} \\ L_U &= L_\odot \times 10^{[0.4\times(5.51-M_U)]} \\ L_R &= L_\odot \times 10^{[0.4\times(4.49-M_R)]} \end{aligned} \tag{5.4}$$

Here $L_\odot = 4 \times 10^{33}$ is the bolometric luminosity of the Sun.

The luminosity function of galaxies in B-band and its evolution for $z \leq 1$ is taken from Loveday *et al.* (1992) and Lilly *et al.* (1995). We apply k-correction on 'blue' and 'red' galaxies (for meaning of blue and red galaxies see Lilly *et al.* 1995) using the k-corrections given by Coleman, Wu, and Weedman (1980). The luminosity function in other wave-bands can be obtained by using the spectral energy distribution given by Yoshii & Takahara (1988). For simplicity we assume the galaxy spectral distribution to remain unchanged for $z \leq 1$.

The redshift range for a given magnitude limit for the four IPN fields is given in Table 5.7. The range refers to the 1σ deviation from the mean redshift. Comparing this table with Table 5.6 we notice that the redshift range corresponding to the limiting magnitude of observed field overlaps with the redshift range from which the GRBs originate in all four cases. Therefore the GRB host might lie in the observed field.

If GRBs are associated with galaxies then it is natural to ask whether the observed fields have any plausible candidates for the GRB hosts. While studies such as ours have not been able to identify any host candidates (e.g. Schaefer 1992), the lack of such candidates had lead investigators (see e.g. Woods & Loeb 1995 and Schaefer

2000 for earlier references) to suggest that there exists a 'no host' problem. However, most of these studies have assumed GRBs to be standard candles, while our study (Chapter 4) shows that the GRB luminosity function is quite broad. This basically means that the redshift range from which the GRBs originate is also quite broad, as is evidenced by Table 5.6. Therefore, although some of the objects seen inside the error boxes could be potential candidates, we can not rule out the possibility of the host being fainter than the magnitude limit of our survey.

Table 5.7: Redshift Estimation: IPN host galaxies

GRB	Limiting Magnitude	z-range (mean $\pm 1\sigma$)
GRB 920720	B = 22.8	0.26 - 0.62
GRB 920517	B = 22.0	0.19 - 0.53
GRB 920525	V = 22.7	0.28 - 0.64
GRB 920325	R = 20.9	0.18 - 0.5

Bibliography

[1] Atteia, J.-L. *et al.* 1987, ApJSS, 64, 305

[2] Bahcall, J. N. & Soneira, R. M. 1980, ApJS, 44, 73

[3] Coleman, G. D., Wu, C., Weedman, D. W. 1980, ApJS, 43, 393

[4] Greiner, J. & Wenzel, W. 1990, *Gamma Ray Bursts: Observations, Analyses and Theories*, proc. of the workshop, (ed). Ho, C., Epstein, R. I. & Fenimore, E. E. p. 119

[5] Hudec, R. 1990, *Gamma Ray Bursts: Observations, Analyses and Theories*, proc. of the workshop, (ed). Ho, C., Epstein, R. I. & Fenimore, E. E., p. 107

[6] Hudec, R. 1993, A & AS, 97, 49

[7] Hurley, K. *et al.* 2000, ApJ, 533, 884

[8] Kippen, M. R. *et al.* 1998, ApJ, 492, 246

[9] Kron, R. G. 1980, ApJS, 43, 305

[10] Laros, J. G. *et al.* 1998, ApJS, 118, 391

[11] Larson, S. B. McLean, I. S., Becklin, E. E. 1996, ApJL, 460, L95

[12] Larson, S. B. 1997a, ApJ, 491, 86

[13] Larson, S. B. McLean, I. S., Becklin, E. E. 1997b, ApJ, 491, 93

[14] Lilly, S. J., Tresse, L., Hammer, F., Crampton, David, Le Fevre, O. 1995, ApJ, 455, 108

[15] Loveday, J., Peterson, B. A., Estathiou, G., Maddox, S. J. 1992, ApJ 390, 338

[16] Petrosian, V. 1976, ApJ, 209, L1

[17] Richer, H. B. & Fahlman, G. G. 1992, Nature, 358, 383

[18] Schaefer, B. E. 1987, ApJ, 313, 226

[19] Schaefer, B. E. 1989, ApJ, 340, 455

[20] Schaefer, B. E. 1990, ApJ, 364, 590

[21] Schaefer, B. E. 1990, *Gamma Ray Bursts: Observations, Analyses and Theories*, proc of the workshop, (ed). Ho, C., Epstein, R. I. & Fenimore, E. E., p. 107

[22] Schaefer, B. E. 1998, In 4hGRB, p. 595

[23] Schaefer, B. E., 1992, In 2hGRB, p. 382

[24] Valdes, F. 1993, *FOCAS User's Guide*

[25] Vrba, F. J. *et al.* 1995, ApJ, 446, 115

[26] Vrba, F. J., 1998, In 4hGRB, p.*

[27] Woods, E. & Loeb, A. 1995, 453, 583

[28] Yoshii, Y. & Takahara, F. 1988, ApJ, 326, 1

Chapter 6

Clustering of GRBs on the Sky.

Abstract

The two-point correlation of the 4th (current) BATSE catalog is calculated. It is shown to be consistent with zero at nearly all angular scales of interest. Assuming that GRBs trace the large scale structure in the universe we calculate the angular correlation function for the standard CDM (sCDM) model. It is shown to be $\leq 10^{-4}$ *at* $\theta \simeq 5^{\circ}$ *if the BATSE catalog is assumed to be a volume-limited sample up to* $z \simeq 1$. *Combined with the error analysis on the BATSE catalog this suggests that nearly* 10^5 *GRBs will be needed to make a positive detection of the two-point angular correlation function at this angular scale.*

6.1 Introduction

Although afterglow observations have provided direct evidence that GRBs are hosted by faint galaxies (typically $R = 26.0$ mag) at cosmological distances, there remain many open issues viz. their progenitors, actual triggering mechanism and their environments. The fraction of GRBs for which counterparts are detected is $< 1\%$, and therefore statistical analysis plays an important role in establishing their distance scales. Various kinds of statistical tests have been performed in the literature viz. tests to correlate GRBs with known objects, to search for correlation among observed parameters and importantly to constrain Galactic v/s cosmological origin.

One of the statistical test which can reveal the distance scale of GRBs and give useful hints about their progenitors is the two-point angular correlation function. In section §3. we describe the estimators of angular two-point correlation function. Our

analysis of 4th (current) BATSE catalog is based on the argument that if GRBs are cosmological in origin, they should show clustering properties as expected of other cosmological population of objects. In section §4. we present the methodology and results of correlation analysis and we draw our conclusions in section §5.

6.2 Statistical Approaches in GRB Studies - A Brief Review

Tests to support Galactic origin consisted of Nearest Neighbour (NN) analysis (Quashnock & Lamb 1993a, 1993b; Narayan & Piran 1993), Likelihood analysis (Luo *et al.* 1996), time-dependent two point correlation function analysis (Brainerd *et al.* 1995), correlation of angular positions with time of occurrence of GRBs using survival analysis technique (Petrosian & Efron 1995), Spherical harmonics (Hartmann & Epstein 1989) and so on. Most of these tests searched for GRB repeaters based on the following argument: In the absence of transient or quiescent counterparts to GRBs only distance indicator is angular distribution of GRBs. Although dipole and quadrupole moment measurements (Meegan 1992) indicate their isotropic property, a careful visual examination of the diagram (Fig. 1.2) shows regions where 2 or more GRBs are clustered together. Each GRB has a location error associated with its position and it is possible that at such clusterings their error boxes are overlapping. It has been argued that clustering is an indication of multiple bursts occurring from a single source if the angular separation between the pairs in clusters is $\leq$ typical size of error boxes in the catalog. Such repeating bursts can be explained by Galactic models and therefore clustering provides an evidence for galactic origin of GRBs. But in case of cosmological models GRB is a catastrophic event where the source might be completely destroyed and therefore GRB sources are not believed to give rise to repeated bursts and this is consistent with the current observations.

Although some of these analyses claimed the existence of repeaters (Quashnock & Lamb 1993a, 1993b ; Wang & Lingenfelter 1993, 1994), many others didnot find evidence for repeaters (Narayan & Piran 1993; Rutledge & Lewin 1993; Nowak 1993; Hakkila *et al.* 1996; Luo 1996; Brainerd *et al.* 1995).

Tests supporting cosmological origin involved computation of two-point correlation function (Hartmann & Blumenthal 1989 ; Blumenthal, Hartmann & Linder 1994) and power spectrum analysis (Lamb & Quashnock 1993). The aims of such

analyses were several : (a) if GRBs are cosmological then the value of two-point correlation can be used to put a lower bound on the distance scale of GRBs and (b) if the GRBs show a non-zero two-point correlation function then its correlation properties can be compared to the correlation properties of the known extra-galactic objects. This can in principle give clues on the possible hosts of GRBs. All the earlier results, perahps owing to the small GRB sample, showed that the two-point correlation functions were consistent with zero.

6.3 Estimators of Two Point Correlation Function

Two-point angular correlation function is one of the tools to measure the degree of clustering of objects in a given sample. This technique is widely used in cosmology to study the clustering properties of galaxies, Rich clusters, High redshift quasars, Lyman-α clouds and so on and to quantify the large scale structure in the universe (see e.g. Peebles 1993).

Given a two-dimensional distribution of N point objects in a solid angle Ω, the two-point angular correlation function is defined using the relation (Peebles 1980):

$$dP = n[1 + w(\theta)]d\Omega \tag{6.1}$$

where dP is a probability defined in the following way: if an object is chosen at random then dP gives the average number of neighbours within an angular separation θ and $\theta + d\theta$. n is the density of points $n = \frac{N}{\Omega}$. $w(\theta)$ is the angular two-point correlation function. Therefore $w(\theta)$ measures the excess of neighbours over a random Poisson distribution at a given separation θ. If the objects are isotropically distributed then $w(\theta) = 0$ for all θ.

To estimate the two-point correlation from a given distribution of objects, it is not very convenient to use Eq. (6.1) directly. Several estimators of two-point correlation function have been discussed in the literature. One of the earliest estimators was given by Peebles and Hauser (1974):

$$w(\theta) = \frac{DD}{RR} - 1 \tag{6.2}$$

Here DD is the number of pairs in the angular separation interval $(\theta\ ,\ \theta + d\theta)$ in the

data sample and RR is the number of pairs in a mock, random, isotropic sample with angular separation in the same interval.

The above estimator for correlation function is widely used. But several alternative estimators of two-point correlation function have also been suggested. The estimator by Davis & Peebles (1983) is given by:

$$w(\theta) = \frac{DD}{DR} - 1. \tag{6.3}$$

Here DR is the number of random points in an interval θ and $\theta + d\theta$ averaged over centers taken as the data points.

The error in estimating the two point correlation function (the standard deviation) can be computed for these estimators:

$$\delta w(\theta)^2 \simeq \frac{1}{DD} + \frac{4}{N} \tag{6.4}$$

The first term on the RHS is from Poisson fluctuations (Peebles 1980). The second term comes from a more careful analysis and gives the correlated component of the variance (Mo *et al.* 1992). The second term dominates the variance once $DD \geq N/4$. This condition is reached for large angular scales and small $w(\theta)$. For the GRB BATSE catalog the smallest angle at which reliable information can be obtained is $\simeq 5°$ and at this angle $w(\theta) \ll 1$; and therefore it is the second term of RHS of above relation that dominates the variance in this case. i.e, the error in both the above estimators is $\propto \frac{1}{N}$.

The above estimators have a limitation that their variance is limited by uncertainty in mean density. Hamilton (1993) proposed an estimator given by:

$$w(\theta) = \frac{DD \times DR}{(DR)^2} - 1 \tag{6.5}$$

Here the variance in $w(\theta)$ is not dependent on the uncertainty in the mean density of sample objects, but is given by uncertainty in pair-counts (the first term in Eq. (6.4). Landy & Szalay (1993) introduced an improved estimator which is also unbiased:

$$\omega(\theta) = \frac{DD - 2DR + RR}{RR}. \tag{6.6}$$

The variance of this estimator is also Poissonian. The estimators by Hamilton

(1993) and Landy & Szalay (1993) are more reliable on large scales where correlation function is small. In our present work we report the results using the estimator given by Landy & Szalay (1993).

6.4 Results

Assuming BATSE catalog to be a flux-limited, homogeneous sample we computed $\omega(\theta)$ for 4th (current) catalog for angular scales $> 5°$ which is larger than the typical location errors in BATSE catalog, so that we could ignore the effects of location errors on correlation function. We generate mock samples of points isotropically distributed on the sphere and count the number of pairs at a given angular separation in data-data, random-random and data-random sample. The uncertainty in $\omega(\theta)$ has been computed using the first term of Eq. (6.4)

In Fig. 6.1 we show the angular correlation function with 1σ error bars for current BATSE (2494 objects) catalog. We also plot the 1σ errors. The main conclusions of our analysis are:

1. The two-point angular correlation function is consistent with zero on nearly all angular scales of interest.

2. From Fig. 6.1 it is seen that at several angular scales a 1σ detection of the correlation function seems to be possible. To make a definitive statement about a detection we need to take into account several uncertainties in our analysis. One of the dominant source of uncertainty is the heterogeneity of the sample with respect to the error in angular positions of the GRBs (the localization uncertainty varies from $\simeq 1°$–$10°$). This means that errors at $\theta \leq 10°$ are much larger than seen in Fig. 6.1 Another major source of uncertainty comes from anisotropic exposure function of the BATSE instrument, which results in a non-zero correlation function even for a completely isotropic intrinsic distribution[1]. Though it is possible that some of the signal at large angular scales is not an artifact, more careful analysis would be required to confirm it.

[1]for more details see `http://www.batse.msfc.nasa.gov/batse/grb/catalog/`

6.5 Conclusions and Summary

The two-point correlation function of the 4th (current) BATSE catalog (2494 objects) is consistent with zero at nearly all angular scales that can be probed in the BATSE catalog. This result is consistent with theory if the GRBs are assumed to trace the dark matter distribution with some bias and are a complete sample up to $z \simeq 1$ (Sethi *et al.* 1999).

When can a detection of the two-point correlation function become possible? The error in the two-point correlation function scales as $DD^{-1/2}$ (first term of Eq. (6.4)) and $DD \propto N^2$, N being the number of objects in the catalog. Therefore the error

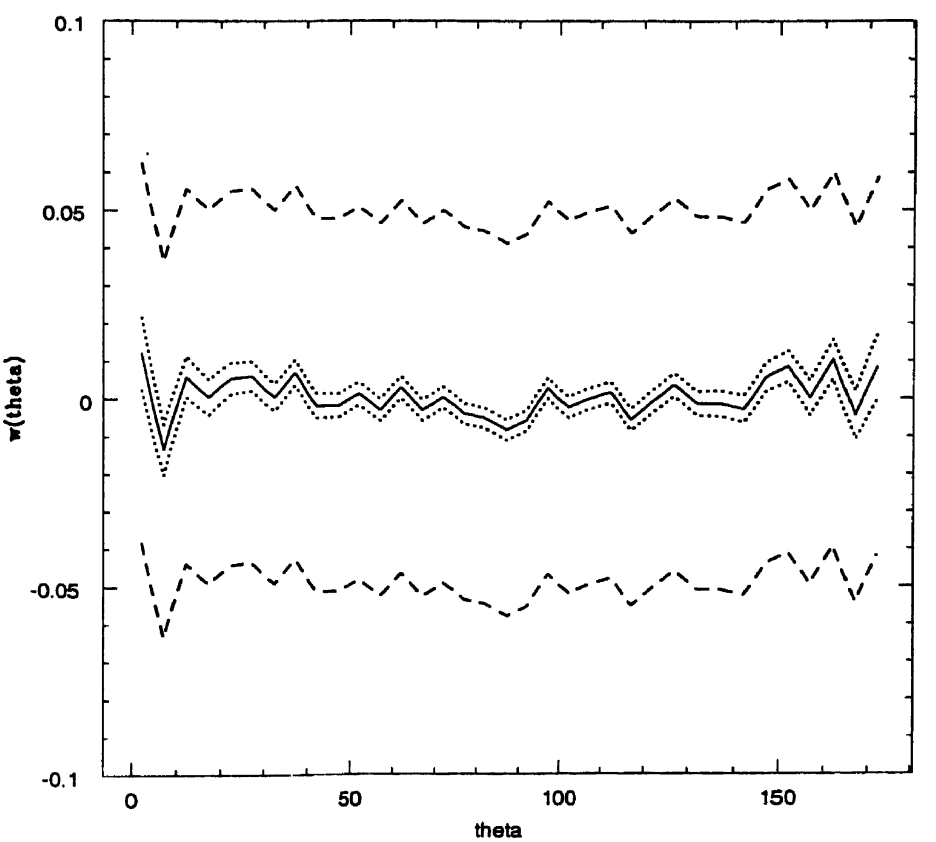

Figure 6.1: The two-point angular correlation function for the BATSE catalog (2494 objects) and the 1σ error bars are shown. The *solid* line corresponds to the two-point correlation function. The *dotted* lines show the 1σ errors given by Eq. (6.4).

in estimating the two-point correlation function scales as $1/N$. Theory suggests (Sethi *et al.* 1999) that the value of correlation function at $\theta = 5°$ is $\leq 10^{-4}$ if the GRB sample is assumed to be complete up to $z \simeq 1$. We check that DD at $\theta \simeq 5°$ is $\simeq 10^{-2}$ times the total number of pairs ($\simeq N^2/2$) in the GRB sample. This would suggest that a detection might become possible at this angular scale when the number of objects in the sample exceeds 10^5.

Recently launched *HETE-II* and future surveys like *Swift* will localize the GRBs to a few arc-minutes. This means smaller angular scales could be probed. And as the theoretically-predicted two-point correlation function scales as $\sim \theta^{-1}$, the probability of detection will increase. The *Swift* instrument after the successful launch will detect nearly 1000 objects over a period of 3 years with an angular resolution $\leq 1''$. However, though the two-point correlation function is large at these angular scales, the average separation between 1000 objects on the complete sky is $\simeq 6°$. Therefore as long as $w(\theta) \leq 1$, the probability of finding an object within a few arcseconds of the other is negligible. It is possible that $w(\theta) \gg 1$ at sub-arcsecond scales. However, detailed analysis, taking into account the non-linear correction to the power spectrum of density perturbation, is needed to make precise theoretical predications for the future surveys.

Appendix: Theoretical Predictions

The two-point angular correlation function can be related to the two-point three-dimensional correlation function $\xi(r)$ using Limber's equation (for details see Peebles 1980). If we assume that the GRBs constitute a volume-limited sample up to a distance $r_{\rm max}$ and that the comoving number density of objects is constant, the Limber's equation reduces to:

$$w(\theta) = \frac{\int_0^{r_{max}} \int_0^{r_{max}} r_1^2 r_2^2 dr_1 dr_2 \xi(r_{12}, z_1, z_2)}{\left[\int_0^{r_{max}} r^2 dr\right]^2} \tag{6.7}$$

Here

$$r_{12}^2 = r_1^2 + r_2^2 - 2r_1 r_2 \cos\theta. \tag{6.8}$$

r is the coordinate distance in an isotropic, homogeneous universe. The two-point correlation function is related to the power spectrum $P(k)$ of the density fluctuations as:

$$\xi(r,t) = b^2 \frac{1}{2\pi^2} \int_0^\infty k^2 dk P(k,t) \frac{\sin(kr)}{kr}. \tag{6.9}$$

b, the bias factor, denotes the clustering of visible matter relative to the dark matter. While its absolute value is still uncertain, the relative bias between nearby rich clusters of galaxies and optically-identified galaxies is $\simeq 5$. And hence if GRBs originate in clusters rather than ordinary galaxies their correlation can be 25 times larger. In this paper, we use the linear perturbation theory predictions for $P(k,t)$. We have checked that for the angular scales of interest ($\theta \geq 5°$) it is a reasonable assumption. We use the BBKS fit (Bardeen *et al.* 1986) for the linear power spectrum of the standard CDM (sCDM) model and some of its variants. We normalize the power spectrum requiring $\sigma_8 = 0.7$. The time dependence of linear power spectrum is $P(k,t) \propto (1+z)^{-2}$, which is also the time dependence of the two-point correlation function. It should be noted that in general the two-point correlation function depends on both the separation between two points and their redshifts, as indicated in Eq. (6.7). However, the two-point correlation function is negligible for points separated by a large enough redshift difference. Therefore, for most purposes $\xi(r,t) \propto (1+z)^{-2}$, where z refers the redshift of any of the two points.

In Figure 6.2 we show the theoretically predicted angular two-point correlation function using the assumptions of P(k,t) for sCDM model. The bias b is taken to be one. If observed GRBs constitute a complete sample up to $z \simeq 1$ and they are assumed to be associated with highly biased structures like rich clusters, the value of correlation function is $\leq 10^{-4}$ at 5°. This is the smallest angular scale at which information is possible in the BATSE catalog. At larger angles the correlation function typically scales as θ^{-1}.

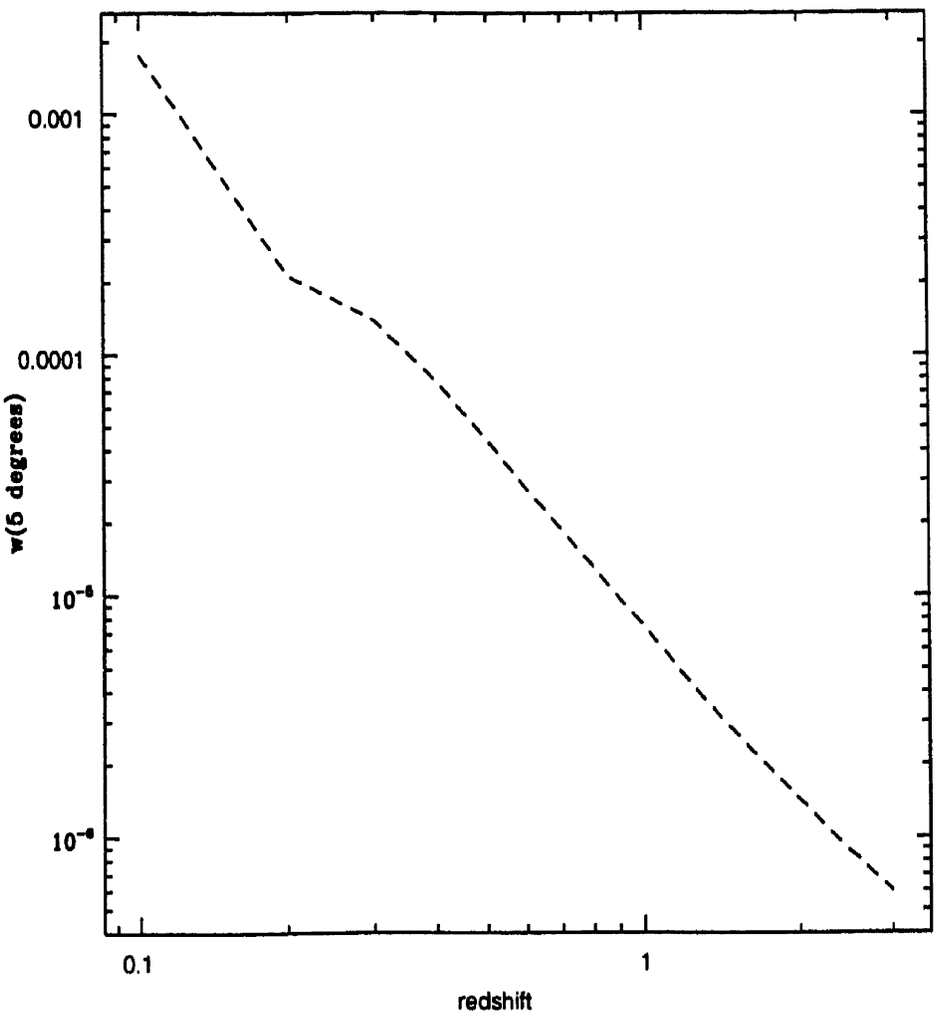

Figure 6.2: Theoretical two-point angular correlation function using the predictions for the sCDM model is shown as a function of depth (redshift) of the sample. The quantity plotted is the absolute value of the two-point correlation function at $\theta = 5°$.

Bibliography

[1] Bardeen, J. M., Bond, J. R., Kaiser, N., & Szalay, A. S. 1986, ApJ, 304, 15

[2] Blumenthal, G. R., Hartmann, D. H., & Linder, E. V. In 2hGRB*, p.117, New York (1994).

[3] Brainerd, J. J. *et al.* 1995, ApJ, 441, L39-L42

[4] Davis, M. & Peebles, P.J.E. 1983, ApJ, 267, 465

[5] Hakkila, J. *et al.* 1996, *AIP*, vol.384

[6] Hamilton, A. J. S. 1993, ApJ, 417, 19

[7] Hartmann, D. H. & Blumenthal, G. R. 1989, ApJ, 342, 521

[8] Lamb, D. Q. & Quashnock, J. M. 1993, ApJ, 415, L1

[9] Landy, S. D. & Szalay, A. S. 1993, ApJ, 412, 64-71

[10] Luo, S. *et al.* 1996, In 2hGRB*, p.477

[11] Meegan, C. A. 1992, Nature, 355, 143

[12] Mo, H.J. *et al.* 1992, ApJ, 392, 452-457

[13] Narayan, R. & Piran, T. 1993, MNRAS, 265, L65-L68

[14] Nowak, M. A. 1994, MNRAS, 266, L45-L49

[15] Peebles, P. J. E. 1993, *Principles of Physical Cosmology*, Princeton university Press

[16] Peebles, P. J. E. 1980,*Large scale structure of the universe*, Princeton University Press, Princeton.

[17] Peebles, P.J.E. & Hauser, M. G. 1974, ApJS, 28, 19

[18] Petrosian, V. & Efron, B. 1995, ApJ, 441, L37-L38

[19] Quashnock, J. M. & Lamb, D. Q. 1993a, MNRAS, 265, L59-L64

[20] Quashnock, J. M. & Lamb, D. Q. 1993b, MNRAS, 265, L45-L50

[21] Rutledge, R. E. & Lewin, W. H. G. 1993, MNRAS, 265, L51-L56

[22] Sethi, S. K., Bhargavi, S. G. & Greiner, J. 1999, In 5hGRB*, p.107; astroph/0001006

[23] Wang, V. & Lingenfelter, R. E. 1993, ApJ, 416, L13

[24] Wang, V. & Lingenfelter, R. E. 1994, In 2hGRB*, p-160

* see bibliography of Chapter. 1 for abbreviated notations.

Chapter 7

Conclusions

7.1 Thesis summary and Conclusions

This thesis mainly presents the studies of the GRB fields carried out to investigate their optical counterparts. The afterglows of GRB 000301c and GRB 010222 were observed and the results of analysis have been presented. Several models were proposed in the literature for the afterglow of GRB 000301c - from standard jet model, gravitational lensing, transition from relativistic to non-relativistic phase and so on. In this thesis, two-burst model is proposed. In case of GRB 010222 different authors arrived at different fit parameters for the light curve and hence diverse suggestions. This could be mainly due to different data sets presented by each author. Perhaps it is time to think of a central facility where all data is pooled together and treated in same manner.

In the cases of GRB 000131 and 010214 afterglows were reported at $\sim 24^{th}$ magnitude. We didnot detect the afterglow down to the detection limits of our telescope. In case of GRB 000131 no independent observations have confirmed the presence of afterglow. In case of GRB 010214 observations by same group after a couple of months indicated that the object reported as afterglow didnot decline in brightness casting doubt on its association with the GRB. One can not rule out the possibility that there might be several variable objects at a faint level of 24^{th} mag in any given field. Such studies need bigger telescopes and so far no systematic surveys have been conducted to study the variability at such fainter levels.

Thesis presents the studies carried out to address two important and timely problems in GRB astronomy concerned with their cosmological nature, viz., clustering

properties and luminosity functions. An attempt has also been made to derive useful results from the IPN-GRB data observed and analysed before the 'afterglow era' by applying the results obtained from the luminosity functions of GRBs. Currently statistical approaches are the only way to study clustering and LF of GRBs. A good sample of measured redshifts is required to derive the LF. The future mission '*Swift*' is expected to provide large number of redshifts.

A summary of current status of research in GRB astronomy with ample references for further reading have been presented. Hopefully this thesis makes an incremental step towards the understanding of the mysterious sources.

7.2 Open issues and Future Prospects

Having established that GRBs are at cosmological distances we now know that they are the most powerful sources in the universe. However, there remain many open questions to be answered, which makes this field ever-exciting in astronomy.

- The progenitors driving the GRB are still not known.
- A careful study of all the light curves of GRB afterglows detected so far shows a diversity in their properties. A large sample of afterglow observations is therefore necessary for the classification of the bursts for subsequent theoretical modelling.
- Whether a sub-class of GRBs associated with SN exist and whether afterglows exist for short duration GRBs is yet to be understood.
- Another application of the z-measurements would be in the study of galaxy evolution (Perna & Loeb). From afterglow studies we know that GRBs occur in host galaxies at a wide range of redshifts ($0.4 < z < 3.42$). Detailed study of such galaxies would provide important information on their evolutionary properties at various look-back times. Afterglow studies of GRBs have also provided evidences that GRBs are associated with star-forming regions. Thus SF histories can be studied at a wide range of redshifts.
- Occurence of GRBs at large redshifts will find application in the study of IGM and Ly_α clouds.

- The data on repeatedly observed GRB fields would be of interest to other branches of astronomy too; There have been interesting objects in such fields e.g. Asteroids. One could make a study of density of variable objects in these data set and also make a catalog of faint galaxies. It is my feeling that, once an OT is confirmed, the focus of the community is just restricted to monitoring the fading behaviour of the candidate object. To my knowledge no report appeared, saying that full FOV/error box has also been monitored to look for other variable objects. From the available data for over 40 afterglow GRBs such a study can be conducted.

- The bad sky conditions at the present observatory hampered our afterglow observations over several years. With the newly commissioned 2-m telescope at Indian Astronomical Observatory, Hanle in the Himalayan region, (longitude = 78°57′51″E, lattitude = 32°46′46″N), we expect to observe large number of GRB afterglows both in the optical and in the IR-bands and make a significant contribution to GRB astronomy. Furthermore, with the commissioning of the GMRT near Pune, we will also be able to carry out studies in the radio band from $\sim$ 150 MHz to $\sim$ 1400 MHz.